UNIVERSITY OF CALIFORNIA
SANTA CRUZ

SEDIMENT SUPPLY AS A DRIVER OF RIVER BED SURFACE GRAIN SIZE AND MOBILITY, WITH CONSEQUENCES FOR AQUATIC HABITAT

A dissertation submitted in partial satisfaction of the
requirements for the degree of

DOCTOR OF PHILOSOPHY

in

EARTH SCIENCES

by

Allison M. Pfeiffer

December 2017

The Dissertation of Allison M. Pfeiffer
is approved:

Noah J. Finnegan, Chair

Andrew T. Fisher

Amy E. East

Tyrus Miller
Vice Provost and Dean of Graduate Studies

Table of Contents

List of Figures

List of Tables

Abstract

Sediment supply as a driver of river bed surface grain size and mobility, with consequences for aquatic habitat

by

Allison M. Pfeiffer

Bed surface grain size and mobility are fundamental characteristics of a river. The size of coarse sediment on the bed of a river controls channel slope, shapes channel plan form morphology, and provides the architecture for aquatic habitat. Despite its importance to river morphology and habitat, the controls on bed surface grain size are imperfectly understood. Varying sediment supply, armoring of the bed surface, roughness effects, and patchiness complicate predictions. Because of its importance, understanding the controls on bed surface grain size is essential despite these complications.

The goal of this dissertation is to further understanding of the controls on the size and mobility of surface grains in gravel bed rivers. The first study, Chapter 2, focuses on predicting reach-averaged grain size at the drainage basin scale. I build on previously proposed methods for grain size prediction, and demonstrate the effectiveness of a new method for predicting grain size in Scott Creek, a small gravel-bedded drainage in the Santa Cruz Mountains, California. This work is then applied to salmon spawning habitat prediction. As a part of that project, I show that grain size is much smaller in Scott Creek than the grain size predicted based on threshold channel theory. This finding motivates the second study in my dissertation. In Chapter 3, I show that there are significant regional trends in the ratio of bankfull Shields stress to critical Shields stress (τ_{bf} / τ_c) across North America. These trends are explained by differences in sediment supply. In

Chapter 4, I consider the implications of these regional trends on the mobility of bed surface grains, and the potential implications for benthic habitat.

To Ben and Nancy, who taught me to love landscapes and data

Acknowledgments

First and foremost, I want to thank my advisor, Noah Finnegan, for teaching me how to tell the stories found within a dataset. I feel enormously grateful to have a mentor who is not only a talented scientist, but one who approaches the world with generosity, self-deprecating humor, and steady good nature. Thank you for allowing me ownership of my intellectual journey while remaining an ever-available source of sound advice and patience.

I am indebted to my committee members, Amy East and Andy Fisher, who took a genuine interest in both my work and my professional growth. Amy has been an important advocate and thoughtful critic, whose advice has been especially helpful in navigating the world of academic publication. Andy has been the model of a thorough, precise, and generous scientist.

I want to thank the members of the UCSC Geomorphology Lab for the years of comradery. I am a better communicator thanks to your shared wisdom and honest, but kind, criticism. I feel lucky to have been in the company of such sharp minds.

This research would not have been possible without the generosity of more than a dozen field assistants who volunteered their time measuring hundreds of pools and thousands of pebbles. Special thanks to Larry Bush, Sam Anderson, and Sarah Reuter for weeks of work and patience with my process.

Funds from the ARCS Foundation, the UCSC EPS Lawson Hydrology Award, and Mildred E. Mathias Graduate Student Research Grant allowed me to complete field campaigns and attend conferences that have been instrumental to my intellectual growth. I thank the generous individuals who made these funds available for budding researchers like myself.

Navigating the academic world was made easier by a number of mentors and

advocates who, while playing no official role in my dissertation research, provided opportunities and guidance at crucial junctures. I am especially grateful to Patrick Fulton, Melanie Michalak, Hilde Schwartz, Jon Perkins, and Kerri Johnson.

I am enormously grateful to Grace, Stephanie, Claire, Sarah, and Danica, the co-founders of GEODES (Geoscientists Encouraging Openness and Diversity in the Earth Sciences), for giving me the opportunity to be a part of such an intentional, deliberate, and positive process. GEODES has nurtured my sense of commitment to and belonging within the geoscience community.

I thrived in Santa Cruz thanks to a group of truly extraordinary friends, at the same time level-headed, playful, brainy, and caring. I am grateful for the support you have given me through unforeseen challenges during these years, and especially for the shared adventures and delicious meals.

Professor Mary Savina first opened my eyes to the science of landscapes. Her quiet guidance and belief in my abilities laid the foundation for this degree.

I want to thank my parents, Nancy and Ben, and the Domudgeons for their genuine curiosity and probing questions about the workings of rivers. Your enthusiasm never failed to reinvigorate my own.

Finally, I thank my partner, Dan, for his unequivocal support through this process, and for bringing laughter and perspective to each day we spend together.

The text of this dissertation includes the following previously published material:

> Pfeiffer, A. M., and N. J. Finnegan (2017), Basin-scale methods for predicting salmonid spawning habitat via grain size and riffle spacing, tested in a California coastal drainage, Earth Surf. Process. Landforms, 42(6), 941 - 955, doi:10.1002/esp.4053.

(Chapter 2, herein)

> Pfeiffer, A. M., N. J. Finnegan, and J. K. Willenbring (2017), Sediment supply controls equilibrium channel geometry in gravel rivers, Proc. Natl. Acad. Sci., 114(13), 3346 - 3351, doi:10.1073/pnas.1612907114.

(Chapter 3, herein. Co-author Jane Willenbring provided data and guidance regarding data analysis.)

Chapter 1

Introduction

Bed surface grain size and mobility are fundamental characteristics of a river. The size of coarse sediment on the bed of a river controls channel slope (*Sklar and Dietrich*, 2006), shapes channel plan form morphology (*Buffington and Montgomery*, 1997), and provides the architecture for aquatic habitat. Among the many physical characteristics that drive salmon spawning site selection (e.g. water depth, velocity, hyporheic exchange, bedform morphology *Bjornn and Reiser*, 1991; *Geist and Dauble*, 1998; *Montgomery et al.*, 1999a), grain size exerts a fundamental control on the distribution of available spawning habitat because a fish must be able to mobilize bed sediment in order to excavate a nest, or redd, in which eggs are buried (*Kondolf and Wolman*, 1993; *Riebe et al.*, 2014). For this reason, the ability to predict the size and occurrence of gravel within both a drainage network and an individual reach is central to salmon habitat protection and restoration efforts. Despite its importance to river morphology and habitat, the controls on bed surface grain size are imperfectly understood. Varying sediment supply, armoring of the bed surface, roughness effects, and patchiness complicate predictions. Because of its importance, understanding the controls on bed surface grain size is essential despite these complications.

Gravel river beds provide an ephemeral architecture for the benthic inhabitants of river ecosystems. Periphyton and benthic macroinvertebrates that live on or within the gravel are subject to catastrophic disruption upon mobilization of the surface gravel during floods. Mobilization of river gravel is often associated with a dramatic reduction in benthic macroinvertebrates density (*Robinson et al.*, 2004; *Power et al.*, 2008; *Gibbins et al.*, 2007). The ecological effects of bed mobilizing flows can persist for months (*Scrimgeour et al.*, 1988; *Power et al.*, 2008), determined by the gradual recolonization by macroinvertebrates. The timing and intensity of bed mobility defines the disturbance regime for river ecosystems. Ecological theories suggest that disturbance regime may control community structure and abundance (*Townsend et al.*, 1997). While the ecological implications of varying bed mobility intensity and timing are substantial, there has been only limited (*Lisle et al.*, 2000) work within the process geomorphology community on this subject.

The stability of an individual grain on the bed surface is a function of the balance between the drag exerted by the flow and the weight of a grain holding it in place. This relationship, which provides a starting point for studies of bed surface grain size and mobility, is expressed as:

$$\tau^{\star} = \frac{\rho h S}{(\rho_s - \rho) D_{50}} \tag{1.1}$$

where ρ_s is the density of sediment, ρ is the density of the water, h is bankfull depth, S is channel slope, and D_{50} is the median grain size on the bed surface and $\tau^{\star}$ is the non-dimensional shear stress, or Shields stress. The critical Shields stress ($\tau_c^{\star}$) is defined as the value of $\tau^{\star}$ that exceeds a threshold value so that sediment transport is initiated on the bed. This critical value of Shields stress is empirically determined. While there is substantial scatter in the data *Buffington*

and Montgomery (1997), incipient motion of the median grain size tends to occur between $\tau_c^\star$ =0.03 and 0.06.

On the drainage basin scale grain size tends to decrease downstream as source material shifts from freshly weathered blocks sourced from headwater streams to finer material sourced from the lowlands (*Sklar and Dietrich*, 2006). Threshold channel theory (*Li*, 1975) suggests that alluvial channels adjust their dimensions so that at any point in the channel, the median grain size is at the threshold for motion at bankfull flow. In terms of Shields stress, this means that bankfull Shields stress, $\tau_{bf}^\star$, is very near $\tau_c^\star$. Taking this simplified approach to explaining the grain size in a channel, knowledge about the bankfull depth and slope of a river should be enough to predict the median grain size. While this approach is useful at the broad scale, and produces accurate grain size predictions in some places (*Snyder et al.*, 2013), factors such as shear stress partitioning between the grains on the bed and other roughness elements (e.g. *Buffington et al.*, 2004) and surface grain size patchiness (*Nelson et al.*, 2010) complicate the realities of predicting grain size in a natural channel from channel morphology.

In natural channels, roughness elements extract momentum from the flow so that only a part of the total bankfull shear stress in the river acts on the bed. This 'partitioning'of shear stress by in-channel wood (*Manga and Kirchner*, 2000), bedforms *Buffington and Montgomery* (1999a), and coarse grains (*Yager et al.*, 2007) causes the effective stress acting on the bed to decrease, thereby decreasing the competent grain size. In addition, channels with very high sediment supply (*Sklar and Dietrich*, 2008) may maintain bankfull stresses well in excess of what is required to initiate motion. Though not strictly 'partitioning' of shear stress away from the bed, this excess shear stress beyond the threshold for motion is an additional component of shear stress to be accounted for at bankfull flow, and

thus represents a complication to the simple threshold channel theory. We can thus frame total shear stress (τ_{total}) in terms of these components,

$$\tau_{total} = \rho g h S = \tau_c + \tau_{roughness} + \tau_{Qxs} \tag{1.2}$$

where $\tau_{roughness}$ is the portion of shear stress accommodated by roughness elements such as wood and bedforms, τ_{Qxs} is the excess shear stress needed to transport a high sediment flux. Because the grain size in the channel is in equilibrium with only a part of the total shear stress, reach-averaged median grain size may be far smaller than would be predicted from the threshold channel theory and equation I.1 in rivers that have adjusted to high sediment supply and abundant roughness elements such as large in-channel wood.

Sediment transport, which I consider here through the lens of river bed mobility, is a function of channel geometry, flow regime, and the grain size distribution of the bed surface. There is an active field of research focusing on sediment transport (e.g. *Parker*, 1990a; *Church and Hassan*, 2002; *Wilcock and Crowe*, 2003; *King et al.*, 2004; *Turowski et al.*, 2010; *Bunte et al.*, 2013), but only limited work has focused on comparing the mobility of different riverbeds (*Lisle et al.*, 2000). The timing of bed mobility is largely determined by the timing of high flows (e.g. high-discharge storms or seasonal snowmelt). The intensity of bed mobility is a more complex function of evolving channel geometry and grain size effects. Shear stress, and therefore bed mobility, increases with water discharge as the depth of flow increases. The rate of increase of flow depth with discharge is moderated by channel geometry (which, in turn, reflects the integrated effects of bed mobilizing flows). The relationship between flow depth and sediment transport intensity is a function of hiding effects: small grains are less mobile when hidden in pockets between large grains. A realistic treatment of bed mobility requires

well-calibrated rating curves to relate discharge and channel geometry as well as sediment transport equations that account for hiding effects.

Chapter 2

Basin-scale methods for predicting salmonid spawning habitat via grain size and riffle spacing, tested in a California coastal drainage

2.1 Abstract

Basin-scale predictive geomorphic models for river characteristics, particularly grain size, can aid in salmonid habitat identification. However, these basin-scale methods are largely untested with actual habitat usage data. Here, we develop and test an approach for predicting grain size distributions from high resolution LiDAR (Light Detection and Ranging)-derived topographic data for a 77 km^2 watershed along the central California Coast. This approach improves on previ-

ous efforts in that it predicts the full grain size distribution and incorporates an empirically calibrated shear stress partitioning factor. The predicted grain size distributions are used to calculate the fraction of the bed area movable by spawning fish. We then compare the 'movable fraction' to 7 years of observed spawning data. We find that predicted movable fraction explains the paucity of spawning in the upper reaches of the study drainage, but does not explain variation along the mainstem. In search of another morphologic characteristic that may help explain the variation within the mainstem, we measure riffle density, a proxy for physical habitat complexity. We find that field surveys of riffle density explain 64% of the variation in spawning in these mainstem reaches, suggesting that within reaches of appropriate sized gravel, spawning density is related to riffle density. Because riffle density varies systematically with channel width, predicting riffle spacing is straightforward with LiDAR data. Taken together, these findings demonstrate the efficacy of basin-scale spawning habitat predictions made using high-resolution digital elevation models.

2.2 Introduction

When salmon return to their natal streams to breed, they build their nests (redds) in reaches with specific hydrologic and geomorphic characteristics. The ability to identify and predict the in-stream physical conditions that drive the redd site selection process is important to salmon habitat protection and restoration efforts. Among the many physical characteristics that contribute to drive spawning site selection (e.g. water depth, velocity, hyporheic exchange, bedform morphology; *Bjornn and Reiser*, 1991; *Crisp and Carling*, 1989; *Geist and Dauble*, 1998; *Hanrahan*, 2007; *Montgomery et al.*, 1996, 1999a; *Soulsby et al.*, 2001), grain size exerts a fundamental control on the distribution of available spawning habitat

because a fish must be able to mobilize bed sediment in order to excavate a nest, or redd, in which eggs are buried (*Buffington et al.*, 2004; *Kondolf and Wolman*, 1993; *Riebe et al.*, 2014).

Given the importance of grain size to spawning site selection, geomorphologists have proposed several methods for predicting bed surface grain size (*Wilkins and Snyder*, 2011; *Gorman et al.*, 2011; *Buffington et al.*, 2004) to determine the distribution of spawning gravel at the basin scale. It has been asserted that these methods represent a potentially valuable tool for watershed managers; however, these assertions are largely untested. To our knowledge, the accuracy of a grain size prediction method has only been tested in one study, (*Snyder et al.*, 2013), which focused on formerly glaciated rivers in Maine. Furthermore, with only one exception (*Buffington, J. M. et al.*, 2003), no proposed methods of basin-scale salmonid habitat prediction (e.g. *Buffington, J. M. et al.*, 2003; *Burnett et al.*, 2007; *May and Lisle*, 2012) have been tested against habitat use data. This lack of testing of basin-scale habitat prediction methods with actual habitat use data represents an important gap in the literature.

Here we take advantage of a unique opportunity to both make predictions of reach-scale habitat suitability (focusing on grain size and riffle spacing) and test those predictions with habitat use data. We focus on a small mountainous drainage in the central California Coast Range, Scott Creek, with widely varying grain size and well-monitored salmonid populations. The unique combination of high-resolution aerial LiDAR-derived topographic data (hereafter referred to as 'LiDAR data') and multiple years of complete spawning season redd surveys in Scott Creek enable this effort. Our goal is to develop and test a method for predicting salmonid spawning habitat on the drainage basin scale, based on remotely sensed topographic data and limited field calibration.

The method we propose builds on previously proposed methods, specifically, *Buffington et al.* (2004) and *Snyder et al.* (2013), in that we predict median bed surface grain size by explicitly empirically calibrating a relationship for the amount of the total bankfull stress available to transport the grains on the bed. In addition, recognizing that a salmon's ability to move sediment is affected by the full grain size distribution present on the bed (*Riebe et al.*, 2014), not just the median grain size, we extend our model to make predictions of bed surface grain size distributions. From these grain size distributions, we can predict the fraction of the bed area movable by a salmonid of a given length. We then test the strength of this metric ('movable fraction', developed by *Riebe et al.*, 2014) as a predictor of spawning site selection by comparing our movable fraction predictions to observed coho salmon (*Oncorhynchus kisutch*) and steelhead trout (*O. mykiss*) spawning survey data.

Finally, we explore the extent to which the density of riffle bedforms along Scott Creek can explain the variation in observed redd density between reaches with similar movable fraction. It is widely recognized that salmonids tend to spawn in channels with pool-riffle morphology, specifically at the tail of a pool and start of a riffle (e.g. *Briggs*, 1953; *Shapovalov and Taft*, 1954; *Geist and Dauble*, 1998; *Montgomery et al.*, 1999a; *Hanrahan*, 2007). Preference for these sites is likely due to the fact that hyporheic exchange, which causes flow of oxygenated water and flushes metabolic waste away from the incubating eggs, is induced by changes in bed topography such as riffles (*Tonina and Buffington*, 2009). Additionally, riffle density may be viewed as a proxy for physical habitat complexity. In forested mountain streams, riffles are often forced by large in-channel wood (LW; *Montgomery et al.*, 1995), which provides cover and hydraulic refuge for salmonids (*Roni and Quinn*, 2001). Pool-riffle couplets also create hydraulic habitat com-

plexity, creating zones of slack water refuge as well as swift water drift-feeding habitat for juveniles (*Booker et al.*, 2004). Thus, where bed surface grain size is in the range for spawning (*Kondolf and Wolman*, 1993), the presence of riffles is often correlated with spawning site selection (e.g. *Hanrahan*, 2007).

Many factors beyond grain size and riffle spacing also drive redd site selection. For instance, flow velocity and depth are widely recognized as controls on redd distribution within a reach (e.g. *Knapp and Preisler*, 1999; *Geist et al.*, 2000; *Moir and Pasternack*, 2008). Additionally, the distribution of redds within a drainage varies from year to year (*Isaak and Thurow*, 2006). The approach we take here is a simplified prediction, focusing solely on reach-averaged channel characteristics that we can estimate from LiDAR data and limited field calibration. However, we recognize that many other factors influence redd site selection at both the reach (e.g. habitat connectivity *Isaak et al.*, 2007) and sub-reach (e.g. depth, velocity) scale. The value of our approach lies in its potential application to rapid, basin-scale identification of spawning habitat for protection and restoration efforts.

Table 2.1: Reach averaged data

Tributary	ID	Reach length m	S^a m/m	w^b m	A^a km^2	h^c m	D_{50}^{ad} m	D_{84}^{ad} m	Avg annual redd density [e] $count/km/yr$	Reach Morph. [f]	Riffles/ km[g] $count/km$
Scott Creek	3	566	0.0039	32.1	71.9	2.17	0.022 (0.024)	0.074 (0.043)	3.79	P-R	15.7
Scott Creek	4	583	0.0047	24.7	70.7	2.16	0.053 (0.027)	0.12 (0.064)	8.83	P-R	20.6
Scott Creek	5	514	0.0051	18.3	54.4	1.97	0.052 (0.026)	0.115 (0.015)	9.46	P-R	23.4
Scott Creek	6	509	0.0039	13.8	35.6	1.73	0.028 (0.009)	0.063 (0.013)	6.22	P-R	27.5
Scott Creek	7	822	0.0049	16	35	1.72	0.03 (0.008)	0.061 (0.012)	10.09	P-R	32.9
Scott Creek	11	772	0.006	11.6	20.1	1.44	0.029 (0.014)	0.063 (0.019)	14.81	P-R	37.6
Scott Creek	12	699	0.0056	12.9	19.2	1.42	0.034 (0.008)	0.078 (0.013)	13.49	P-R	30
Big Creek	24	561	0.0165	11.9	28.4	1.61	0.117 (0.029)	0.239 (0.049)	8.92	PB	5.3
Big Creek	25	568	0.0285	12.1	27.2	1.59	0.123 (0.033)	0.299 (0.052)	1.76	S-P	0
Mill Creek	31	768	0.0237	6	7.6	1.05	0.062 (0.031)	0.174 (0.06)	4.84	PB	-
Mill Creek	32	790	0.0733	6.6	6.3	0.99	0.131 (0.046)	0.337 (0.073)	1.99	CA	-

S (channel slope), w (bankfull channel width), A (drainage area), h (bankfull water depth), D50 (measured median bed-surface grain size), D84 (84th percentile bed surface grain size), average annual redd density, reach morphology, and riffle density are all reach-averaged values.

[a] Mean of measurements made for 100 m spaced grain size measurement stations

[b] Mean of 15 m spaced width measurements made using HEC-RAS

[c] From hydraulic geometry scaling with drainage area.

[d] In parentheses: standard deviation of the mean of the 100-m spaced grain size measurement stations within each reach.

[e] Averaged over 7 years of redd count data.

[f] P-R = pool-riffle, PB = plane bed, S-P = step-pool, CA = cascade. Surveyed in the field.

[g] Surveyed in the field. Mill Creek reaches were not surveyed for riffle spacing.

2.2.1 Study Site

Our study focuses on Scott Creek, a coastal watershed with a drainage area of 77 km^2 in the Santa Cruz Mountains, north of Monterey Bay, California (Figure 2.1). The drainage runs over Miocene aged mudstone, with Cretaceous granodiorite in the upper reaches of its two main tributaries, Big Creek and Mill Creek (*Brabb*, 1989). The Santa Cruz Mountains have a long-term rock uplift rate of 0.1-0.8 mm/yr (*Bürgmann et al.*, 1994; *Anderson*, 1990) and erosion rates of 0.1-0.6 mm/yr (*Gudmundsdottir et al.*, 2013). The region has a Mediterranean climate with cool, rainy winters and dry summers. No dams or diversions regulate flow in the drainage. Average annual precipitation is 113 cm (*PRISIM Climate Group*, 2004). The dominant riparian vegetation shifts going upstream from alder and willow in the lower reaches to coastal redwood (Sequoia sempervirens) in the upper reaches and tributaries. In the early 1900s, a large portion of the watershed was clear-cut for lumber (*Cal Poly Swanton Pacific Ranch*, 2012); since then, logging has been by selective harvest (Drew Perkins, personal communication). Near-infrared (non-bathymetric) LiDAR data for Scott Creek was collected in March 2011 by the National Center for Airborne Laser Mapping (NCALM). The LiDAR-derived point cloud has a density of approximately 10 points/m^2, from which a 1-m resolution digital elevation model (DEM) of the bare-earth ground surface was made for this study.

Within the Scott Creek drainage, our study focuses on portions of the mainstem of Scott Creek as well as its two largest tributaries, Big Creek and Mill Creek, which drain 29 km^2 and 10 km^2, respectively (Figure 2.1). The study areas include seven reaches in Scott Creek and two reaches in both Mill and Big Creeks, respectively, for a total of 11 reaches. These study reaches were selected by National Marine Fisheries Service (NMFS) for repeat spawning surveys. The

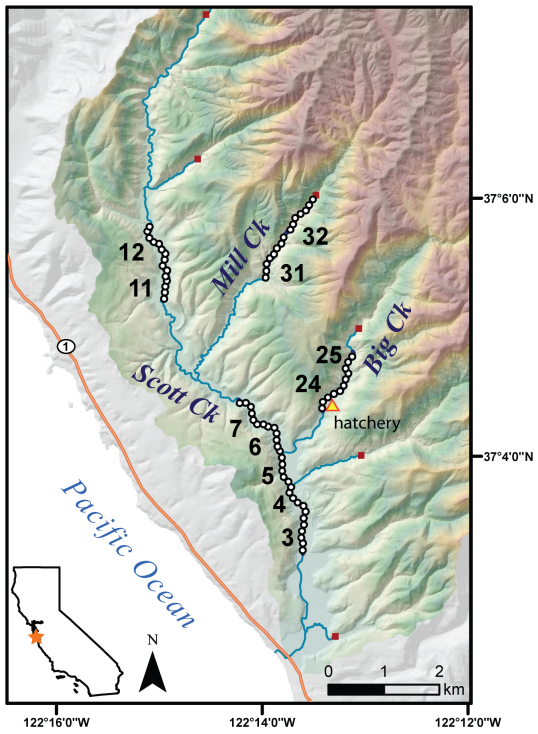

Figure 2.1: Study area, with 100 m spaced field measurement sites marked with black and white dots. Reach numbers, labeled in black, correspond to those listed in Table 2.1. Red squares mark the location of natural barriers to fish migration.

reaches (509-821 m in length) range in slope from 0.4% to 7.3%, and in median grain size from 0.022 m to 0.13 m (Table 2.1). Previous workers found that that stream temperature varies by less than 1° C between upstream and downstream reaches (*Sogard et al.*, 2012). Coho salmon in the coastal streams of central California are listed as endangered under the Federal Endangered Species Act (*NOAA*, 2012), while steelhead trout in this region are listed as threatened (*NOAA*, 2011). The Santa Cruz Mountains mark the southern extent of coho salmon habitat (*NOAA*, 2012). Between 2007 and 2013, the estimated average annual return of coho salmon and steelhead trout to the Scott Creek drainage has been 10 and 185, respectively (Sean Hayes, unpublished data, 2013). Barriers to fish passage that mark the upstream extent of anadromous fish habitat are located 13.0 km (Scott Creek), 9.6 km (Mill Creek), and 6.3 km (Big Creek) upstream from the outlet of Scott Creek into the Pacific Ocean. There is a small hatchery located on Big Creek (Figure 2.1), operated since 1982 by a non-profit organization (Monterey Bay Salmon and Trout Project) in association with the California Department of Fish and Game.

2.3 Methods

We make and test predictions of the median bed surface grain size, D_{50}, for 100-m spaced sites throughout our 11 study reaches in the Scott Creek watershed using three methods: two previously proposed and one that we present below. We then make predictions of the whole grain size distribution, from which we calculate the fraction of the bed area movable by a salmonid of a given length (F_m). Next we compare F_m to observed redd density. Additionally, in the field we measure riffle spacing and compare it to redd density. Lastly, we show that riffle spacing can be predicted from channel width. Extending these methods beyond

the 11 reaches surveyed in the field, we make predictions of F_m, and riffle spacing for all reaches in the Scott Creek drainage that are accessible to steelhead trout and coho salmon. The workflow for the method is shown in Figure 2.2.

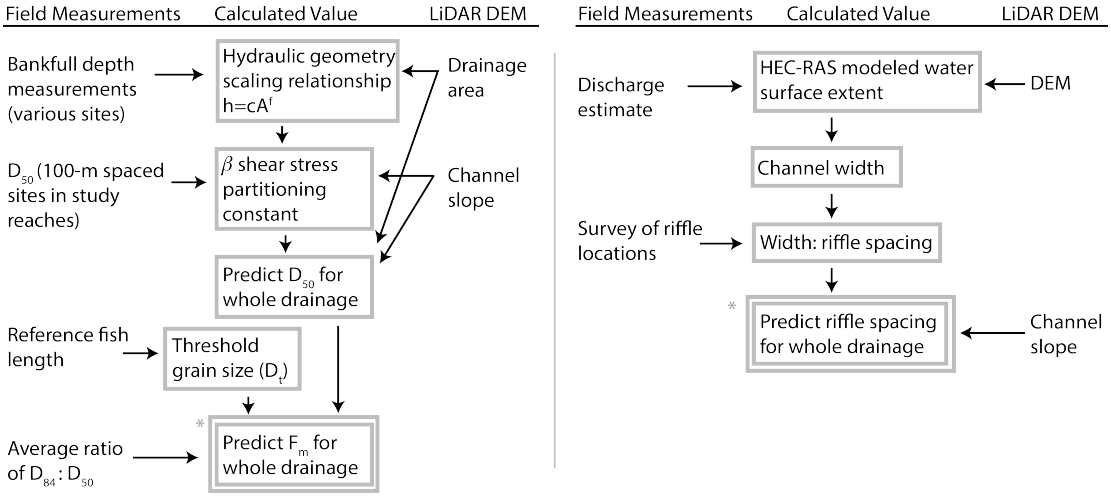

Figure 2.2: Workflow for the method presented in this paper.

2.3.1 Median Grain Size (D_{50}) Prediction

A number of grain size prediction methods have been proposed in the literature (*Buffington et al.*, 2004; *Gorman et al.*, 2011; *Wilkins and Snyder*, 2011). These methods typically assume that the channel in question has evolved so that its entire bankfull reach-averaged bed stress (*Wilkins and Snyder*, 2011) or some fraction of it (*Buffington et al.*, 2004) is available to act on the grains deposited on the bed. This approach allows for the prediction of grain size by first assuming that the stress necessary to move the median grains on the bed occurs at bankfull conditions and then solving for median grain size in the Shields equation (*Paola and Mohrig*, 1996),

$$\tau_{bf}^{\star} = \frac{\rho h S}{(\rho_{sed} - \rho) D_{50}} \tag{2.1}$$

eqn

where $\tau_{bf}^{\star}$ is the bankfull Shields number, g is the acceleration due to gravity (9.8 m/s^2), ρ is the density of water (1000 kg/m^3), ρ_{sed} is the density of the sediment (roughly 2650 kg/m^3), h is reach-average bankfull depth, S is reach-average channel slope, and D_{50} is the median grain size on the bed surface. Importantly, in order to predict grain size from bankfull shear stress in a channel with substantial roughness, it is necessary to 'partition' shear stress between that which acts on grains on the bed and that which acts on roughness elements including in-channel wood (*Manga and Kirchner*, 2000), bedforms (e.g. *Buffington and Montgomery*, 1999a) and boulders (*Yager et al.*, 2007). In addition, channels with very high sediment supply (*Sklar and Dietrich*, 2008) or vegetated banks (*Parker et al.*, 2007) may maintain bankfull stresses well in excess of what is required to initiate motion.

In this study, we make grain size predictions using the (*Wilkins and Snyder*, 2011) and (*Buffington et al.*, 2004) methods; additionally, here we develop a new approach to predict median grain size using a single empirically calibrated shear stress partitioning coefficient. For a thorough review and explanation of the previously proposed methods, see *Snyder et al.* (2013).

This Study

We describe the critical shear stress (τ_c) for the initiation of grain motion as one component of total bankfull shear stress (τ_{bf}) in a reach of river, such that

$$\tau_{bf} = \rho g h S = \tau_c + \tau_{bedforms} + \tau_{LW} + \tau_{Qxs} + \tau_{other} \tag{2.2}$$

(*Buffington and Montgomery*, 1999a; *Manga and Kirchner*, 2000; *Sklar and Dietrich*, 2008) where $\tau_{bedforms}$ is the portion of shear stress associated with momentum loss due to bedform roughness, τ_{LW} is the shear stress associated with large in-channel wood, τ_{Qxs} is the excess shear stress (above critical stress) associated with mobile sediment at bankfull flow (*Sklar and Dietrich*, 2008), and τ_{other} represents other channel conditions (such as bank vegetation or sinuosity) that extract momentum from the flow. Framing critical shear stress in this way, we can describe it in terms of a proportion (β) of bankfull shear stress, such that

$$\beta = \tau_c/\tau_{bf} \tag{2.3}$$

Thus, β represents the magnitude of the partitioning of bankfull shear stress, where a value of $\beta = 1$ corresponds with no partitioning of shear stress ($\tau_c = \tau_{bf}$) and $\beta < 1$ corresponds with momentum losses and excess shear stress that result in τ_c being less than τ_{bf}. We then non-dimensionalize equation (3) with equation (1) to solve for median grain size (D_{50}),

$$D_{50} = \frac{\beta\tau_{bf}}{(\rho_{sed} - \rho)g\tau_c^\star} \tag{2.4}$$

where $\tau_c^\star$ is the critical Shields number and ρ_{sed} is the density of sediment, approximated as 2650 kg/m^3. Rather than selecting a single value of $\tau_c^\star$ (e.g. 0.03), we chose to use the slope-dependent critical Shields number relation (*Lamb et al.*, 2008): $\tau_c^\star = 0.15S^{0.25}$. Thus, our equation for median grain size becomes:

$$D_{50} = \frac{\beta\rho hS^0.75}{0.15(\rho_{sed} - \rho)} \tag{2.5}$$

The magnitude of shear stress partitioning (β) depends on conditions that vary both by reach and regionally. For example, in gravel-bedded channels, it

has been proposed that bedform roughness should be lowest in reaches with plane bed morphology and higher in pool-riffle reaches (*Buffington et al.*, 2004), making partitioning dependent on channel-reach morphology. Additionally, because the density of LW varies between and within streams, depending on natural wood loading and transport as well as management choices (*Benda and Sias*, 2003; *Bilby and Ward*, 1991), partitioning due to LW may vary. Furthermore, gravel flux typically increases downstream, increasing the magnitude of τ_{Qxs} (*Sklar and Dietrich*, 2008). Because the relative magnitude of each of the terms in equation 2.2 can vary greatly depending on local conditions, we proceed with the simplest assumption: that regional effects (catchment erosion rates, etc.) will outweigh between-reach differences (number of pieces of LW, sinuosity, etc.) in partitioning. We therefore assume that β is roughly constant within the extent of the drainage available to spawning salmon. This assumption is tested below.

Buffington et al. (2004) method

The *Buffington et al.* (2004) method for predicting D_{50} forms the basis of the method we propose above; however, it differs in that it incorporates partitioning of shear stress by assuming a power law scaling between shear stress and critical Shields stress $\tau_c^\star = k(\tau_{bf})\mathrm{m}$, such that

$$D_{50} = \frac{(\rho h S)^{(1-m)}}{(\rho_{sed} - \rho) k g^m}. \tag{2.6}$$

In this method, separate values of k and m are empirically determined for different channel-reach morphologies (i.e. plane bed, pool-riffle, step-pool, cascade) (*Montgomery and Buffington*, 1997). When applying this method across whole drainage basins, channel-reach morphology is inferred from reach-averaged channel slope (*Buffington et al.*, 2004). Where channel slope is between 1.5% and

3%, large wood (LW) can force plane bed channel morphology into forced pool-riffle channel morphology; as a result, it is necessary to select which of the two morphologies is most likely in the study area.

Wilkins and Snyder (2011) method

Wilkins and Snyder (2011) use Manning's equation (*Manning*, 1891) and mass continuity ($Q = whv$, where v is average water velocity and w is bankfull channel width) to substitute bankfull channel width for water depth in the Shields equation (equation 1), yielding

$$D_{50} = \rho n^{3/5} Q_2^{3/5} w^{-3/5} S^{7/10} / (\rho_{sed} - \rho) \tau_c^{\star} \tag{2.7}$$

where Q_2 is the 2 year recurrence interval flood discharge, a rough estimate for the bankfull discharge (*Leopold et al.*, 1964). Q_2 is calculated for any point in the drainage network through a scaling relationship with drainage area (A), $Q = bA$. This method has the potential to be useful in an entrenched alluvial channel such as Scott Creek, in which it is possible to measure w from high resolution LiDAR data, but in which h cannot be estimated remotely. The potential drawbacks of the method are the omission of stress partitioning, the need to define a flood recurrence interval relationship (difficult in un-gaged rivers), and the uncertainty in estimating a Manning's roughness coefficient (n).

2.3.2 Model inputs: GIS and Field Data

We tested the three D_{50} prediction methods using data from 11 study reaches within the Scott Creek drainage network. Within each of these reaches, we sampled grain size in the field at cross-sections spaced 100 m apart (71 in total) and pre-determined in a GIS database. By sampling at fixed intervals, regardless of

the bedform or morphologic unit, we ensured that our field measurements captured a representative sampling of the grain size patches in each reach. In order to compute the reach-averaged bankfull stress ($\tau_{bf} = \rho g h S$), we used a combination of field and digital elevation model (DEM) based topographic measurements. Following the methods described by *Snyder et al.* (2013), we measured channel thalweg slope and drainage area for the 100 m spaced stations in ArcGIS from the LiDAR DEM. We made slope measurements using a centered difference approach, calculating channel slope over 200 m intervals centered at each 100 m spaced station (Snyder et al., 2013). The depth-slope product yields reliable predictions of bed surface shear stress when calculated for reaches longer than the backwater length (h/S, *Paola and Mohrig*, 1996). By measuring slope over 200-m increments, we make measurements over a distance greater than the backwater length for just over half of our sites (median h/S = 245). Although previous grain size prediction efforts have successfully used the depth-slope product to predict grain size over length scales less than the backwater length (*Snyder et al.*, 2013), we acknowledge this as a potential source of error and explore it in the discussion. In the field, we measured grain size at each 100-m spaced station using a (*Wolman*, 1954) pebble count, using a ruler to measure the intermediate axis diameter of 100 or more grains at each site. Average bankfull flow depth (h) estimates were made only where indicators of bankfull flow height (e.g., debris on banks or in trees, changes in vegetation) were present within 20 m upstream or downstream of a 100 m sampling site. Fitting these measurements we found a bankfull depth (m) to drainage area (m^2) hydraulic geometry scaling relationship *Leopold and Maddock* (1953) (Supporting Information Figure 1a):

$$h = 0.0062 A^{0.32} \tag{2.8}$$

Combining channel slope measurements from the LiDAR DEM, extrapolated bankfull depth from equation 2.8, slope-dependent critical bankfull Shields stress ($\tau_c^\star$) (*Lamb et al.*, 2008), and measured D_{50}, we minimized root mean square error to find the partitioning (β) value that yielded the best fit between the median grain size predicted via equation 2.5 and observed median grain size at each of the 71 study reaches. These values were then averaged by reach. We use this optimized value of β along with Equation 2.8 and S and A measurements from the DEM to predict D_{50} throughout the entirety of the Scott Creek drainage network using Equation 2.5.

In addition to the estimates of h and S, the *Wilkins and Snyder* (2011) method requires estimates of Q2, w, and Manning's n. We estimated w using HEC-RAS a 1-dimensional hydraulic model, according to the method described by (*Finnegan and Balco*, 2013). Because near-infrared LiDAR does not penetrate the water surface, our HEC-RAS modeled flows are superimposed on top of the low-flow water surface captured when the LiDAR data were collected, and do not represent the actual discharge at bankfull flow. We input values of roughness and discharge sufficient to yield a modeled water surface that filled the incised channel, which we identified visually from the LiDAR-derived DEM. Because channel width varied substantially within each reach, we measured bankfull channel width for cross sections spaced every 15m throughout Scott Creek and its two tributaries, Mill Creek and Big Creek. To do this, we used ArcGIS to 'clip' the channel cross section lines, which are created automatically as a part of the HEC-RAS channel topography extraction, to the width of the modeled water surface extent. We then calculated the length of the resulting (clipped) cross section lines, yielding an estimate of bankfull channel width (w) at each 15 m spaced cross section. Using HEC-RAS allowed us to make >1500 width estimates throughout the drainage

(which we also use to estimate riffle density, below), a task that would be cumbersome by hand. Following the method described by *Snyder et al.* (2013), we used these point measurements to calibrate a basin-wide hydraulic geometry scaling relationship *Leopold and Maddock* (1953) to relate w (m) and A (m^2) (Supporting Information Figure 1b):

$$w = 0.0028A^{0.49} \tag{2.9}$$

Using this relationship, we calculated a representative channel width for each 100 m station. Following the methods in *Wilkins and Snyder* (2011), we visually estimated Manning's n in the field (*Barnes*, 1967), and determined that it varies between (and sometimes within) study reaches from 0.03-0.05. Calculating the 2-year recurrence interval discharge (Q^2) for Scott Creek, a required input for the (*Wilkins and Snyder*, 2011) method, proved problematic in Scott Creek, for which a long term stream gage record does not exist. A USGS stream gage operated in Scott Creek intermittently from 1937 to 1973, with a total of 19 years of data (including both daily average flow and peak annual flood). Given the potential for error when estimating a 2-year recurrence interval discharge calculated with only 19 years of data, we compared the Scott Creek record to that for Soquel Creek, a nearby drainage of a similar area, precipitation gradient, and similar flood stage hydrographs (Supporting Information Figure 2) with a 62 year USGS stream gage record (1950-2012, including both daily average flow and peak annual flood). From the Soquel Creek data, we found that the years of Scott Creek data yielded a Q_2 9% lower than the Q_2 based on the complete dataset. Based on this finding, we adjusted our Scott Creek Q_2 to be 9% higher than that from the years on record. Using this adjustment and a linear scaling between discharge (m^3/s) and drainage area (m^2) (*Snyder et al.*, 2013) the bankfull discharge to drainage

area relationship is:

$$Q_2 = (4.365x10^{-7})A \tag{2.10}$$

2.3.3 Predicting Grain Size Distributions and Movable Fraction

We make predictions of 'moveable fraction' (F_m), a metric that quantifies the suitability of a grain size distribution to salmon spawning in terms of the fraction of the bed area movable by a salmon of a given body length (*Riebe et al.*, 2014). The movable fraction approach builds on the long-held observation that salmon spawning gravel size has an upper limit; *Kondolf and Wolman* (1993) found that salmonids of many species spawn in gravel with surface D_{50} up to 10% of their body length. F_m is suggestive of good spawning gravel, though it should be noted that F_m does not account for the negative impact of sand and silt on spawning gravel suitability.

In order to predict F_m, we need an estimate of the complete bed surface grain size distribution, not just the D_{50}. To predict the grain size distribution at each one of our sample sites, we take advantage of the fact that river gravels, including those in Scott Creek, tend to have roughly log-normal grain size distributions (*Bunte and Abt*, 2001). We caution that this assumption should be tested with field data, especially in channels with large fine sediment accumulations or lag deposits. Using the observed ratio between D_{84} and D_{50} from our field measurements of grain size in Scott Creek, as well as our predicted values of D_{50} (from Equation 5), we can calculate the geometric mean ($\log(D_{50})$) and standard deviation ($\log(D_{84}/D_{50})$) of the grain size distribution for each site (*Bunte and Abt*, 2001; *Riebe et al.*, 2014). Based on those values, we are able to create synthetic

log-normal grain size distributions for any site in the Scott Creek drainage network.

In order to determine the suitability of a grain size distribution for salmonid spawning, we compare each predicted grain size distribution to a representative maximum movable grain size for the salmonids spawning in the Scott Creek drainage. Using the median body length of the 597 returning adult female coho salmon and steelhead trout captured in Scott Creek between 2007 and 2013, 0.65 m, we calculate a threshold spawning gravel size according to the relationship $D_t = 0.115(5L/3)^{0.62}$ (*Riebe et al.*, 2014), where L is the median fish length in meters. Our analysis includes only female fish, as they are the ones that perform the majority of the digging during redd construction. Redd observations were not linked to individual species during the spawning surveys (described below), which prevents us from comparing species specific F_m to redd density; thus, we did not utilize separate threshold grain sizes for steelhead trout and coho salmon. However, the threshold grain size for coho salmon (which make up only 5% of the returning fish, median length = 56.5 cm) is only 0.01 m smaller than the threshold grain size for steelhead trout (median length = 65 cm, $D_t = 0.12$ m), resulting in little difference in F_m between these two species. In a river with multiple salmonid species of significantly different size, species specific calculation of F_m would be warranted. Using the species aggregate threshold grain size ($D_t = 0.12$ m) we can make a prediction of F_m for any reach in the Scott Creek drainage by calculating the fraction of the reach-averaged synthetic grain size distribution that is smaller than D_t. In the results presented below, we calculate F_m at each 100-m spaced station, then find the average of those values to determine the reach-scale F_m. Moveable fraction, as originally conceived by *Riebe et al.* (2014), describes the fraction of movable particles within the grain size patch surrounding a redd.

However, the distribution of available grains should, in principle, limit spawning habitat suitability beyond the microhabitat scale. Boulder-bedded reaches will tend to have fewer pockets of suitable spawning habitat than their gravel-bedded counterparts. Here, we extend the application of F_m to a reach scale. Below, we test the effectiveness of reach-scale F_m in identifying spawning habitat by comparing it to reach-scale redd density.

Also of note, F_m is a prediction of the movable fraction of the grains on the bed surface, which is likely different than the movable fraction of the subsurface grain size distribution. During redd excavation, salmonids mobilize both the surface and subsurface grains. However, the bed surface tends to be coarsened relative to the subsurface grain size distribution (*Parker et al.*, 1982) making predictions of F_m an estimate of the mobility of the coarsest grains encountered by a salmonid during redd excavation.

2.3.4 Survey of riffles in Scott Creek

With the goal of explaining the variation in redd density within areas of high F_m (good spawning gravel), we mapped riffles in the field throughout the mainstem of Scott Creek and in Big Creek during baseflow conditions. We did not conduct a field survey of riffles in the study reaches of Mill Creek. Bedforms were classified as riffles if they had two of the following three qualities: 1) area of steeper water surface slope, juxtaposed with the shallow water surface slope of pools during base flow (*Leopold et al.*, 1964), 2) a shallow depth with deeper pools immediately upstream and downstream, and 3) located between alternating bars where the thalweg traverses sides of the channel (*Keller and Melhorn*, 1978). We recorded the center point of each riffle crest using a handheld global positioning system (GPS). As a part of the riffle survey, we also noted large in-channel wood in the

study reaches. We counted the number of large wood structures, either individual pieces or jams, greater than 10 cm in diameter and more than 1 m long within the bankfull channel, recording the location of each large wood structure with a handheld GPS.

2.3.5 Predicting Riffle Density

With the goal of estimating riffle density from the LiDAR data, we made predictions of channel-reach morphology and, within the reaches of predicted pool-riffle morphology, predictions of riffle density. We predicted channel-reach morphology from channel slope according to the classification system of (*Montgomery and Buffington*, 1997). We classified all reaches of slopes <1.5% as emergent pool-riffle morphology (*Buffington et al.*, 2004). Where abundant large wood (LW) is present, forced pool-riffle morphology may form in slopes up to 3% (*Buffington et al.*, 2004). Thus, we verified the morphology of these reaches (slope 1.5-3%) in the field. Within pool-riffle reaches, bedforms tend to display rhythmic spacing (*Keller and Melhorn*, 1978), with riffles spaced an average of 5-7 channel widths apart (e.g. *Leopold et al.*, 1964; *Hanrahan*, 2007). In wood-rich environments, the spacing of bedforms tends to decrease to 2-4 widths or less (*Montgomery et al.*, 1995). Taking advantage of this previously observed relationship between channel width and riffle density we made an estimate of reach-average relative riffle density for reaches of appropriate channel slope for pool-riffle morphology (<1.5%). Averaging the 15 m-spaced bankfull channel width estimates (from HEC-RAS, described above) by reach, we predicted riffle density by assuming that riffle density scales with bankfull channel width (assuming riffle spacing (number of channel widths between riffle crests) is 2.5). Using HEC-RAS to estimate width allowed us to automate average channel width calculations (n > 33 cross section mea-

surements per reach) for all reaches in the drainage. We calculate observed riffle spacing for each reach by dividing the reach length (m) by the product of the reach-average channel width and the number of riffles observed in that reach.

2.3.6 Redd Counts

We compared the above measures of habitat suitability, F_m and riffle spacing, against redd count data collected by the National Marine Fisheries Service (NMFS) from 2007 to 2013. Each year's redd count began when the seasonal lagoon at the mouth of Scott Creek breached in the late fall or early winter, and ended two weeks after the last new redd was sighted. Trained surveyors walked the length of the 11 study reaches weekly, marking redds with flagging to prevent duplicate entries. In this study, we compare F_m and riffle spacing to observed average annual redd density (redds/km/yr) for each of the 11 study reaches. Salmonids inhabit a wide variety of fluvial systems; in this study we focus on a small, forested mountain drainage, while other studies have focused on spawning habitat in reaches with an order of magnitude greater channel width (e.g. *Geist et al.*, 2000). Because our study reaches are narrow (bankfull widths listed in Table 2.1), and redds are rarely observed side by side in the channel (Sean Hayes, personal communication), we treat available spawning habitat as a one-dimensional problem, ignoring the direct effects of channel width on the distribution of redds. In large channels, where redds are often aligned side by side, perpendicular to the flow (e.g. *Geist et al.*, 2000; *Moir and Pasternack*, 2010, 2008), channel width would be a necessary consideration.

2.3.7 Data Analysis

Predictions of grain size and F_m

To quantify the accuracy of each of the three grain size prediction methods described above, we compared predicted and observed median grain size for the 100 m spaced sites throughout Scott Creek and its tributaries. We compared the root mean square error (RMSE) between observed and predicted D_{50} values for each of the three methods (Equations 2.5, 2.6, and 2.7). Because F_m is calculated from D_{50} and two coefficients which remain constant for all sites in the study area, successful prediction of D_{50} is directly related to successful prediction of F_m. The relationship between D_{50} and F_m is illustrated in Supporting Information Figure A.3.

Predictions of spawning habitat

To determine whether the differences in average redd density (redds/km/yr) between study reaches were statistically significant, we performed a Kruskal-Wallis rank sum test. We used linear regression to test whether F_m and riffle density explain the variation in redd density between reaches. Because of the small sample size of study reaches (n = 11 reaches of redd data, and n = 7 reaches of pool-riffle morphology), we used a bootstrap-resampling technique to calculate the uncertainty associated with both the correlation between riffle spacing and channel width and the correlation between F_m and redd density. We generated a bootstrapped dataset of 10,000 random samples with replacement from the original F_m and riffle density data, calculating a correlation coefficient (r) for each of these random samples. From the distribution of bootstrapped r values, we calculate the 95% confidence interval associated with the correlation (*Efron*, 1987). This non-parametric analysis is based on the assumption that our data on redd

density and riffle spacing data are representative of the redd density and riffle density in the drainage.

2.4 Results

Within our study areas, observed median grain sizes range over almost two orders of magnitude, from 0.005 m in the lower mainstem of Scott Creek to 0.21 m in upper Mill Creek (100 m spaced sites), though the ratio of D_{84} to D_{50} ($D_{84} = 2.29D_{50}$; $r^2 = 0.86$) remains constant throughout the creek (Figure 2.3). This scaling relationship is nearly identical to that computed from an independent analysis of 141 D_{84}-D_{50} pairs compiled from multiple datasets (*Rickenmann and Recking*, 2011). Reach average channel slope also varies over more than an order of magnitude between reaches, from 0.4% to 7.3% (Table 2.1).

Using the shear stress partitioning method (Equation 2.5), we predict median grain size (D_{50}) throughout Scott Creek, calibrating these predictions with data from 71 points (100 m spaced sites) throughout the study reaches. By minimizing root mean square error (RMSE) between predicted and observed grain size at the 71 100-m spaced grain size measurements sites in Scott Creek, we find that 28% of the total bankfull shear stress in Scott Creek goes to setting grain size ($\beta = 0.28$). Additionally, when separately calculated for each of the 11 study reaches, β varies from 0.18 to 0.39 (Standard deviation = 0.06), and does not change systematically with channel slope within our study area (Figure 2.4).

Comparing the values of D_{50} predicted using the *Wilkins and Snyder* (2011), *Buffington et al.* (2004), and shear stress partitioning (presented here) methods to measurements made in the field, we find that all three methods predict D_{50} to within a RMSE of 0.034 m, given the right inputs (Table 2.2). We note that the *Wilkins and Snyder* (2011) method is sensitive to user choices of plausible

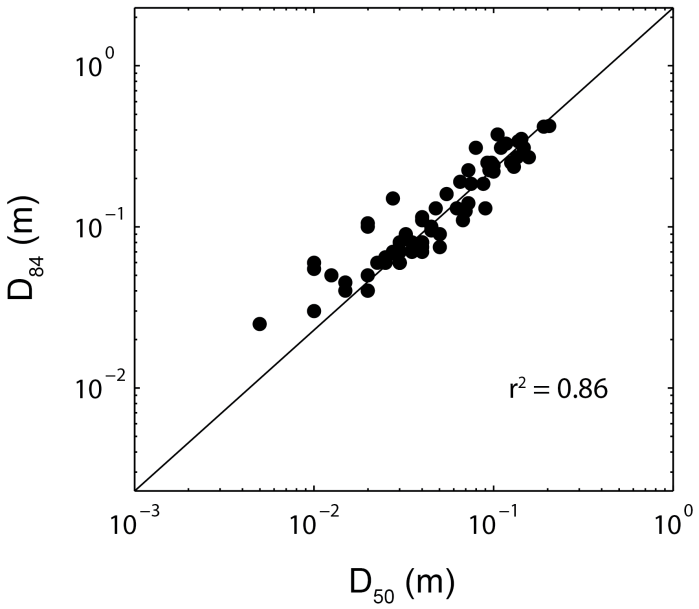

Figure 2.3: Comparison of D_{84} and D_{50} measured at each 100 m spaced grain size station in the study area (n=71) using Wolman (1954) 'pebble counts'. Regression line takes the form D_{84}= 2.29 D_{50}.

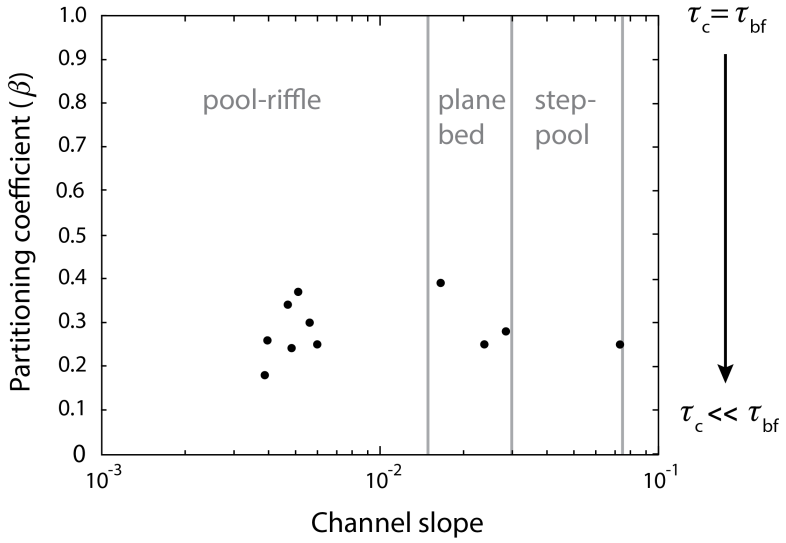

Figure 2.4: Bankfull shear stress partitioning (portion of total bankfull shear stress that sets grain size, equation 2) of each study reach plotted against channel slope. In the case of no partitioning, all points should fall on the line β=1. Channel morphology-slope relationships (Buffington et al., 2004) marked for reference.

Table 2.2: Accuracy of D_{50} predictions

Method	Root mean squared error (RMSE) (m)
Stress partitioning (this study) [a]	0.025
Wilkins and Snyder method [b] (n = 0.03, $\tau_c^\star = 0.05$)	0.025
Wilkins and Snyder method [b] (n = 0.05,$\tau_c^\star = 0.03$)	0.1
Buffington method [c] (w/FPR)	0.037
Buffington method [c] (no FPR)	0.032

[a] Equation 5
[b] Equation 6, *Wilkins and Snyder* (2011)
[c] Equation 7, *Buffington et al.* (2004)

values of Manning's n and $\tau_c^\star$. By varying Manning's n between 0.03 and 0.05, the estimated range observed in the field, and varying $\tau_c^\star$ within a standard range (0.03 and 0.05) (*Buffington and Montgomery*, 1997), we find that RMSE varies by a factor of four, from 0.025 m to 0.10 m. Conversely, we find that D_{50} prediction success for the (*Buffington et al.*, 2004) method is relatively insensitive to user choice of $\tau_c^\star$ - τ_{bf} scaling in Scott Creek. Selecting either the values of k and m for forced pool-riffle or for plane-bed morphology, a necessary choice for reaches with channel slope between 1.5% and 3%, has a minor effect on the overall grain size prediction success in Scott Creek (Table 2.2). Using the shear stress partitioning method proposed in this paper, our optimized predictions match observed D_{50} (Table 2.2) with an RMSE of 0.025 m. Averaging these 100-m spaced station D_{50} predictions and observations by reach (Figure 2.5), we find our grain size predictions are within +/- 30% of observed reach-average D_{50} for 10 out of the 11 study reaches. Extending our D_{50} predictions beyond the surveyed reaches, we use the stress partitioning method to make predictions of D_{50} for all reaches in the Scott Creek drainage that are downstream of barriers to anadromous fish

migration. Predicted reach-average D_{50} in the Scott Creek drainage ranges from 0.03 to 0.21m.

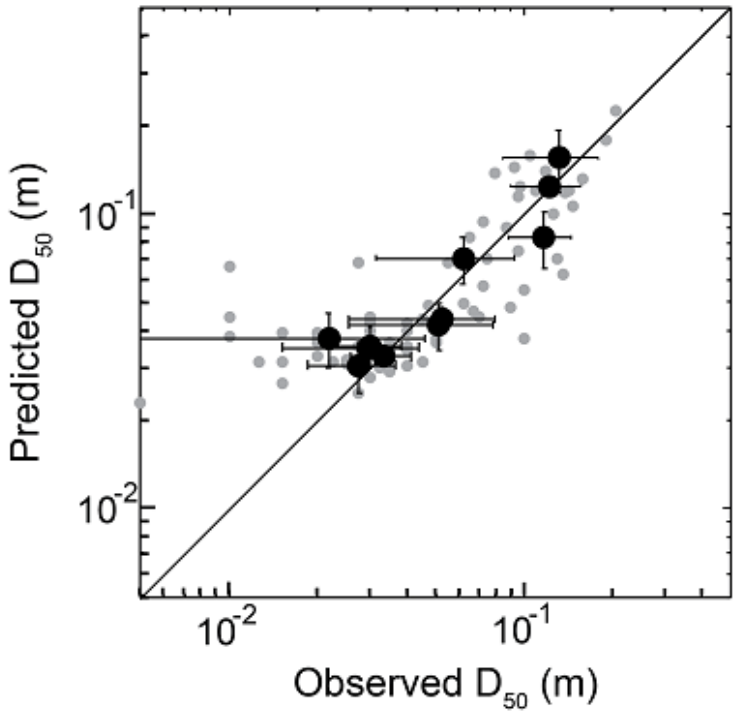

Figure 2.5: Comparison of measured and predicted median grain size (using method developed here, Equation 5, partitioning coefficient (β) = 0.28) throughout Scott Creek. Grey dots mark predictions and measurements made for 100 m spaced points throughout the study area, black dots denote reach-averaged values. Error bars represent one standard deviation within binned data. Diagonal line indicates 1:1 agreement.

A comparison of field-measured grain size distributions and their synthetic counterparts is shown in Figure 2.6a. Because we binned all observed grain size measurements below 0.005 m into a single category (fines), we do not capture the fine-grained tail of the cumulative grain size distribution curve. Additionally, several sites had substantial mismatch in the lower half of the grain size distribution (e.g. site marked in green, Figure 2.6). Predictions matched observations more closely in the coarser half (>50% finer or, equivalently, D_{50}) of the distribution

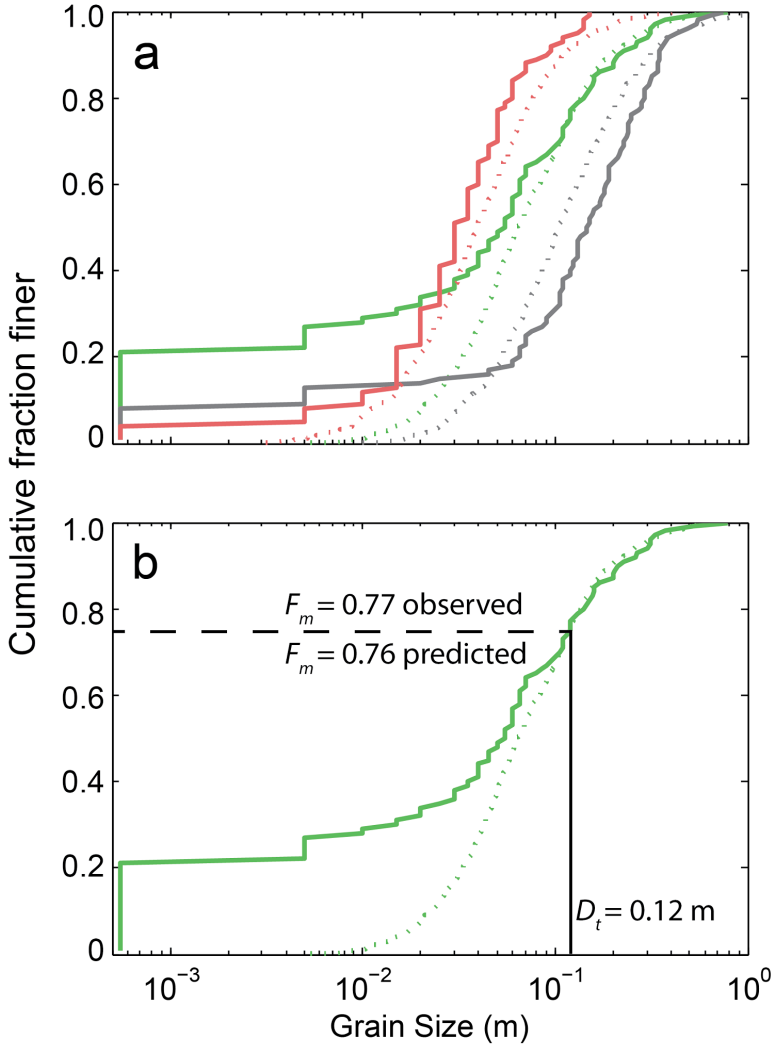

Figure 2.6: (a) Examples of predicted and observed grain size cumulative distribution curves for three 100-m spaced sampling sites in the study area. Observed (solid lines) and predicted (dashed lines) data for a given site are marked in the same color. (b) Graphical representation of the method for calculating Fm from D_t and the grain size distribution curve. Note that the misfit in prediction and observation in the lower portion of the grain size distribution has no effect on the predicted F_m at this site.

curves for most sites. While the individual observed grain size distributions do not perfectly match the measured distributions (Figure 2.6), the metric we are ultimately concerned with predicting is F_m. Because the threshold grain size for F_m ($D_t = 0.12$ m) is greater than the reach-average D_{50} for 87% of the sites, these poor predictions of the fine grained portion of the distribution have no effect on F_m. We illustrate this in Figure 2.6b. Using both the observed and predicted grain size distributions to calculate movable fraction (F_m), we find that, averaging our 100-m spaced stations by reach, observations match predictions +/- 6% for 9 out of 11 reaches (Figure 2.7). The remaining sites have a misfit between predicted and observed movable fraction of less than 15%. Reach average observed F_m, calculated from grain size measurements in the field, ranges from 0.49 to 0.98, while reach averaged predicted F_m ranges from 0.39 to 0.95. As with D_{50}, we make predictions of F_m for all reaches in the Scott Creek drainage that are within the extent of anadromy. Predicted F_m within the drainage ranges from 0.24 to 0.95 (Figure 2.8).

Within surveyed reaches with channel slope <1.5% (n = 7), riffle density (riffles/km) varies strongly as a function of bankfull channel width (Figure 2.9a). On average, within these reaches, riffles are spaced 2.2 channel widths apart (standard deviation = 0.3 widths). The dotted line in Figure 2.9 represents a prediction of riffle density (riffles/km) assuming riffle spacing of 2.5 channel widths. Using this metric and the measured channel widths, we make predictions of riffle spacing for all reaches within the Scott Creek drainage (Figure 2.8c). Of note, channel slopes in three of the 11 study reaches are between 1.5 and 3%. As a result, the channel reach morphology could be predicted to be either forced pool-riffle or plane bed (*Buffington et al.*, 2004). One of these three reaches, the downstream study reach in Mill Creek (Reach 31), was not surveyed for riffle density. Of the two reaches

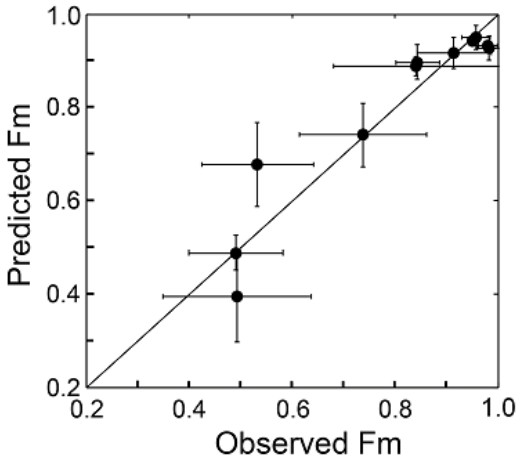

Figure 2.7: Predicted and observed values of movable fraction of the bed area (Fm), averaged by reach. Diagonal line marks equality. Error bars show standard deviation of the observed and predicted Fm values for the 100 m spaced sites within each reach.

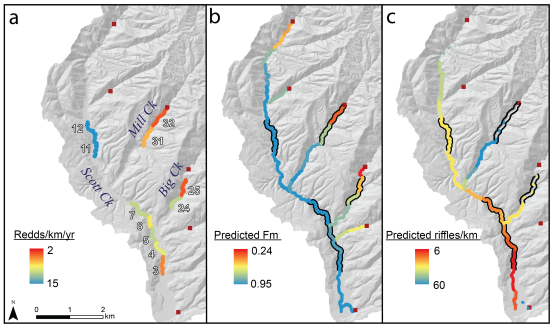

Figure 2.8: (a) Observed redd density (redds/km/yr) for all surveyed reaches. Reach numbers (marked in white) correspond to the data in Table 2.1. Red dots mark barriers to fish passage. (b) Prediction of movable fraction of the bed area (Fm) for reaches throughout Scott Creek and its tributaries. The 11 surveyed study reaches are outlined in black. (c) Predictions of riffle density (riffles/km) made by assuming pool riffle morphology occurs where channel slope is <1.5% and riffles are spaced an average of 2.5 bankfull channel widths apart. Reaches marked with dashed lines have slopes 1.5-3%, suggesting that they may be either plane bed or forced pool-riffle morphology (Buffington et al., 2004). Unmarked reaches situated downstream from barriers to anadromy (marked with red boxes) have slopes >3%, and are predicted to have no riffles.

with channel slope between 1.5 and 3% surveyed for riffles (both in Big Creek), the lower was classified as plane bed morphology and the other was classified as step-pool (Table 2.1) based on field observations. Riffle spacing in the lower reach averaged 15.7 channel widths, and no riffles were observed in the upper reach.

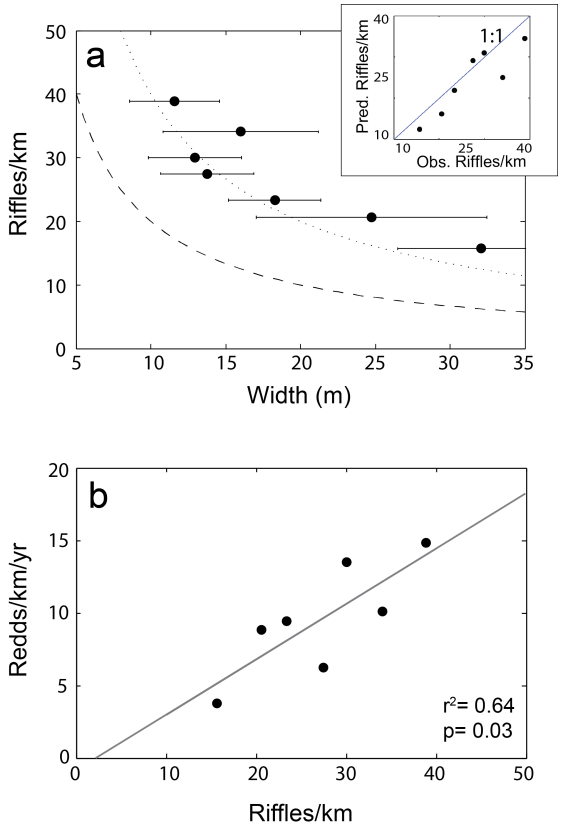

Figure 2.9: (a) Observed riffle density as a function of channel width, measured by reach for all reaches of pool-riffle morphology (n = 7) in Scott Creek. Dashed line represents predicted riffle spacing of 5 channel widths. Dotted line represents riffle spacing of 2.5 channel widths. Error bars show the standard deviation of channel width measurements for each reach. Inset shows a comparison of measured riffle density and predictions of riffle density (assuming 2.5 channel width spacing). (b) Redd density as a function of riffle density for reaches in the mainstem of Scott Creek.

Redd counts performed between 2007 and 2013 indicate that the average annual density of redds ranged between study reaches from 1.8 to 14.8 redds per kilo-

meter per year of survey (Table 2.1). There are significant differences in spawning density between the study reaches (Kruskal-Wallis test: $\chi^2 = 28.1$; df = 10, p = 0.0018). That said, because a comparison between 11 reaches involves 55 unique pair-wise comparisons, non-parametric post hoc tests such as Mann-Whitney U have little power to detect significant differences between reaches. However, considering the distribution of redd densities for all of the seven years of redd survey data, trends remain consistent over time. For example, in all 7 years of record, redd density was higher in the two upstream-most reaches of the mainstem (Reaches 11 and 12, Figure 2.8, Table 2.1) than in the uppermost reaches in both Big Creek and Mill Creek (Reaches 25 and 32).

We observe variation in redd density associated with both predicted (Figure 2.10a) and observed (Figure 2.10b) reach-average movable fraction of the bed area. Linear regression suggests that variation in predicted F_m explains 47% (r^2=0.47, p=0.02) of the variation in spawning density in Scott Creek. The bootstrapped 95% confidence interval for the positive correlation between F_m and spawning density ($0.09 < r < 0.94$) is greater than 0, thus the positive correlation is significant. The two surveyed reaches with the lowest predicted F_m, the uppermost surveyed reaches in Mill and Big Creeks, have the lowest redd densities. This trend of low spawning density in the lowest F_m reaches was consistent in all 7 years of the spawning survey; this is illustrated in the data for individual years of spawning survey, shown as open circles in Figure 2.10a. However, reaches with high movable fraction do not have uniformly high redd density. Within reaches of $F_m > 0.88$, we observe more than threefold variation in redd density. Considering the variation in movable fraction spatially (Figure 2.8b), the upper reaches of Mill Creek and Big Creek have low F_m and correspondingly low spawning density. On the other hand, in the mainstem of Scott Creek, F_m is uniformly high, but spawning

density varies greatly. A comparison of redd density and D_{50} yields equivalent results because predicted F_m is a function of D_{50} and a constant ratio of D_{84}/D_{50} (Supporting Information Figure A.3).

Within the high F_m reaches of the mainstem, redd density is positively correlated with riffle density (Figure 2.9b). Using linear regression, we find that the variation in riffle density explains 64% ($r^2 = 0.64$, p = 0.03) of the variation in redd density within finer grained mainstem reaches, all of which have > 88% F_m. Despite the small dataset, the bootstrapped 95% confidence interval for the correlation coefficient (95% C.I.: $0.30 < r < 0.99$) is positive, meaning that this positive correlation is statistically significant.

2.5 Discussion

F_m and riffle density as predictors of spawning suitability A primary goal of this work is to test the extent to which F_m, and as a corollary, grain size, can be used to explain salmonid spawning distribution. Comparing the predicted values of F_m to average observed redd density over the 7 years of observation, we find that F_m explains 47% of the variation in spawning density (Figure 2.10a). We observe the lowest redd densities (redds/km/yr) in the two reaches with the lowest movable fractions. This corresponds well with observations of spawning cited in the literature. While F_m of a reach can theoretically vary from 0 - 1, data from *Riebe et al.* (2014) strongly suggest that spawning tends to occur where F_m is high, with almost all spawning happening in reaches where $F_m > 0.75$ (Figure 2.10c). Their data, many of which come from previously published observations of spawning, record the bed surface grain size at the redd site, rather than at the spawning reach scale. However, reach average spawning gravel suitability is directly related to the cumulative suitability of each grain size patch within that

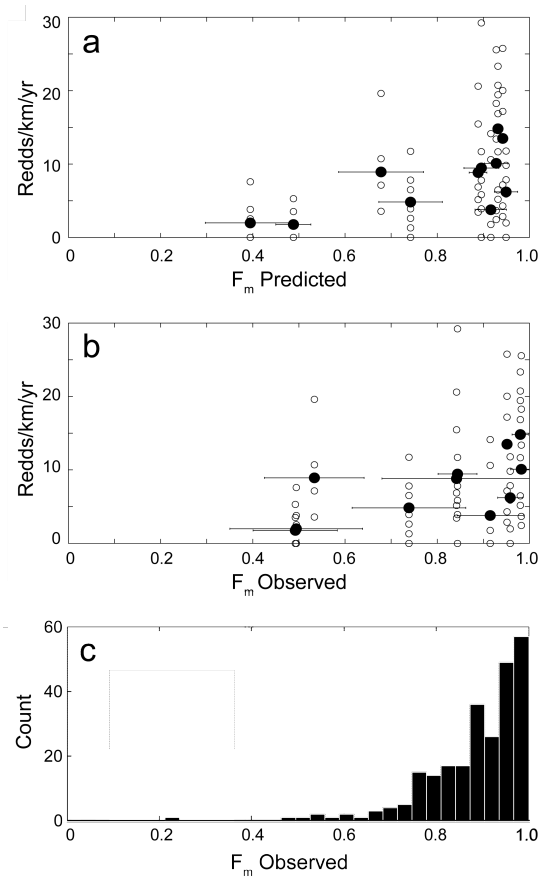

Figure 2.10: (a) Comparison of predicted movable fraction (Fm) and observed redd density (redds/km/yr). Hollow circles mark the redd density observed in each reach in each of the 7 years of study. Black dots denote the average observed redd density (redds/km/yr) over the 7 year period. Horizontal error bars mark the standard deviation of predicted Fm from the 100 m spaced sites in each reach. (b) Same as (a), showing observed Fm calculated using field measured grain size distributions. (c) Histogram of Fm of spawning reaches, calculated from data from former studies (Riebe et al. (2014) (Chinook data only, Supplementary Information, table 3); Kondolf and Wolman (1993) (Table 2.1, only fish >0.4 m in length). Note that Fm is high (> 0.8) in the majority of reaches where spawning occurs.

reach. In the Scott Creek drainage, the reaches with highest observed redd density have high movable fraction, $F_m > 0.88$, however not all reaches with high movable fraction have high redd density. Considering the spatial trends in F_m throughout the Scott Creek drainage network, low spawning density in the upper reaches of both tributaries (Reaches 25 and 32, Figure 2.8a) can be well explained by large grain size, and thus low F_m. However, variation in spawning within the mainstem, where movable fraction is uniformly > 0.88 throughout, cannot be explained by grain size. A comparison of reach 3 to reaches 11 and 12 illustrates this point: F_m is high in all three reaches (> 0.92), while redd density is higher in reaches 11 and 12 than in reach 3 during 6 out of the 7 years on record (average 3.8, 14.8, and 13.5 redds/km/yr, respectively, Table 2.1). This supports the idea that reaches with suitably sized spawning gravel (high F_m) are not all equally suitable for spawning. Thus, models of reach-averaged F_m may be useful in predicting reaches of low spawning suitability but, alone, these models cannot be used to explain where in a drainage network the highest spawning density will occur.

In order to explain the variation in redd density within the mainstem of Scott Creek, we turn to another geomorphic characteristic that has been correlated with spawning sites and is predictable from LiDAR data: riffle bedforms. Observed riffle density, as mapped in the field, explains 64% of the variation in redd density in the mainstem ($p = 0.02$, Figure 2.9b). This regression suggests that the prediction, or direct identification, of riffles from remotely sensed data such as LiDAR-derived DEMs is a valuable tool for predicting the distribution of salmon spawning in a drainage network. Because the LiDAR data for Scott Creek are near-infrared and, thus, record the water surface rather than channel bathymetry, direct identification of riffles in the DEM was not possible. The increasing availability of airborne green wavelength LiDAR, which yields a bathymetric DEM,

may allow for the direct identification of riffles remotely (*Hilldale and Raff*, 2008; *McKean et al.*, 2008).

Despite the fact that we do not see variations in bed topography directly, we show that it is possible to make an estimate of riffle density from channel width, as measured from a traditional 1-m airborne LiDAR dataset. In Scott Creek, riffle density varies systematically with channel width (Figure 2.9a). Despite the presence of large in-channel wood throughout the drainage (Supporting Information Figure 4), this finding is analogous to data from emergent pool-riffle morphology, in which pool-riffle couplets are rhythmically spaced at 5-7 channel width intervals (e.g. *Leopold et al.*, 1964; *Hanrahan*, 2007). However, in contrast to this commonly observed bedform spacing, we observe a much tighter average riffle spacing of 2.2 channel widths, which agrees with the findings of *Carling and Orr* (2000) and *Wyrick and Pasternack* (2014), as well as the finding that large wood decreases pool-spacing (*Montgomery et al.*, 1995). The positive correlation between narrower channels and greater spawning density agrees well with the findings from coastal British Columbia of (*Rosenfeld et al.*, 2000), who observed significantly higher abundance of juvenile coho salmon and cutthroat trout in narrow channels compared to wide channels. We propose an increase in riffle density with decreasing channel width as a possible mechanism driving high spawning rates in narrower channels.

There is uncertainty associated with predicting riffle spacing in channels of slope 1.5-3%, which are likely to be either plane bed or forced pool-riffle morphology depending on the abundance of large wood (*Buffington et al.*, 2004). As a result, channel width and slope alone do not give us enough information to estimate riffle spacing in these reaches (marked with dashed lines, Figure 2.8c). Plane bed reaches, with less bed topography (and therefore less hyporheic flow) than

pool-riffle reaches, are less suitable for spawning than forced pool-riffle reaches (*Montgomery et al.*, 1999b), making this distinction important in drainage systems with substantial channel length in this slope range (*Buffington et al.*, 2004). For example, an abundance of LW, which presumably forces pool-riffle morphology, could change a reach of high predicted F_m but slope 1.5-3% from less-suitable (low riffle density) to highly suitable (high riffle density). Our study area included three reaches with channel slopes 1.5-3%. During our field survey, we observed few riffles in these reaches, despite the presence of LW. Notably, in addition to being less suitable for spawning in terms of riffle density, these reaches had lower movable fraction than the low-slope emergent pool-riffle reaches. Thus, in the case of our study area, reaches with slopes of 1.5-3% are inferior to the high-F_m emergent pool-riffle reaches in terms of spawning habitat even before consideration of channel reach morphology (and, as a corollary, riffle spacing). When predicting riffle spacing, field validation of channel reach morphology classification is especially important in reaches of slope 1.5-3%. While spawning habitat suitability is an important driver of redd distribution within a drainage, it cannot explain the totality of the observed variation. Coho and steelhead populations vary widely from year to year, and extreme low flows during drought years make some reaches inaccessible to migrating adults. Thus, the distribution of redds within the catchment will inevitably vary between years. Additionally, the lower reach of Big Creek, immediately adjacent to a hatchery (Figure 2.1) where steelhead trout and coho salmon that will eventually be released into Scott Creek are raised, deserves special note. This reach has the third lowest movable fraction and plane bed morphology, yet it has higher redd density than many of the reaches in the mainstem. This anomaly matches the observation made by previous workers in Scott Creek (*Hayes et al.*, 2004), who found that juvenile steelhead trout raised at the Big

Creek hatchery returned in disproportionately large numbers to Big Creek over other tributaries. Despite the fact that both grain size and riffle density should deter spawning relative to reaches in the mainstem, 11% of the spawning within the study area occurred in this reach. The finding is in line with observations of salmonid homing to natal reach, not just natal drainage network (*Neville et al.*, 2006; *Thurow*, 2000). This suggests that the location of the hatchery causes fish to 'home' to, and spawn in, what is otherwise marginal habitat in Scott Creek.

2.5.1 Grain size prediction methods

While all three grain size (D_{50}) prediction methods used in this analysis can have similar model success given the right inputs (Table 2.2), the stress-partitioning method for predicting D_{50} developed in this paper has the advantage of yielding accurate predictions while requiring fewer assumptions. As our results show, grain size predictions using the (*Wilkins and Snyder*, 2011)method are highly sensitive to the choice of Manning's n and $\tau_c^\star$ (Table 2.2). Altering Manning's n and $\tau_c^\star$ has the same effect as selecting a different β, but lacks the physical significance. For example, an increase in n represents an increase in channel roughness, but would result in an increase rather than decrease in predicted grain size.

In Scott Creek, the *Buffington et al.* (2004) method yielded predictions of D_{50} similar to those made with the shear stress partitioning method we present here. This is despite the fact that we did not independently calibrate the shear stress to Shields stress relationships ($\tau_c^\star = k\tau^m$) in Scott Creek. We speculate that this reflects the fact that their calibrations were made using data from streams in Southeast Alaska and on the Olympic Peninsula, WA. These regions, like Scott Creek, are heavily forested and experiencing regional uplift (*Larsen et al.*, 2003;

Pazzaglia and Brandon, 2001), both of which may contribute to similar partitioning of shear stress. Using the method for calculating β described above, their data yield $\beta = 0.28$ and 0.37, for SE Alaska and the Olympic Peninsula, respectively (*Buffington and Montgomery*, 1999a). On the other hand, the three rivers studied by Snyder et al. (2013) yield β values between 0.70 and 0.92 (Snyder, personal communication). So, while the *Buffington et al.* (2004) method worked well in Scott Creek, areas of different partitioning would still require the calibration of new τ - $\tau_c^\star$ relationships for each channel reach morphology, making it a potentially more cumbersome method to calibrate.

The similarity between β calculated for Scott Creek and that for the Olympic Peninsula and Southeast Alaska suggests that it may be reasonable to assume a value of β given knowledge of the wood loading, sediment supply, and climatic conditions in a watershed. As further evidence that stress partitioning is a regionally consistent quantity, we compare our Scott Creek value of β to measurements of bankfull depth, slope, and grain size made at 13 sites in the San Lorenzo River drainage (*Klier*, 2014), which lies adjacent to Scott Creek in the Santa Cruz Mountains. Rearranging equation (5) to solve for β, we calculate β for each site in the San Lorenzo River drainage, and find that the average value is 0.28. So, while our method for determining β in this study involves a curve-fitting exercise, we propose that, for future use, it may be possible to estimate stress partitioning in regions with similar conditions. Of note, predictions of D_{50} made using the shear stress partitioning method closely match observed D_{50} despite being based on a single value of β, which is assumed constant throughout the drainage. The success of the shear stress partitioning method predictions is encouraging and suggests that, despite the reach-to-reach variability in a river, a conceptually simple and spatially averaged approach to grain size prediction can be effective. There

is no a priori reason to assume that β remains constant throughout Scott Creek; likewise, we know of no mechanistic explanation for a power-law shear stress to Shields stress ($\tau_c^\star = k\tau^m$) relationship such as that used by (*Buffington et al.*, 2004). Because we find that β does not change with large wood loading (Supporting Information Figure 4), channel slope (Figure 2.4), or, as a corollary, drainage area, we believe a constant value of β is a reasonable choice. It is important to note that we use a channel slope-dependent critical Shields number (*Lamb et al.*, 2008). Calculating β with a constant Shields number (e.g. 0.03) would result in a decrease in β in steep channels. The fact that we do not see changes in β associated with shifts in channel reach morphology contradicts the prediction of morphology-dependent partitioning supported by (*Buffington et al.*, 2004), as well as the prediction of increased partitioning with excess sediment flux in high drainage areas as proposed by (*Sklar and Dietrich*, 2008). These findings suggest that, for small drainages such as Scott Creek, it may be reasonable to assume that partitioning of shear stress is constant (when calculated using a slope-dependent $\tau_c^\star$) throughout the gravel-bedded portions of the river. If this is the case, a single partitioning relationship (β) could be used to make grain size predictions for rivers throughout large regions of similar climatic and geologic setting.

2.5.2 Limitations of the approach

Using predictions of F_m, we are able to identify reaches where an abundance of large grains (low F_m) likely limit coho salmon and steelhead trout spawning in the Scott Creek drainage; however, there is also a lower limit to appropriate grain size for salmon spawning, where gravel transitions to sand (*Davey and Lapointe*, 2007), which is less clearly identifiable using these grain size prediction methods. This is of little consequence in Scott Creek, where only a small portion of the

creek is sand-bedded, but would be important in areas where the gravel-sand transition lies farther upstream. In the fine-grained downstream reach of Scott Creek (reach 3, Table 2.1), we observe a wide spread in observed median grain size (D_{50}), but our model predicts little variation (Figure 2.5). For the finest observed sizes, the model consistently overpredicts D_{50}. In fact, this pattern is apparent in all three prediction methods (see *Snyder et al.*, 2013), a result of the wide variation of grain size and low variation in channel slope. *Snyder et al.* (2013) attribute this pattern to the gravel-sand transition. We suggest that it could also be a function of the heterogeneity of grain size clustering in pool-riffle reaches, in which grains are sorted into finer and coarser patches within a single reach (*Milne*, 1982). The result of these patches and the fact that, like *Snyder et al.* (2013), we measure grain size at a single cross section, is a wide spread in observed grain sizes within a single reach, despite the fact that slope and depth remain nearly constant. All three grain size prediction methods used here begin to fail in fine grained reaches for three likely reasons: a) the slopes of the fine-grained reaches are low, meaning our approximations of shear stress are made over a distance (200 m) smaller than the backwater length (h/S) (*Paola and Mohrig*, 1996), b) they are based on shear stress-grain size relationships for gravel bedded rivers that do not hold true for sandy beds (*Wilcock and Crowe*, 2003), and c) they cannot predict grain size patchiness (e.g. *Buffington and Montgomery*, 1999a). A geomorphic tool for identifying the gravel-sand transition from topographic variables would further aid in efforts to predict the impact of grain size on spawning distribution.

The approach to habitat prediction we take here operates at a reach-averaged spatial scale, and it should be noted that this approach does not predict the location of individual riffles or variations in grain size at the scale of individual bedforms. As discussed above, the use of bathymetric LiDAR would allow for the

identification of individual bedforms; however, grain size predictions made using the method we present here would remain a reach-averaged parameter. Rather than a function of the resolution of topographic data inputs, this limitation is inherent in using a Shields stress based approach to grain size prediction. Because Shields stress ($\tau_c^\star$) depends on the depth-slope product, an approximation only appropriate at the reach-average scale (*Paola and Mohrig*, 1996), these prediction methods, by nature, cannot account for patchiness of grain size. Many studies focusing on within-reach redd sites selection have emphasized the importance of hydraulic factors such as velocity and depth in redd-site prediction, suggesting that grain size and riffle location alone may be insufficient to predict spawning site selection at the within-reach scale (*May et al.*, 2009; *Moir and Pasternack*, 2010). Additionally, because patches of suitable habitat can occur in reaches of plane bed or step-pool morphology (e.g. *Montgomery et al.*, 1999a), which lack riffles, or in cobble- and boulder-bedded streams (*Kondolf and Cada*, 1991), reach-averaged F_m and riffle spacing are inadequate to predict all suitable spawning habitats. For these reasons, the grain size and morphology based method we present here has the potential to be a useful tool for management and restoration decisions that will impact a river at the reach, rather than microhabitat, scale.

2.6 Conclusions

Here, we present and test a method for identifying reaches of suitable and less-suitable coho and steelhead spawning habitat within a catchment. This method relies on a simplified conceptualization of spawning habitat requirements, focusing purely on grain size (via moveable fraction, F_m) and riffle bedform spacing, two reach-scale physical habitat characteristics that we show can be predicted from LiDAR data and minimal field calibration. Both riffle density and F_m are

necessary to predict the distribution of spawning habitat within a drainage. Comparing movable fraction to observed spawning data, we see that little spawning occurs in coarse grained reaches; however, we observe a wide range of redd densities within reaches of uniformly high movable fraction. Thus, movable fraction or, as a corollary, grain size, is insufficient to explain the trends in spawning throughout the finer-grained mainstem of the creek. In order to explain residuals in spawning density within the finer grained reaches, we turn to riffle spacing, a stream characteristic that we show can be predicted via channel width from high-resolution DEMs. We find that variation in spawning within the fine-grained reaches is explained well by the density of riffles. Alone, riffle density would be insufficient to explain the distribution of spawning habitat, especially in coarse-grained drainages. Together, F_m and riffle density form complementary pictures of spawning potential throughout the drainage. Setting aside the effects of the hatchery, F_m tells us where salmon are likely or less likely to spawn. Within those areas of highly suitable grain size, a prediction of riffle density tells us where salmon have the greatest density of potential spawning sites.

These methods can be applied to other drainage networks where high resolution topographic data are available. In order to apply our D_{50} prediction method to other drainages, partitioning (β), and a depth-to-drainage area scaling relationship are the only relationships that must be calibrated with field data. To predict movable fraction (F_m), the ratio of D_{84} to D_{50} is also needed, though this ratio can be obtained from the grain size data used to calibrate β.

The method we present here provides a tool for rapid assessment of basin-wide spawning habitat suitability at the reach-scale. It would be well paired with additional tools such as the Intrinsic Potential habitat classification (*Burnett et al.*, 2007), which is aimed at identifying reaches of suitable juvenile coho and steel-

head overwintering habitat at the basin scale. Together, these two methods give watershed managers quantitative tools for prioritizing habitat protection efforts or prioritizing the removal of barriers to anadromy. These basin scale tools for characterizing habitat suitability provide a framework for making the best use of available funds, focusing habitat protection efforts on regions that have the greatest inherent habitat potential (*Burnett et al.*, 2007).

Chapter 3

Beyond the threshold for motion: river channel geometry and grain size reflect sediment supply

3.1 Abstract

In many gravel-bedded rivers, floods that fill the channel banks create just enough shear stress to move the median-sized gravel particles on the bed surface (D_{50}). Because this observation is common and is supported by theory, the coincidence of bankfull flow and the incipient motion of D_{50} has become a commonly employed assumption. However, not all natural gravel channels actually conform to this simple relationship; some channels maintain bankfull stresses far in excess of the critical stress required to initiate sediment transport. We use a database of >300 gravel-bedded rivers and >600 ^{10}Be-derived erosion rates from across North America to explore the hypothesis that sediment supply drives the magnitude of bankfull shear stress relative to the critical stress required to mobilize the median

bed surface grain size ($\tau^{\star}_{bf}/\tau^{\star}_{c}$). We find that $\tau^{\star}_{bf}/\tau^{\star}_{c}$ is significantly higher in West Coast river reaches (2.35, n=96) than in river reaches elsewhere on the continent (1.03, n=245). This pattern parallels patterns in erosion rates (and hence sediment supplies). Supporting our hypothesis, we find a significant correlation between upstream erosion rate and local $\tau^{\star}_{bf}/\tau^{\star}_{c}$ at sites where this comparison is possible. Our analysis reveals a decrease in bed surface armoring with increasing $\tau^{\star}_{bf}/\tau^{\star}_{c}$, suggesting channels accommodate changes in sediment supply through adjustments in bed surface grain size, as also shown through numerical modeling. Our findings demonstrate that sediment supply is encoded in the bankfull hydraulic geometry of gravel bedded channels through its control on bed surface grain size.

3.2 Introduction

What determines the shape of alluvial rivers? These self-formed channels emerge through the interaction of flowing water and transported sediment. Explaining widely observed trends in river channel hydraulic geometry remains an ongoing challenge in the field of geomorphology. Gravel-bedded alluvial rivers (whose bed and banks are comprised of sediment transported by the river) approach equilibrium geometry through feedbacks between deposition, erosion and bed surface armoring as well as through channel slope change (*Dietrich et al.*, 1989; *Parker*, 1990b; *Mueller and Pitlick*, 2013). These responses in channel geometry and surface grain size accommodate perturbations in the water and sediment supply regimes. Thus, sediment supply is among the key controls on the morphology of all river channels, and understanding linkages between sediment supply and channel morphology is a central question in much of fluvial geomorphology, civil engineering and river restoration.

Decades of observations in gravel-bedded alluvial channels support the pervasiveness of threshold channels (*Andrews*, 1984; *Mueller et al.*, 2005; *Parker et al.*, 2007) in which the channel dimensions adjust such that the threshold for motion of the median bed surface grain size (D_{50}) occurs at, or just below, bankfull flow. These observations are reinforced by theoretical work (*Parker*, 1978) showing that at bankfull flow, a straight channel with non-cohesive banks will maintain a stable channel width with a shear stress in the center of the channel that just exceeds that required to move the median sized grains on the bed surface.

The seeming ubiquity of threshold channels provides a convenient constraint on gravel-bedded river morphology, suggesting that the near equivalence of the stress required for sediment motion (critical Shields Stress, $\tau_c^\star$) and the mean bankfull bed stress ($\tau_{bf}^\star$) may be a criterion to which all gravel rivers must conform (*Phillips and Jerolmack*, 2016). The critical Shields stress ($\tau_c^\star$) describes the amount of stress needed to initiate median grain motion, normalized for the grain size, and is generally between 0.03 and 0.08 (*Buffington and Montgomery*, 1997). The bankfull Shields stress ($\tau_{bf}^\star$) describes the stress acting on the bed during bankfull flow, and (at the reach scale) is approximated as:

$$\tau_{bf}^\star = \frac{\rho g R_{bf} S}{(\rho_s - \rho) D_{50}} \tag{3.1}$$

where ρ is the density of water (1000 kg/m3), ρ_s is the density of sediment, g is the gravitational constant, R_{bf} is the bankfull hydraulic radius, and S is the channel slope (note: all Shields stresses referred to herein apply to D_{50}).

However, the orders of magnitude global variability in basin-wide erosion rates (and hence sediment yields) (*Willenbring et al.*, 2013) points to a potential problem with widespread application of a threshold channel model. In tectonically active settings, channels, as the primary conduits of material off the landscape,

must be adjusted to move high sediment loads. The sediment transport capacity of a channel is often modeled as a function of the excess stress, or difference between the bankfull and critical stress ($\tau^{\star}_{bf}$ - $\tau^{\star}_{c}$)(*Fernandez-Luque and Van Beek*, 1976). Consequently, all else being equal, it would seem that higher bankfull stresses are needed to transport large volumes of material in tectonically active settings. The requirement to transport a high sediment supply ($\tau^{\star}_{bf} > \tau^{\star}_{c}$) is seemingly at odds with the threshold channel assumption ($\tau^{\star}_{bf} = \tau^{\star}_{c}$).

Previous work has hinted at a relationship between sediment supply and $\tau^{\star}_{bf}$/ $\tau^{\star}_{c}$. The difference between the grain size predicted by rearranging eqn (1) and observed grain size can theoretically be used to predict sediment supply (*Buffington and Montgomery*, 1999b), although this idea has yet to be validated with field data. Further, $\tau^{\star}_{bf}/\tau^{\star}_{c}$ has been shown to increase with decreasing bed stability (*Bunte et al.*, 2013), which is likely correlated with sediment supply. On the other hand, further confirmation of the ubiquity of threshold channels has continued to appear in the literature (*Phillips and Jerolmack*, 2016).

While there is not a well-accepted link between sediment supply and $\tau^{\star}_{bf}/\tau^{\star}_{c}$, it is clear that sediment supply can affect many aspects of channel morphology. Rivers with very high sediment supply are often braided (*Mueller and Pitlick*, 2013) and aggradation occurs when the sediment supply to a channel is in excess of the channel's capacity to transport that sediment (*Eaton and Church*, 2009). Additionally, the bed surface can armor through size selective transport in low supply conditions (*Dietrich et al.*, 1989; *Parker*, 1990b) or the bed surface grain size can fine in response to high sediment supply (*Madej et al.*, 2009). Despite the prevalence of these observations, we lack a coherent understanding of how these responses are expressed in $\tau^{\star}_{bf}$, which is a function of both grain size and channel geometry. Though it is clear that sediment supply impacts channel morphology,

this does not necessarily translate to an impact on $\tau^{\star}_{bf}$ $/\tau^{\star}_{c}$. One can imagine that a river channel might respond to an increase in sediment supply through a decrease in bed surface armoring (reducing surface D_{50}) while maintaining a constant, threshold $\tau^{\star}_{bf}$ $/\tau^{\star}_{c}$ value through a concurrent decrease in S or R_{bf}, via widening. It could also be the case that a river channel would respond to an increase in sediment supply through a reduction in bed surface armoring without a change in channel geometry, yielding an increased $\tau^{\star}_{bf}$ $/\tau^{\star}_{c}$. Here, we address the question: do all gravel-bedded rivers, regardless of sediment supply, tend towards an equilibrium that maintains threshold conditions, or can $\tau^{\star}_{bf}/\tau^{\star}_{c}$ vary with sediment supply?

To the extent that we understand and restore rivers according to their sediment supply regime, a clearer understanding of the relationship between sediment supply, bed surface grain size, and the hydraulic geometry of river channels is needed. A unifying model should explain both the widespread observation of threshold channels and the need for channels in tectonically active areas to transport large coarse sediment loads. Here we adopt and test the hypothesis that the balance between bankfull shear stress and bed surface grain size reflects not only the need to initiate sediment motion, as is commonly argued, but also the requirement that channels convey the load supplied from upstream (*Buffington and Montgomery*, 1999b).

To explore the controls on bed surface grain size and bankfull hydraulic geometry, and their relationship to sediment supply, we compiled a dataset of D_{50} and hydraulic geometry for 341 reaches of gravel-bedded rivers in North America (Figure 3.1a). Using these data, we explore patterns in $\tau^{\star}_{bf}$ across the continent. Channel geometry and grain size reflect basin lithology, large wood loading, landslide history, land use history, hydrology, and relative roughness, among other

factors; rather than attempting to control for all of these factors in a small subset of drainages, we take a continent-wide approach to addressing this problem. By gathering a large dataset across a wide variety of lithologies, climates, and land use histories we gain sufficient statistical power to see past the 'noise' that is inherent to such a compilation.

We compare patterns in $\tau^{\star}_{bf}/\tau^{\star}_{c}$ to sediment supply, which we infer from an independent compilation of ^{10}Be-derived erosion rates from across North America (*Balco et al.*, 2013; *Willenbring et al.*, 2013) (Figure 3.1d) (Methods). ^{10}Be erosion rates, which measure long term (10^3 year) averages, are very often (*Matmon et al.*, 2003; *Ganti et al.*, 2016) but not always (*Kirchner*, 2001; *Reusser et al.*, 2015) in close agreement with short term erosion rates. Also, the ratio of coarse sediment (which impacts gravel bed morphology) to fine sediment (which has no known bed-forming role in gravel-bed rivers), depends on lithology (*O'Connor et al.*, 2014) and can vary widely between drainages and flood stages (*Turowski et al.*, 2010). With the understanding of these caveats, we proceed assuming that ^{10}Be erosion rates are a proxy for coarse (bedload) sediment supplied to a channel, and further address these assumptions below.

3.3 Sediment supply as a driver of high $\tau^{\star}_{bf}/\tau^{\star}_{c}$

Calculating values of $\tau^{\star}_{c}$ based on channel slope (*Lamb et al.*, 2008) (Methods), we find that the ratio of bankfull to critical Shields stress ($\tau^{\star}_{bf}/\tau^{\star}_{c}$) is significantly higher in West Coast rivers (median $\tau^{\star}_{bf}/\tau^{\star}_{c} = 2.35$) than in other rivers ($\tau^{\star}_{bf}/\tau^{\star}_{c} = 1.03$, Welch's t-test for unequal variance, $p = 3\text{x}10^{-12}$) (Figure 3.1b). This difference exists despite the wide spread in observed $\tau^{\star}_{bf}/\tau^{\star}_{c}$ within both categories. The near-equivalence of critical and bankfull Shields stress across most of the continent is in keeping with previous research (*Parker*, 1978; *Mueller et al.*, 2005)

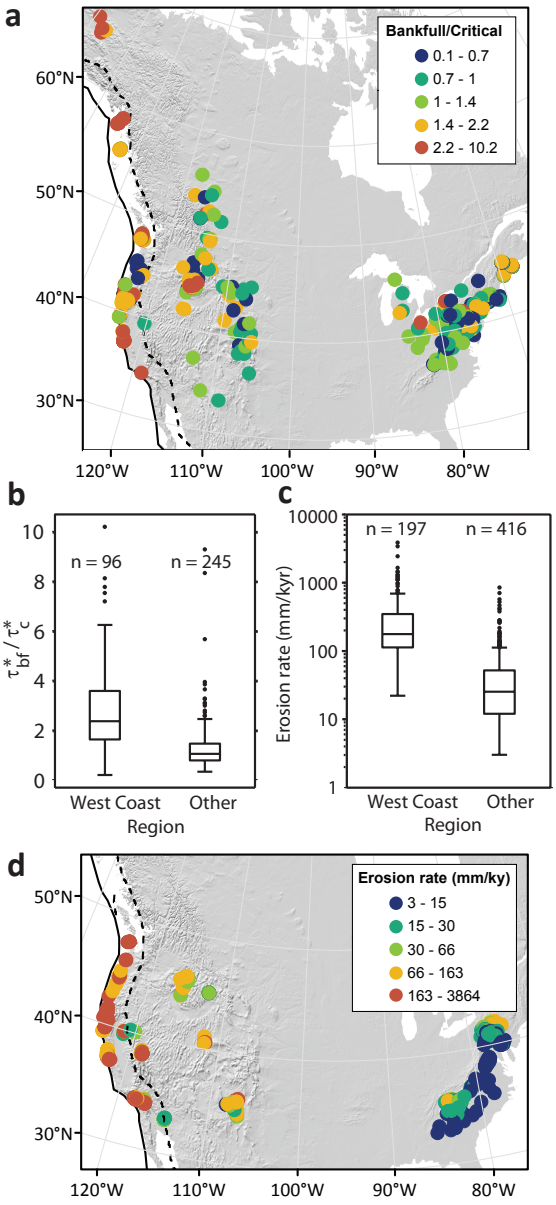

Figure 3.1: Ratio of $\tau^\star_{bf}/\tau^\star_c$ and 10Be erosion rate data across North America. a, Location of all hydraulic geometry sites in our data compilation. Boxplots showing b, the distribution of $\tau^\star_{bf}/\tau^\star_c$ separated by region, and c, the distribution of 10Be-derived erosion rates separated by region. d, Location of 10Be erosion rate sites in our data compilation. Solid line corresponds to the Pacific-North American Plate boundary used in this analysis (see Methods). Dashed line marks the boundary between 'West Coast' and 'Other' sites. Data are separated into color bins by quintile.

and supports the threshold channel model. In contrast, the systematically high bankfull Shields stress in West Coast rivers has, to our knowledge, never been documented. Using depth, h, in place of R_{bf} in equation 3.1, a common simplification (*Buffington and Montgomery*, 1999a; *Parker et al.*, 2007), results in only modest differences in $\tau^{\star}_{bf}/\tau^{\star}_{c}$ (median 'Other' = 1.12, 'West Coast' = 2.81).

In order to test whether high sediment supply drives this pattern in hydraulic geometry, we estimate sediment transport capacity (Methods), which we compare to ^{10}Be-derived catchment-averaged erosion rates from across North America (*Balco et al.*, 2013; *Willenbring et al.*, 2013). As with $\tau^{\star}_{bf}/\tau^{\star}_{c}$, ^{10}Be erosion rates are very statistically significantly higher ($p = 1.6x10^{-14}$) on the West Coast (median E = 177 mm/ky) when compared to the rest of the continent (E = 25 mm/ky, Figure 3.1c). Normalizing both ^{10}Be-derived basin-wide erosion rate and sediment transport capacity (Methods) by their means, we find that sediment transport capacity and erosion rate decrease by about an order of magnitude moving east from the plate boundary (Supplementary Figure B.1). These data suggest that more coarse sediment is being transported in regions with high sediment supply. This supports our assertion that coarse sediment fluxes scale with ^{10}Be-derived catchment-averaged erosion rates.

Isolating the sites for which we have both ^{10}Be and channel geometry data, we see that there is a statistically significant trend of increasing $\tau^{\star}_{bf}/\tau^{\star}_{c}$ with increasing erosion rate (Figure 3.2). This pattern persists in both long term (^{10}Be) and short term erosion rates. This consistency lends support to our assertion that ^{10}Be erosion rates are a valid proxy for coarse sediment supply at timescales relevant to channel adjustment. The assertion is further supported by recent work (*Ganti et al.*, 2016) showing that basins dominated by fluvial incision do not exhibit a time scale bias in erosion rates. The magnitude of variation in background erosion

rates across the continent is substantially greater than the differences in sediment supply generally attributed to land use effects (*Reusser et al.*, 2015). Below, we discuss some of the factors that likely drive the scatter in Figure 3.2. Because we do not know the error associated with the $\tau^{\star}_{bf}/\tau^{\star}_{c}$ data, we cannot determine the slope of the true functional relationship between erosion rate and $\tau^{\star}_{bf}/\tau^{\star}_{c}$ (*Mark and Church*, 1977). Regressions (Figure 3.2) represent a lower bound; $\tau^{\star}_{bf}/\tau^{\star}_{c}$ is likely more sensitive to erosion rate than suggested in Figure 3.2 (*Mark and Church*, 1977).

We note that the least-squares fit to our paired sites data nearly crosses the intersection of the median erosion rate and $\tau^{\star}_{bf}/\tau^{\star}_{c}$ for both the 'West Coast' and 'Other' populations. This suggests that the paired sites are representative of the larger data compilation. Thus, both continent-wide trends and paired sites suggest that rivers in high erosion rate landscapes, where sediment supplies are high, have adjusted to maintain high bankfull Shields stresses rather than maintaining threshold conditions at bankfull flow.

3.4 Sediment supply accommodated through armoring

The association between erosion rate and $\tau^{\star}_{bf}/\tau^{\star}_{c}$ suggests that high sediment supply channels are some combination of deeper (greater bankfull depth), steeper (higher slope), and finer (smaller bed surface grain size) than their low sediment supply counterparts. Substantial work has been done connecting sediment supply conditions with bed surface armor ratio (D_{50}/D_{50ss}, where D_{50ss} is the median grain size of the subsurface) (*Dietrich et al.*, 1989; *Buffington and Montgomery*, 1999b; *Madej et al.*, 2009; *Mueller and Pitlick*, 2013). Although it is difficult to

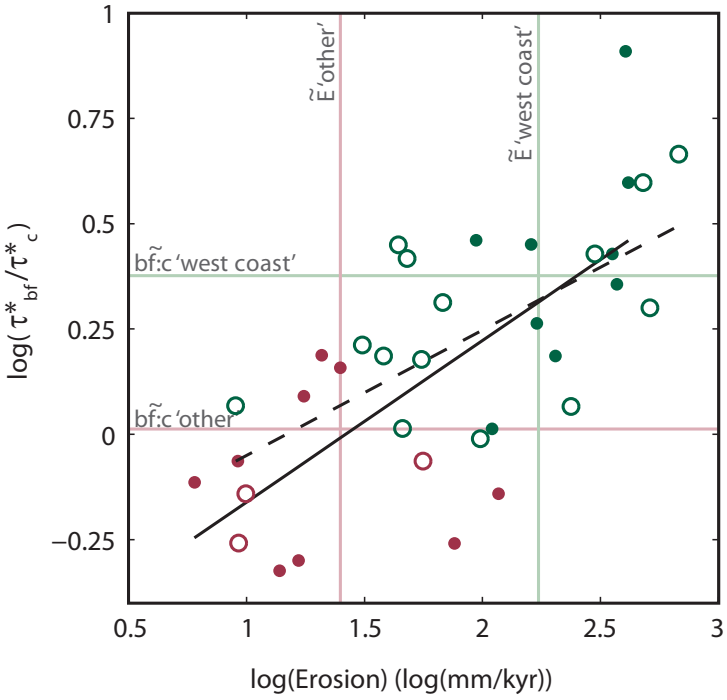

Figure 3.2: Paired erosion and $\tau^{\star}_{bf}/\tau^{\star}_{c}$ sites. The solid dots and solid line represent 10Be erosion rates, while the open circles and dashed line represent short term erosion rate measurements. 'West Coast' data in green; 'Other' in maroon. There is a statistically significant relationship between erosion rate and the ratio of bankfull to critical stress, a relationship that holds true with both long term ($p = 0.001$, $r2 = 0.50$) and short term ($p = 0.002$, $r2 = 0.47$) erosion rates. The colored lines mark the median 10Be erosion and $\tau^{\star}_{bf}/\tau^{\star}_{c}$ values, color-coded by region.

observe armoring of channels during high flow conditions, the armor ratio of the channel measured at low flow appears to provide an index of the sediment supply and transport conditions during the formative flows (*Wilcock and DeTemple*, 2005; *Hassan et al.*, 2006; *Parker et al.*, 2006). Bed surface armor forms through the selective transport of finer bed surface particles relative to coarser particles (*Parker et al.*, 1982). In high sediment supply conditions, however, armor formation is reduced, leaving the bed surface more closely matching the grain size distribution of the subsurface (*Eaton and Church*, 2009). This connection between low armor ratio and high sediment supply suggests that high $\tau^{\star}_{bf}/\tau^{\star}_{c}$ primarily results from bed surface fining.

Using subsurface grain size measurements available for a subset of our sites, we see that, indeed, armor ratio correlates with $\tau^{\star}_{bf}/\tau^{\star}_{c}$ (Figure 3.3). To more directly link armor ratio and sediment transport, we make estimates of instantaneous sediment transport capacity per unit width during bankfull flow, Q_t (m2/s)(*Recking*, 2013)(Methods). Figure 3.3 shows that the low armor ratio, high $\tau^{\star}_{bf}/\tau^{\star}_{c}$ sites correspond with high estimated Q_t. This observation suggests that bed surface grain size adjusts in channels in order to transmit the high sediment load supplied during bankfull flow.

The above approach to predicting sediment transport capacity is simplified and limited by the data available to us; it is based solely on S, R_{bf}, and D_{50}. In order to independently validate the relationship between armor ratio, $\tau^{\star}_{bf}/\tau^{\star}_{c}$, and estimated Q_t, we examine the results of an independent sediment transport model (*Parker*, 1990b) that explicitly incorporates the formation of armor and its effect on sediment transport in natural rivers (Methods). The physically based, empirically calibrated model evolves Q_t and armor ratio from an imposed bedload grain size distribution and Shields stress. Comparing the model output to our data

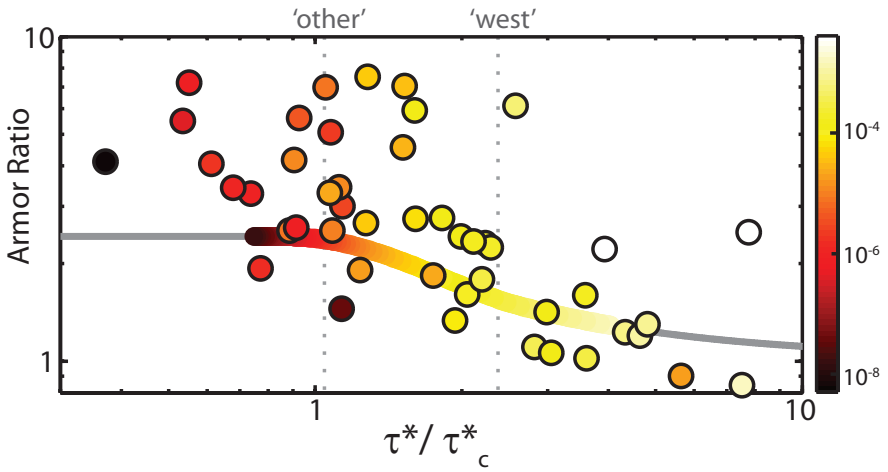

Figure 3.3: Relationship between $\tau^\star_{bf}/\tau^\star_c$, armor, and sediment transport capacity. Points, which represent sites in our data compilation for which we have subsurface grain size measurements, are colored by predicted Qt (43)(Methods). The solid line shows the relationship between armor ratio and $\tau^\star/\tau^\star_c$ predicted using the Parker (3) model. The line is colored by predicted sediment transport capacity in the range of $\tau^\star/\tau^\star_c$ for which the model was calibrated. The vertical dashed lines mark the median $\tau^\star/\tau^\star_c$ values in the 'west' and 'other' populations (Figure 3.1b).

compilation, we find good agreement with the general trends (Figure 3.3): both the independent model and the data from our compilation show decreasing armor ratio with increasing $\tau^\star/\tau_c^\star$ and Q_t. This agreement points to the mechanistic relationship between sediment transport, armor ratio, and $\tau^\star/\tau_c^\star$. At formative flows, a high sediment supply equilibrium channel must maintain high sediment transport capacity, which is a function of $\tau_{bf}^\star/\tau_c^\star$ (e.g. 12). This high transport rate depresses armor formation. We observe these relationships in our data compilation (Figure 3.3), and the mechanistic links are encoded in the model (*Parker*, 1990b). That said, we acknowledge that there are limits to the effectiveness of bed surface armor in absorbing the effects of sediment supply on $\tau_{bf}^\star/\tau_c^\star$. At some high sediment supply point, armor ratio approaches unity and bed surface aggradation begins (*Eaton and Church*, 2009).

3.5 Exploring additional explanations for high $\tau_{bf}^\star/\tau_c^\star$

While our data support the idea that sediment supply is a significant driver of $\tau_{bf}^\star/\tau_c^\star$, other factors certainly influence this ratio. First, roughness elements such as immobile boulders or large in-channel wood can cause some of the total bankfull shear stress to be 'partitioned'away from the bed (*Buffington and Montgomery*, 1999b). As a result of this form drag, the non-dimensional effective shear stress acting on the bed will be lower than the total Shields stress at bankfull flow. However, relative roughness (D_{50}/h_{bf}) does not differ significantly between West Coast and Other channels (Welch's t-test for unequal variance, p = 0.58), suggesting that form drag due to grains is not responsible for the observed patterns in $\tau_{bf}^\star/\tau_c^\star$ (Supplementary Figure B.2). In-channel wood volumes, which

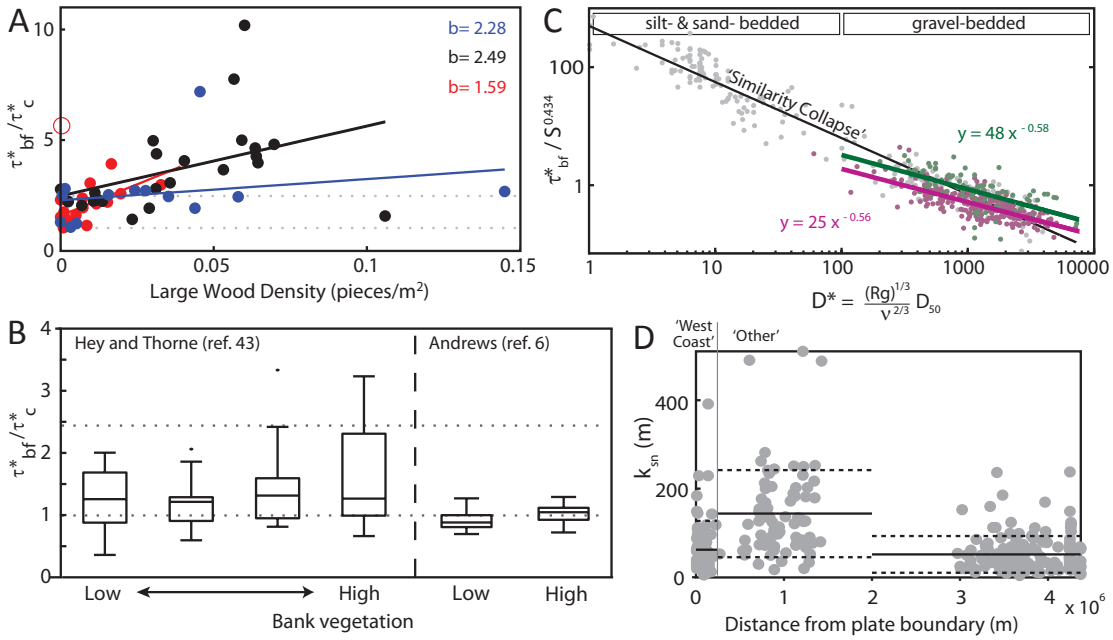

Figure 3.4: Exploring alternative explanations for high $\tau^{\star}_{bf}/\tau^{\star}_{c}$. a, $\tau^{\star}_{bf}/\tau^{\star}_{c}$ as a function of large wood density, separated by sub-region. Olympic Peninsula (Washington) sites in blue, Southeast Alaska sites in black, and Middle Fork Salmon River (Idaho) sites in red. The site marked with an open circle was excluded from the regression. Y-intercept values (b) from linear regressions are shown in colored text. b, Effects of bank cohesion on $\tau^{\star}_{bf}/\tau^{\star}_{c}$. There are no statistically significant differences between bank vegetation classes within either dataset: Hey and Thorne (1986) (ANOVA, p= 0.15) dataset nor Andrews (1984) (ANOVA, p = 0.14). In a and b, the upper and lower dashed grey lines mark the median $\tau^{\star}_{bf}/\tau^{\star}_{c}$ ratio for 'West Coast' and 'Other' sites, respectively. c, Overlay of our data compilation (in color) on the proposed (39) similarity collapse for all alluvial river data (greyscale). 'West Coast' data and regression are in green, 'Other' are marked in maroon. The solid grey line denotes the best-fit regression through all alluvial river data shown by Li et al. (39), which is shown in grey. d, Calculated normalized steepness (k_{sn}) plotted by distance from the plate boundary. Solid lines mark the means of each region; dotted lines mark one standard deviation

may contribute substantially to hydraulic roughness, vary by orders of magnitude between channels (*Buffington and Montgomery*, 1999b), land management types, and biomes (*Benda and Bigelow*, 2014). Figure 3.4a shows the effects of in-channel wood for a subset of our data. Even in West Coast channels devoid of wood, $\tau^{\star}_{bf}/\tau^{\star}_{c}$ is substantially greater than one. So, while high wood loading does have the expected effect of increasing $\tau^{\star}_{bf}/\tau^{\star}_{c}$ (Figure 3.4a), the form roughness associated with in-channel wood cannot alone explain the high $\tau^{\star}_{bf}/\tau^{\star}_{c}$ observed in West Coast channels.

Bank cohesion from vegetation has been suggested as a driver of high $\tau^{\star}_{bf}/\tau^{\star}_{c}$ (*Parker et al.*, 2007). However, reanalyzing data used by Parker and others (*Parker et al.*, 2007) we find no statistically significant difference in $\tau^{\star}_{bf}/\tau^{\star}_{c}$ between bank vegetation classes (Figure 3.4b). Although bank cohesion may not drive high values of $\tau^{\star}_{bf}/\tau^{\star}_{c}$, cohesion is nevertheless fundamentally important to maintaining stable banks under high $\tau^{\star}_{bf}/\tau^{\star}_{c}$ conditions. In the absence of cohesion, the alluvial material making up channel banks should become unstable when $\tau^{\star}_{bf} > 1.2\tau^{\star}_{c}$ (*Parker*, 1978), leading to channel widening which would, in turn, reduce flow depth and bed shear stress. However, fine sediment and vegetation provide cohesion on the banks of many natural channels. In small and mid-sized channels, where the magnitude of shear stress acting on the banks is moderate, vegetation can act to stabilize otherwise mobile banks (*Eaton and Giles*, 2008). The prevalence of meandering gravel-bedded rivers provides further evidence that cohesive banks are common, as stable meander formation requires bank cohesion (*Braudrick et al.*, 2009). In the presence of stable banks, physical experiments suggest that changes in bed surface texture can accommodate a fourfold change in sediment supply before aggradation begins (*Eaton and Church*, 2009). Thus, bank cohesion, while likely not responsible for driving increases in $\tau^{\star}_{bf}/\tau^{\star}_{c}$, is likely

required to stabilize the banks of above-threshold channels.

It could be argued that West Coast channels, even the alluvial-bedded ones included in this study, may have more exposed bedrock and therefore should not conform to threshold channel assumptions. Yet, in low-sediment supply settings, bedrock channels, like their alluvial counterparts, conform to $\tau^{\star}_{bf} = \tau^{\star}_{c}$ (*Phillips and Jerolmack*, 2016). Even in tectonically active channels that incise bedrock, the combined stress needed to move and transport sediment is typically much greater than the stress needed to incise rock (*Sklar and Dietrich*, 2008). This is especially true where bedrock has low tensile strength, as in the case of the young sedimentary rocks that cover much of the West Coast. For example, modeling suggests that 50% of the total bankfull shear stress along the South Fork Eel River in Northern California, USA, is associated with the need to transport sediment and 40% is related to initiating sediment motion (*Sklar and Dietrich*, 2008). Hence, the distinction between channels that incise rock and those that simply convey sediment (i.e., alluvial channels) is neither clear, nor necessarily useful in many settings.

Patterns in basin-averaged erosion rates are not reflected in continent-wide trends in normalized channel steepness (k_{sn}, Methods, Figure 3.4d). According to the stream power model for river incision (*Whipple*, 2004), we might expect channels actively incising uplifting rock to have high k_{sn} to match the high erosion rates (e.g. *DiBiase et al.*, 2010). We do not observe this at the continent scale (Figure 3.1d and Figure 3.4d). So, while k_{sn} may be strongly correlated with erosion rates within a region of similar climate and rock type (e.g. *DiBiase et al.*, 2010) our results suggest that the relationship between grain size and channel geometry ($\tau^{\star}_{bf}/\tau^{\star}_{c}$ or Q_t), rather than channel geometry and drainage area (k_{sn}), may be a more universal indicator of active tectonics, at least to the extent that

it is correlated with coarse sediment supply.

We noted earlier that lithology affects the relationship between basin-wide erosion rates and coarse sediment supply. Rocks of low tensile strength will rapidly abrade during transport, yielding less bedload for a given sediment supply than their high tensile strength counterparts, thereby decreasing the coarse sediment supply felt by the bed of a gravel-bedded river. The $\tau^{\star}_{bf}/\tau^{\star}_{c}$ data from the Oregon Coast Range nicely demonstrate this effect. Oregon Coast Range sedimentary rocks rapidly disintegrate during transport into grain sizes that are transported as suspended load rather than bedload (*O'Connor et al.*, 2014). So, while the erosion rates across the Oregon Coast Range are uniformly high (100-200 mm/kyr (*Balco et al.*, 2013)), the channels sourcing Coast Range sedimentary rocks have remarkably little coarse sediment supply (*O'Connor et al.*, 2014). This manifests in $\tau^{\star}_{bf}/\tau^{\star}_{c}$ values below 1 (e.g. 0.37, 0.18). For lithology to explain the continent-wide trends in $\tau^{\star}_{bf}/\tau^{\star}_{c}$, West Coast basins would need to have substantially stronger bedrock. As a first-order test of the effect of lithology on our results, we determined the percent of basin area underlain by sedimentary rocks for sites in our compilation (SI Appendix 1, Supplementary Figure B.3). On average, there was little difference between 'West Coast' and 'Other' basins, which were underlain by 72% (standard deviation 42%) and 72% (standard deviation 39%) sedimentary bedrock, respectively. This would suggest that our data compilation does not over-sample hard rocks on the West Coast, and lithology does not explain the continent-wide trends we observe. However, the effects of lithology are almost certainly important when comparing between individual basins (*Mueller et al.*, 2016) and likely drive scatter in Figure 3.2.

The dependence of $\tau^{\star}_{bf}$ on both slope (*Lamb et al.*, 2008; *Bunte et al.*, 2013) and grain size can be used to produce a similarity collapse of all alluvial river

data, including both bedload- and suspension-dominated systems (*Li et al.*, 2014). However, some scatter persists. Plotting our data compilation along the same axes used in the similarity collapse (*Li et al.*, 2016) (which are very nearly equivalent to plotting D_{50} on the horizontal axis and $\tau^{\star}_{bf}/\tau^{\star}_{c}$ on the vertical), we see parallel trends in 'West Coast' and 'Other' channels, with West Coast channels having substantially higher $\tau^{\star}_{bf}$ (Figure 3.4c). To the extent that sediment supply drives the difference in trends between the two populations, this suggests that sediment supply is a major hidden variable driving the remaining scatter in the similarity collapse unifying all alluvial river morphology.

Many studies have called attention to the complexity of the incipient motion of grains in gravel bedded rivers (*Lamb et al.*, 2008; *Bunte et al.*, 2013). These studies imply that critical Shields stress should be viewed not as a constant but rather as a representative value used to generalize the stochastic process of grains being swept out of pockets by turbulent sweeps (*Kirchner et al.*, 1990). Recent studies have shown that $\tau^{\star}_{c}$ varies with channel slope (*Mueller et al.*, 2005; *Lamb et al.*, 2008), grain packing geometry, and particle shape, among many other factors; thus, choices of $\tau^{\star}_{c}$ should be made with these factors in mind (*Bunte et al.*, 2013). Similarly, we have shown here that bankfull channel geometry does not simply reflect the conditions required to initiate motion of D_{50}. Roughness, large wood loading, and bedrock exposure can affect $\tau^{\star}_{bf}/\tau^{\star}_{c}$, though our data suggest that these factors likely play a small role relative to sediment supply in driving the difference in $\tau^{\star}_{bf}/\tau^{\star}_{c}$ between 'West Coast' and 'Other' channels. Rather, these, along with flow intermittency (*Hassan et al.*, 2006) and local variability in characteristics such as bed material attrition (*O'Connor et al.*, 2014) and uplift rate likely help drive the scatter in $\tau^{\star}_{bf}/\tau^{\star}_{c}$ that we observe within 'West Coast' and 'Other' channels as well as the scatter about the trend in Figure2parker. We suggest that,

as with $\tau_c^\star$, assumptions of constant $\tau_{bf}^\star/\tau_c^\star$ must be made with caution.

3.6 Conclusions

In summary, our findings provide evidence that river channel hydraulic geometry and grain size are fundamentally linked to sediment supply. 'Threshold' channels may therefore simply reflect settings with low sediment supplies. Because sediment transport rates are a highly non-linear function of stress near the threshold for motion (*Parker*, 1990b), small changes in stress result in large changes in transport capacity. Therefore, on the low end of the sediment supply spectrum, a relatively large range of sediment supply conditions may be accommodated with small changes in $\tau_{bf}^\star/\tau_c^\star$, giving the appearance that channel geometry is set by the critical stress. This explains the observation that channels are, on average, adjusted to 'threshold' conditions across much of the continent (*Phillips and Jerolmack*, 2016). While the average channel may conform to the 'threshold' model, physically meaningful factors drive the scatter in $\tau_{bf}^\star/\tau_c^\star$. Our findings suggest that bankfull stresses can be, and are, maintained well above critical where sediment supplies are sufficiently high to require it. Bankfull Shields stress, bed surface armoring, and sediment supply are fundamentally linked in gravel bedded rivers. Thus, an understanding of sediment supply is key to interpreting, predicting, or restoring bankfull hydraulic geometry in rivers.

3.7 Materials and Methods

3.7.1 Channel geometry and grain size data compilation

In order to determine spatial patterns in bankfull Shields stress across North America, we compiled channel geometry and bed surface grain size data from 341 gravel-bedded river reaches with known locations. We selected reaches with negligible regulation of flow and negligible sediment traps. Additionally, we chose reaches with primarily alluvial beds, and not immediately confined on both sides by bedrock banks. Our data are limited to gravel-bedded rivers, thus excluding the flatlands of the Great Plains where sand-bedded rivers predominate.

We calculated $\tau^{\star}_{bf}$ (eqn. 1) for each reach, substituting bankfull flow depth for hydraulic radius where bankfull width data were unavailable (n = 7). Because $\tau^{\star}_{c}$ varies systematically with channel slope (*Mueller et al.*, 2005; *Lamb et al.*, 2008), it would be misleading to compare $\tau^{\star}_{bf}$ between reaches of different slope. Therefore, we normalize $\tau^{\star}_{bf}$ by an estimated slope-dependent $\tau^{\star}_{c}$ (*Lamb et al.*, 2008):

$$\tau^{\star}_{c} = 0.15S^{0.25} \tag{3.2}$$

For each site, we calculated the distance to the Pacific Plate boundary. Because portions of coastal California are west of the San Andreas Fault, and therefore could be considered a part of the Pacific Plate, we defined the plate boundary as the bathymetrically defined trench or the coast, whichever is farther west, thereby avoiding negative distance values. To compare 'West Coast' sites from those elsewhere in North America, we use a threshold distance of 250 km from the Pacific Plate boundary.

3.7.2 Sediment transport capacity and normalized steepness

We use channel geometry and D_{50} to estimate bankfull sediment transport capacity per unit channel width, Q_t (m^2/s), for sites in the data compilation using the *Recking* (2013) surface-based transport relation. The model, detailed in SI Appendix 2, has been validated using independent field data from a variety of alluvial rivers. We note that sediment transport predictions, especially those based on just D_{50}, can substantially over- or under-predict sediment transport rates (*Gomez and Church*, 1989). However, our analysis relies on the observed trends in Q_t, not the precise values.

Sediment supply should equal sediment transport capacity in alluvial channels that are neither aggrading nor degrading. Thus, our prediction of sediment transport capacity can be viewed as a prediction of sediment supply.

In comparing Q_t to erosion rates, we rely on the assumption that the recurrence interval of bankfull flows is similar across most fluvial regimes (*Leopold et al.*, 1964). While this is a simplification, we note that our dataset covers significant climate gradients across both latitude and longitude, complicating a snowpack or rainfall intermittency explanation for observed patterns. Notably, a wide variety of hydrological environments are represented within the 'West Coast' sites, from snowmelt-dominated streams to highly seasonal streams in Mediterranean climates.

For each of the sites we calculate normalized steepness index (k_{sn} (m)) assuming a reference concavity, θ, of 0.5 (*Whipple*, 2004):

$$k_{sn} = SA^{\theta} \tag{3.3}$$

3.7.3 Parker 1990 Model

The *Parker* (1990b) sediment transport model provides an independent prediction of the relationship between bed surface armoring, $\tau^\star/\tau_c^\star$, and sediment supply. We use the model to evolve Q_t and armor ratio from a given substrate grain size distribution and boundary shear stress (as in ref. 9, Figure 3.3). For a detailed description, see SI Appendix 3.

We the employ the *Parker* (1990b) model because it numerically describes the importance of bed surface armor in moderating the transport of different grain size fractions, and provides us with an independent prediction of the relationships we observe in our larger data compilation. The Parker model was originally written assuming that bed surface armor changes continuously throughout the flood hydrograph. In the intervening years, however, work has shown that armor very likely persists, invariant of flood stage (*Wilcock and DeTemple*, 2005; *Parker et al.*, 2006). In Figure 3.3 we compare to the modeled equilibrium armor ratios and transport capacities for a single channel at a variety of flood stages ($\tau^\star/\tau_c^\star$) to the bankfull conditions ($\tau_{bf}^\star/\tau_c^\star$) and armor ratio (measured at low flow conditions) of the natural rivers in our data compilation. Given the evolution in understanding since the original publication, we believe it is fair to compare the model results (equilibrium transport and armor at various flood stages) to our compilation of bankfull shear stresses and low flow observed armor.

Chapter 4

The timing and intensity of river bed mobility varies by region, controlled by hydrologic regime and sediment supply

4.1 Abstract

Because sediment supply varies by orders of magnitude across North America, and rivers adjust to convey their imposed loads, the intensity of river bed surface mobility varies enormously. Climate also varies widely across the continent, yielding a range of flood timing, duration, and intermittency. Together, the differences in sediment supply and hydro-climate result in diverse regimes of bed surface stability. The frequency and intensity of bed mobility, although difficult to predict, are of paramount importance to the inhabitants of river ecosystems as well to the evolution of bed surface structure. To quantitatively characterize

regional variation in bed mobility regimes, we calculate multi-decadal time series of estimated bed surface mobility using sediment transport equations. The method requires measurements of the bed surface grainsize distribution, channel slope, and longterm stream discharge records. We use the time series to compare bed mobility between rivers and regions. In many snowmelt-dominated rivers of the Rocky Mountains, a period of partial bed mobility (dimensionless transport parameter, $W^\star > 0.002$) generally occurs during the annual melt, and can last for days. In rivers draining the central Appalachians, partial bed mobility is comparatively rare and occurs during short-duration floods. Rivers on the tectonically active West Coast tend to experience partial bed mobility during most winter storms, with brief (hours long) periods of full bed mobility ($W^\star > 0.1555$) during storm peaks. There are statistically significant regional differences in (a) the exceedance probability of bed mobilizing flows ($W^\star > 0.002$), (b) the maximum bed mobility, and (c) the number of discrete bed mobilizing events in a year. These regional patterns can be explained by differences in sediment supply and hydrologic regime, and lead to diverse disturbance regimes for river ecosystems and varying potential for the importance of bed surface memory effects.

4.2 Introduction

Gravel river bed mobility defines the architecture for the benthic inhabitants of river ecosystems. A reductionist view of gravel riverbed mobility based on the threshold channel concept would suggest that, on average, the riverbed just exceeds the threshold for motion during bankfull floods (*Phillips and Jerolmack*, 2016). Because bankfull floods tend to occur an average of once every one to two years (*Leopold et al.*, 1964), we might infer that gravel beds mobilize with the same recurrence interval. However, natural rivers experience a wide diversity in

both hydroclimatic regimes (*Hirschboeck*, 1991) and sediment supply conditions (*Pfeiffer et al.*, 2017). This variability hints at a more complex array of bed mobility timing and intensity among gravel bedded rivers. River bed mobility is a function of channel geometry, flow regime, and the grain size distribution of the bed surface, which is shaped in part by sediment supply (*Dietrich et al.*, 1989). Rivers with high sediment supply tend to have finer bed surface grain size (*Pfeiffer et al.*, 2017), which increases mobility for a given discharge (*Lisle et al.*, 2000). As an extreme example, the rivers draining Mt. Pinatubo responded to the dramtic increase in sediment supply after the 1991 volcanic eruption through fining of the bed surface grain size and reduction in surface roughness, enabling remarkable rates of sediment transport even at low flow (*Montgomery et al.*, 1999b). *Lisle et al.* (2000) explored variability in bed mobility between 6 rivers of different sediment supply. They used grain size mapping and 2-D flow models to characterize the heterogeneity of bed mobility within each reach. They found that a larger portion of the bed was mobile during bankfull flow in sediment rich channels compared to low-supply channels. Importantly, trends in bed mobility calculated using reach-averaged variables generally matched the trends in bed mobility determined using the more spatially precise grain patch maps and flow modeling. However, they did not consider the effects of flow intermittency, simply comparing bed mobility at bankfull flow.

The threshold for sediment motion is defined as the transition from an immobile bed, in which grains are not moving, to a partially mobile bed, in which a small number of grains are mobile. In practice, the threshold for motion (hereafter 'threshold mobility') is commonly defined as the flow at which the the dimensionless transport parameter ($W^{\star}$) exceeds the value of 0.002 (*Parker*, 1990b). $W^{\star}$ is

defined as

$$W^{\star} = \frac{Rgq}{(ghs)^{3/2}} \tag{4.1}$$

where R is submerged specific gravity of sediment, g is gravitational acceleration, q is the volumetric sediment transport rate, h is average flow depth, and S is channel slope. As flow increases beyond the threshold mobility, the proportion of the bed that is mobile increases until nearly all grains on the bed surface are in motion (*Andrews*, 1994). This is the transition from partial mobility to full mobility.

The timing and predictability of river bed mobility are important drivers of aquatic habitat in river ecosystems. The threshold for bed mobility is often associated with a dramatic reduction in benthic macroinvertebrates density (*Robinson et al.*, 2004; *Gibbins et al.*, 2007; *Power et al.*, 2008). In a New Zealand stream, benthic macroinvertebrates returned gradually (both biomass and number of species) over the 3 months following a large storm (*Scrimgeour et al.*, 1988). In the South Fork Eel River of central California, Power et al. (2008) demonstrated that the ecological effects of bed mobilizing flows are even longer-lived. In most winters, bed mobilizing flows reduce armored caddisfly populations, but during drought winters (lacking bed-scouring flows) caddisfly populations go unchecked. The summers following drought winters are associated with robust caddisfly populations and a significantly lower density of green algae, a primary foodsource of the caddisfly (*Power et al.*, 2008). These findings point to the importance of bed mobility frequency to river ecosystems. However, not all bed mobilizing storms result in a loss of macroinvertebrate biomass. In contrast to findings from New Zealand and California, work in Nepalese streams suggests that the monsoonal floods do not represent major ecological disturbance (*Brewin et al.*, 2000). Premonsoon macroinvertebrate density is already low because of low winter produc-

tivity, suggesting that seasonal productivity effects can outweigh the importance of bed-mobilizing floods if the floods align predictably with times of low biological productivity. Thus, a biologically relevant characterization of riverbed mobility should deal with both wait times between bed-mobilizing storms and the seasonal consistency of bed mobilizing events.

In addition to implications for river ecosystem function, the timing of bed mobility and immobility has implications for 'memory' effects in rivers. The flow conditions preceeding a storm can affect the mobility of the bed. Physical experiments have shown that the threshold for riverbed mobility can increase with the duration of pre-mobility low flows (*Masteller and Finnegan*, 2017). This phenomena is associated with subtle reorganization of the bed surface, rendering grains more stable. Thus, the duration of low flow conditions separating storms has the potential to impact the threshold for motion. In addition to this abiotic process, biologically mediated stabilization of gravel during prolonged low-flow, high-productivity periods may represent another memory effect controlled by bed mobility timing. For example, caddisfly larvae build silk nets that bind individual particles together, significantly increasing the threshold for sediment motion during subsequent storms (*Johnson et al.*, 2009; *Albertson et al.*, 2014). Because it may take months for caddisfly populations to rebound after extreme bed-mobilizing flows (*Power et al.*, 2008), the timing and intensity of bed mobilizing storms has the potential to determine the threshold for mobility during subsequent high flow events. While existing sediment transport models do not take these effects into account, bed mobility frequency analysis can provide us with quantification of how variable inter-storm wait times actually are between rivers and regions.

Bed mobility provides a lens through which to consider how sediment transport

and hydroclimatic patterns are reflected in gravel bedded river geometry. Sediment supply and hydrology vary enormously, but differences in river geometry are comparatively subtle. For example, *Pfeiffer et al.* (2017) showed that a 2 order of magnitude variation in sediment supply is associated with only a 2 fold difference in the ratio of the bankfull shear stress to the critical shear stress associated with bed mobility. These findings suggest that channel geometry and grain size reflect sediment supply; however, it is impossible to fully capture/understand how channels reflect variation in sediment supply without recognizing the importance of flow intermittency (*Hassan et al.*, 2006). A channel that experiences sediment mobilizing floods lasting one week a year likely transports substantially more sediment than one that transports sediment at the same rate for only a few hours. To the extent that river channels tend towards a dynamic, quasi-equilibrium between sediment supply inputs and sediment transport outputs, patterns in bed mobility should reflect the combined effects of magnitude and frequency.

Here, we use decades-long series of modeled sediment transport for 31 rivers across the continental US to show that predicted bed mobility varies enormously in gravel bedded rivers. It varies in terms of intermittency, timing, and intensity. We focus on the significant regional trends, and suggest that these trends are a direct function of the differences in hydroclimatic regime and sediment supply between these regions.

4.3 Methods

We calculate multi-decadal time series of predicted bed surface mobility using fractional sediment transport equations (*Parker*, 1990b; *Wilcock and Crowe*, 2003). The method requires measurements of the bed surface grain size distribution, channel slope, and long-term stream discharge records. We calculate the

fraction of the bed surface grain size distribution that is mobile at any given flow, as well as the intensity of transport. We use the time series of predicted bed mobility to compare between rivers and regions.

4.3.1 Site choice

We compiled a dataset of 31 gravel bedded rivers across the continental US (C.1, Figure 4.1). We selected sites with gravel beds and long-term (mean = 24.2 years) USGS continuous discharge (15-minute interval) records. Bed surface grain size and channel slope data came from the literature. The distributions of slope, drainage area, and median grain size (D_{50}) represented in each region are shown in C.1. In the absence of full grain size distributions (n=16), we created synthetic GSDs using reported D_{50} and D_{84} for the reach, assuming a lognormal grain size distribution (as in *Pfeiffer and Finnegan*, 2017). In 5 cases we lacked D_{84}data and estimated D_{84} as $2.1D_{50}$ (*Rickenmann and Recking*, 2011).

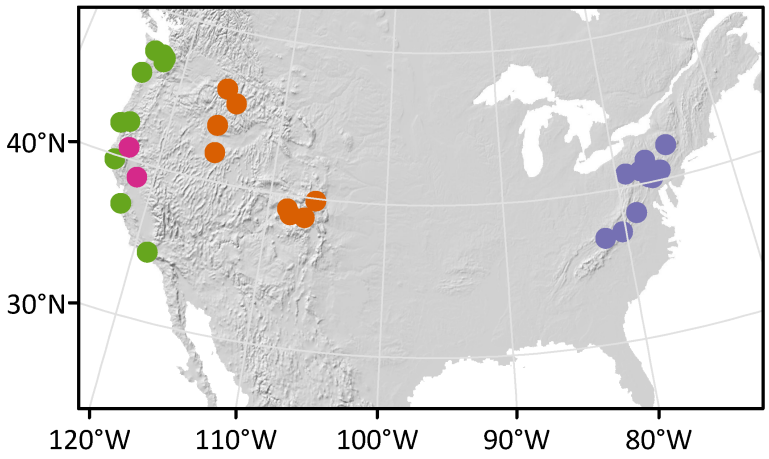

Figure 4.1: Sites used in this study, colored by category. Appalachian sites are shown in purple, Rocky Mountain in orange, West Coast in green, Dammed rivers in pink.

Table 4.1: Sites used in this study.

Site	Slope	D_{50} (m)	Drainage Area (km^2)	USGS Gage	Source
Rocky Mountain					
Jarbidge	0.016	0.095	79.3	13162225	King et al. (2004)
Lochsa	0.0023	0.126	3056	13337000	King et al. (2004)
Selway	0.0021	0.173	4947	13336500	King et al. (2004)
Williams Fork	0.0039	0.04	231	9036000	Segura and Pitlick, 2015; Andrews, 1984
Boise	0.0038	0.076	2150	13185000	King et al. (2004)
Salmon	0.0025	0.038	855	13310700	King et al. (2004)
Gunnison	0.00076	0.074	20520	9152500	Williams et al., 2013
Colorado	0.0024	0.075	22825	9106150	Pitlick and Van Steeter (1998)
EastR	0.0067	0.091	749	9112500	Andrews 1984
West Coast					
Sespe	0.009	0.07	652	11113000	Stillwater Sci (2010)
Elder	0.0222	0.108	17	11475560	Lisle, personal comm.
Chetco	0.00138	0.037	702	14400000	Wallick et al. (2012)
San Lorenzo	0.002	0.026	275	11160500	unpublished data
Applegate	0.0028	0.02776	1994	14369500	O'Connor et al. (2014)
Nehalem	0.00129	0.04954	1844	14301000	O'Connor et al. (2014)
Puyallup	0.00087	0.032	2455	12101500	Czuba, personal comm.
Nisqually	0.007	0.064	344	12082500	Czuba, personal comm.
Carbon	0.013	0.13	204	12094000	Czuba, personal comm.
Skokomish	0.0009	0.02		12061500	Collins, personal comm.
Appalachian					
Yellow Breeches	0.001	0.023	552	1571500	Chaplin (2005)
Spring	0.002	0.0506	152	1546400	Chaplin (2005)
Roanoke	0.0024	0.0657	282	2053800	Keaton et al. (2005)
Sherman	0.001	0.051	536	1568000	Chaplin (2005)
Blockhouse	0.006	0.0819	98	1549500	Chaplin (2005)
Schuylkill	0.001	0.0269	344	1468500	Chaplin (2005)
WB Delaware	0.001	0.0488	860	1423000	Westergard et al. (2005)
Mahoning	0.001	0.0675	226	3034500	Chaplin (2005)
Holston	0.0016	0.0552	572	3488000	Keaton et al. (2005)
South	0.0048	0.123	549	1627500	Keaton et al. (2005)
Trinity	0.0024	0.09	1862	11525500	Viparelli et al. (2011)
Bear	0.001143	0.033	756	11424000	Minear (2010)

We focused our study on three regions: the West Coast, the Rocky Mountains, and the Mid-Atlantic Appalachians. These regions represent a gradient in sediment supply (*Pfeiffer et al.*, 2017), and have varying flood hydrology. The west coast is characterized by high erosion rates (average long-term erosion rate = 336 mm/kyr (*Pfeiffer et al.*, 2017)), and has a Mediterranean climate with dry, warm summers and mild, wet winters (*Hirschboeck*, 1991). The Mid-Atlantic is characterized by low erosion rates (22 mm/kyr mean long-term), and less consistent seasonality to precipitation. Floods result from early autumn tropical cyclones, wintertime 'nor'easters', and, occasionally, intense summer thunderstorms (*Hirschboeck*, 1991). The Rocky Mountain region has moderate erosion rates (114 mm/kyr mean long term erosion rate, with notably lower short term erosion rates (*Kirchner*, 2001)). Rivers in the Mid-Atlantic Appalachians and along the West Coast tend to experience a substantial number of 'flashy' storms (*Smith and Smith*, 2015). This is not the case in the Rocky Mountains, where most floods predictably occur during peak snowmelt in the spring or early summer (*Hirschboeck*, 1991). In addition to these regions, we include two reaches that are just downstream from large dams (Trinity, < 1 km below Lewiston Dam, and Bear, 11 km below New Camp Far West Dam). In compiling these data, we aimed to represent a variety of grain sizes and channel slopes within each region, while maintaining similar averages between the regions.

While USGS instantaneous discharge data exist for hundreds of sites across the continental US, many well-studied sites proved unsuitable for our analysis. In particular, small Rocky Mountain streams tend to be frozen for a large portion of the year, with ice breaking up during the spring high flows. Those missing data impede exceedance probability analysis. We excluded sites that have large, seasonally consistent data gaps. In cases with more moderate winter data gaps

(e.g. East River), where the full duration of the missing data occurred during sub-threshold transport conditions, we filled in the missing data using a linear interpolation between flows of known magnitude.

4.3.2 UGSG gage records

We use the method described by *Phillips and Jerolmack* (2016) to transform long-term USGS discharge records into time series of average flow depth and width for each site analyzed, using channel geometry data from USGS Water Science Centers. Using this information, we create a modified rating curve that relates average flow depth (instead of stage) to discharge. This transformation is necessary because average flow depth has hydraulic significance, whereas stage is simply water height measured above an arbitrary datum. We use our modified rating curves to turn these discharge records into a decades-long timeseries of average flow depth.

We made one modification to the *Phillips and Jerolmack* (2016) method for relating stage and average flow depth. Field measurements are abundant at low and moderate flow and scarce at high flow, but bed mobilizing sediment transport generally occurs only at high flow. In many cases, a linear least squares fit between stage and average flow depth yields a poor match to the highest flows, which are the most important for our bed mobility analysis. To ensure fidelity at the high flows, we forced the stage-depth fit through the highest flow on record. From visual inspection of the modified rating curves, this yielded an improved average flow estimate for nearly all sites. Where appropriate, we reverted to the original method. For sites where published depth-discharge relationships exist, we used those if they produced a (visually determined) better fit than the method described above. For examples, see C.2.

We used the same discharge and channel geometry data to create a rating curve to relate average channel width ($w(m)$) to discharge ($Q(m^3/s)$). These relationships were well-modeled using a standard hydraulic geometry scaling relationship:

$$w = aQ^b \tag{4.2}$$

where a and b are empirical parameters determined through least-squares best-fit analysis.

4.3.3 Estimate bed surface mobility from sediment transport equations

We tested several methods for predicting bed surface mobility. The most mechanistically explicit models calculate separate sediment transport rates for different grain size classes. These fractional transport models can account for the low mobility of very large grains relative to small ones and the importance of hiding and protrusion effects. For our analysis, we used both the *Parker* (1990b) and *Wilcock and Crowe* (2003) fractional sediment transport equations, and modified these equations to account for slope dependence of the threshold for motion. The models are described in detail in Appendix 1.

4.3.4 Modifications

Since the publication of the *Parker* (1990b) and *Wilcock and Crowe* (2003) models, several studies have shown that the threshold for sediment motion is a function of channel slope (*Mueller et al.*, 2005; *Lamb et al.*, 2008; *Pitlick et al.*, 2008; *Prancevic and Lamb*, 2015). The sites in our compilation vary in terms of channel slope (.00076 to .0222), making this effect potentially important to

the accuracy of bed mobility predictions. As a part of a sensitivity analysis, we substituted the reference Shields stress (equation A4 and A15) for the empirical slope-dependent reference Shields stress equation determined by *Mueller et al.* (2005):

$$\tau_r^\star = 2.18S + 0.021; \tag{4.3}$$

as well as the equivalent equation from (*Lamb et al.*, 2008);

$$\tau_r^\star = 0.15S0.25 \tag{4.4}$$

and that of (*Pitlick et al.*, 2008);

$$\tau_r^\star = 0.36S0.46 \tag{4.5}$$

Several of the sites in our compilation have published reference Shields stresses. We explored the sensitivity of our bed mobility calculations by using these published values.

4.3.5 Analysis of transport results

We require a metric to describe bed mobility intensity. *Lisle et al.* (2000) used $\tau^\star$ to make comparisons of bed mobility between different rivers. While the common use of Shields stress make it an attractive choice, we feel it is an imperfect one. Sediment transport is a function of more than Shields stress (and a non-linear one, at that): it also varies with GSD, and depends on the critical (or reference) Shields stress, which varies as a function of channel slope and sand content. There are two commonly used dimensionless parameters that more directly characterize sediment transport, and thus bed mobility: the Einstein transport parameter, $q^\star$,

and the dimensionless transport parameter, $W^\star$. In this analysis, we chose to use compare streams using $W^\star$ because it has a specific, frequently used value associated with bed mobility. By design, the reference transport rate associated with the threshold for motion occurs at $W^\star = 0.002$. It is also helpful to characterize 'full mobility', a transport stage associated with the mobility of nearly all grains on the bed surface, defined by Andrews (*Andrews*, 1994). Andrews found that, in Sagehen Creek, full mobility occurred at roughly twice the critical stress. We can plug this ratio ($\tau^\star/\ \tau_r^\star = 2$) into equation C.20 to find the value of $W^\star$ associated with the transition to 'full mobility' (0.1555).

To characterize bed mobility intermittency, we calculated wait times between bed mobilizing flood events. We counted a mobility event ($W^\star$>0.002) as distinct if it was preceded by at least 24 hours of $W^\star$<0.002.

We tested the statistical significance of differences between regions using a Welch's Analysis of Variance (ANOVA), a test that is robust to analyze data sets of unequal size with unequal variance. Where appropriate, we log-transformed the data before running the ANOVA to account for log-normal (rather than normal) distributions within regions. When statistically significant differences were found (α< 0.05), we employed a Games-Howell post-hoc test to make pair-wise comparisons.

4.3.6 Testing transport against supply

As an order-of-magnitude test of our sediment transport results, we compare predicted average annual bedload transport to estimates of average annual bedload supply ($Q_{supply}(m^3/yr)$) based on data in the literature. If a riverbed is neither aggrading nor incising, the sediment transport through the reach should be in equilibrium with the sediment supply to the reach. Our methods for esti-

mating bedload supply varied by river, depending on the available information. Site specific details are given in Supplementary Table C.1. For most sites, we obtained a bedload supply estimate by assuming that the average total annual sediment supply was the product of the erosion rate, the drainage area, and the bedload fraction (percent of total sediment flux transported as bedload, rather than suspended or dissolved load). The fraction of total sediment transported as bedload is highly variable (*Turowski et al.*, 2010), and is a function of catchment lithology and drainage area (*O'Connor et al.*, 2014), among other factors. Where we could not find published estimates of bedload fraction, we did not attempt to estimate this value.

4.4 Results

The magnitude of bed mobility varied depending on sediment transport model, though the trends between regions were consistent across models. Supplementary Figures C.3 through C.10 show results from the different model runs. In all model runs, West Coast rivers had high maximum mobility ($W^\star$) and high exceedance probability when compared to Rocky Mountain and Appalachian rivers (Fig 4.4 and 4.5). In all model runs, Rocky Mountain rivers have higher maximum bed mobility for a given exceedance probability, when compared to Appalachian rivers (Fig 4.4). For the following analysis, we will focus on sediment transport calculations made using the Parker (1990) equations, modified with slope-dependent reference stress (*Lamb et al.*, 2008), using field measured reference stress data where available for the duration of the results and discussion. This configuration results in good agreement between sediment transport and supply (Figure 4.2). In addition, it did not result in unreasonably high predicted transport rates at low flows (e.g. exceeding reference transport 90% of the time), as was the case for sev-

eral configurations of the *Wilcock and Crowe* (2003) model with slope-dependent reference stress.

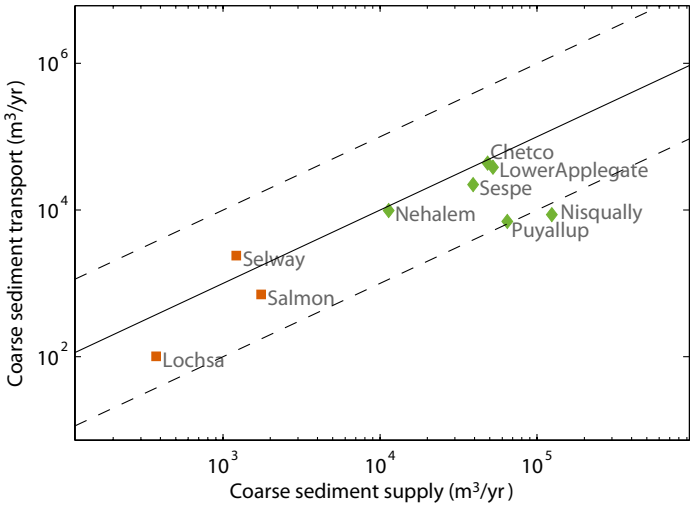

Figure 4.2: Testing the accuracy of our bed mobility predictions: comparing long term predicted sediment transport against sediment supply. The solid black line marks perfect agreement. The dashed lines mark one order of magnitude from perfect agreement. Points are colored by region, as in previous figures.

The first order relationships between hydrology and bed mobility are clear in the time series of bed mobility (Figures 4.3 and 4.4). The Rocky Mountain rivers (Fig 4.3 a and b; Figure 4.4 a-c) have floods that are generally consistent in timing and magnitude between years. Peak floods tend to occur during the late spring, which coincides with snowmelt. In most of the Rocky Mountain streams in our dataset, the threshold mobility (a term we use to refer to $W^{\star} = 0.002$) occurs at approximately bankfull flow.

West Coast rivers experience many short-duration, high bed mobility events

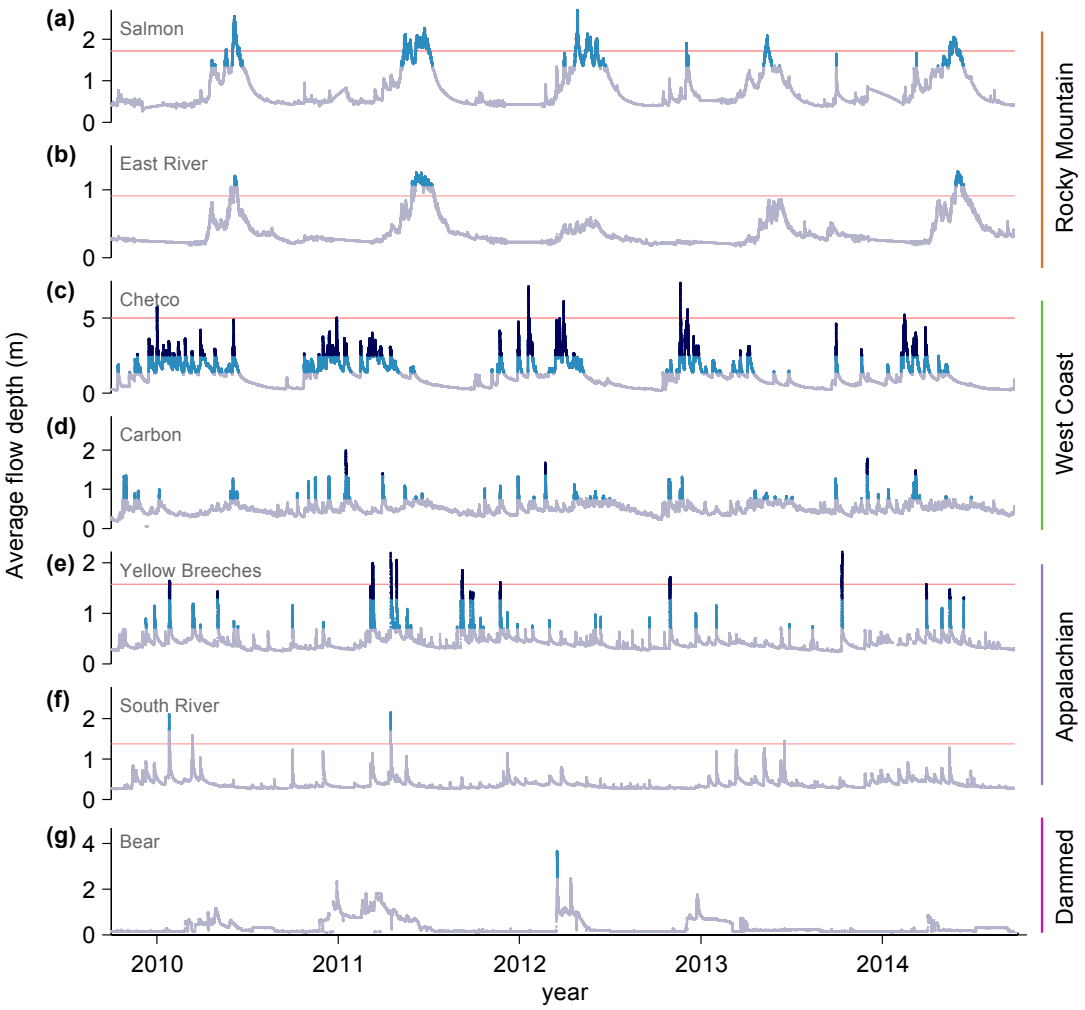

Figure 4.3: Example average flow depth hydrographs for water years 2010-2014, colored by bed mobility. Transport below $W^\star = 0.002$ is shown in grey, 'marginal mobility' in light blue, and 'full mobility' in dark blue. Where available, bankfull depths are shown, for reference, in red.

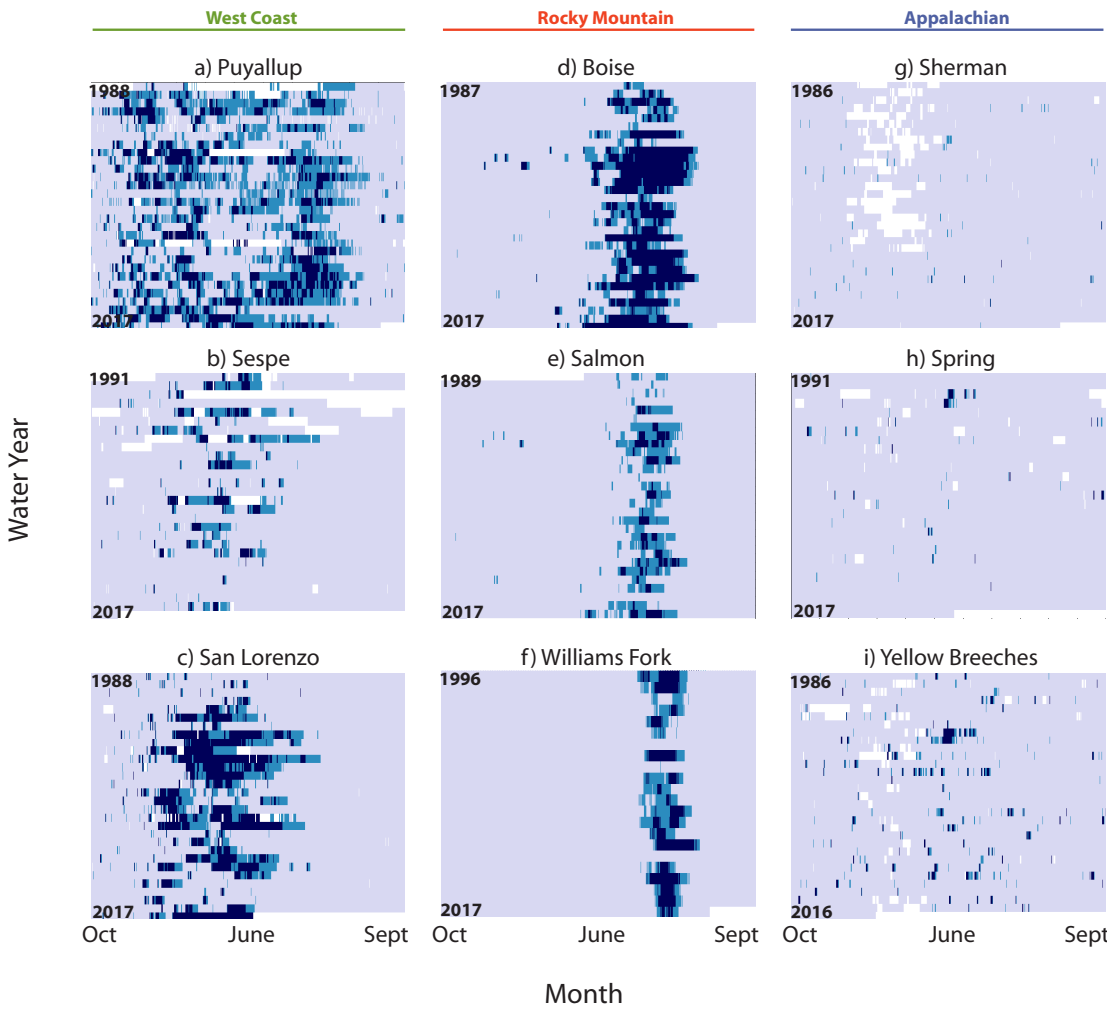

Figure 4.4: Bed mobility intensity through time for 9 example sites, 3 from each geographic region. Data are separated by water year. Water year is on the vertical axis, month within the water year is on the horizontal axis. The color scheme matches figure 2: immobile bed is shown in grey, 'partial mobility' in light blue, and 'full mobility' in dark blue. Data gaps shown in white.

throughout the winter and spring (Figure 2 c and d; Figure 3 d-f). This is the case even for streams in our dataset that drain Mt. Rainier (Carbon, Nisqually, and Puyallup), even though the upper reaches of those basins contain glaciers and receive substantial winter snowfall. In many West Coast streams in our dataset, the peak intensity of bed mobility varies substantially between years. We lack bankfull depth measurements for most of the West Coast rivers in our compilation. However, we predict bed mobility at low recurrence-interval flows.

The Appalachian rivers experience short-duration high flow events throughout the year (Figure 4.3 e and f; Figure 4.4 g-i). The maximum intensity of bed mobility varies substantially between the Appalachian rivers in our compilation. The peak bed mobility events do not have a strong seasonal control, unlike the West Coast and Rocky Mountain rivers. The relationship between bankfull flow and the predicted initiation of bed mobility is inconsistent across Appalachian rivers. In several of the rivers (e.g. Spring Houser, Mahoning), bed mobilization occurs well above bankfull flow. The two gaged sites immediately downstream from major flow- and sediment-regulating dams rarely exceed reference bed mobility $W^{\star}= 0.002$ (Figure 4.5). These two rivers represent end-member cases of flow and sediment regulation. Because bed mobility exceeds the reference value so infrequently, we have excluded dammed rivers from portions of the following analysis. The exceedance probability of bed mobility (Figure 4.5) results from the combined effects of flood hydrology, channel geometry, and bed surface grain size. We observe clear regional trends in the bed mobility exceedance curves. Using $W^{\star}$ to quantify the intensity of bed mobility, we see that the Rocky Mountain and West Coast rivers have gently sloped $W^{\star}$-exceedance probability curves (Figure 4.4). This suggests that infrequent storms have only marginally more mobile beds. On the other hand, the exceedance probability curves for Appalachian rivers are

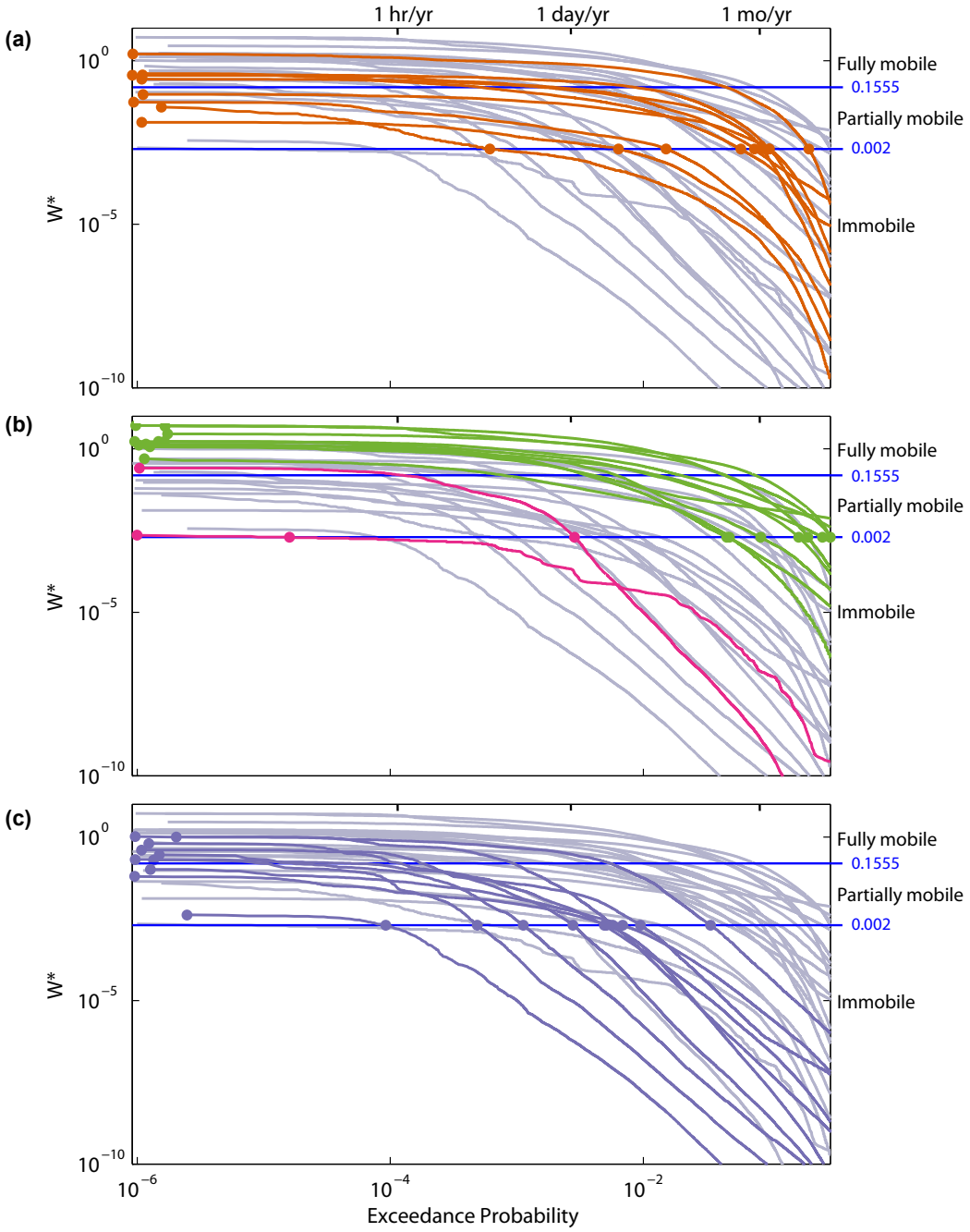

Figure 4.5: Exceedance probability of bed mobility (via the dimensionless sediment transport parameter, W*). Curves are separated and colored by region, as in Figure 1: a) Rocky = orange; a) West Coast= green, and Dammed = fuchsia; c) Appalachian = purple. Grey curves in the background are from all other regions. Horizontal lines at W*=0.002 and 0.1555 separate bed mobility stages.

steep. The regional trends are captured in the relationship between the exceedance probability of reference flows and the maximum bed mobility (Figure 4.6). We see that the data cluster by region. West Coast and Rocky Mountain rivers have statistically significantly higher exceedance probability of threshold mobility (the beds are mobile a large portion of the time) when compared to Appalachian rivers (Welch's ANOVA, Games-Howell post-hoc test, Rocky-Appalach $p = 0.02$; West-Appalach $p < 0.0001$). In terms of maximum bed mobility, West Coast rivers have statistically significantly higher maximum mobility when compared to both Rocky Mountain and Appalachian rivers (Welch's ANOVA, Games-Howell post-hoc test, West-Rocky $p = 0.002$, West- Appalach $p = 0.005$), which are not statistically different from one another.

The number of bed mobilizing events per year varies by region. West Coast rivers experience a mean of 9.7 (+/- 3.2 standard deviation, S.D.) discrete bed mobilizing events per year (median duration = 9.5 days), while Rocky Mountain rivers experience a mean of 2.0 (+/- 1.1 S.D.) discrete bed mobilizing events per year (mean duration = 10 days). Appalachian rivers experience a mean 2.6 discrete bed mobilizing event per year, though the variation between rivers is substantial, with a standard deviation of 2.2. (average duration = 0.73 days). West Coast rivers have statistically significantly more mobility events per year when compared to both Rocky Mountain and Appalachian rivers (Welch's ANOVA, Games-Howell post-hoc test, West-Rocky $p = 0.0002$, West-Appalach $p = 0.006$).

We use the wait time between bed-mobilizing events to quantify bed mobility intermittency. Bed mobilizing events in Rocky Mountain rivers tend to occur after a 3-10 day or 300 day wait time (Figure 4.7). This strong annual frequency is apparent in Fig 4.5 a - c. West Coast channels have similarly bi-modal wait times, though the majority of events happen after a 3-30 day period of sub-reference

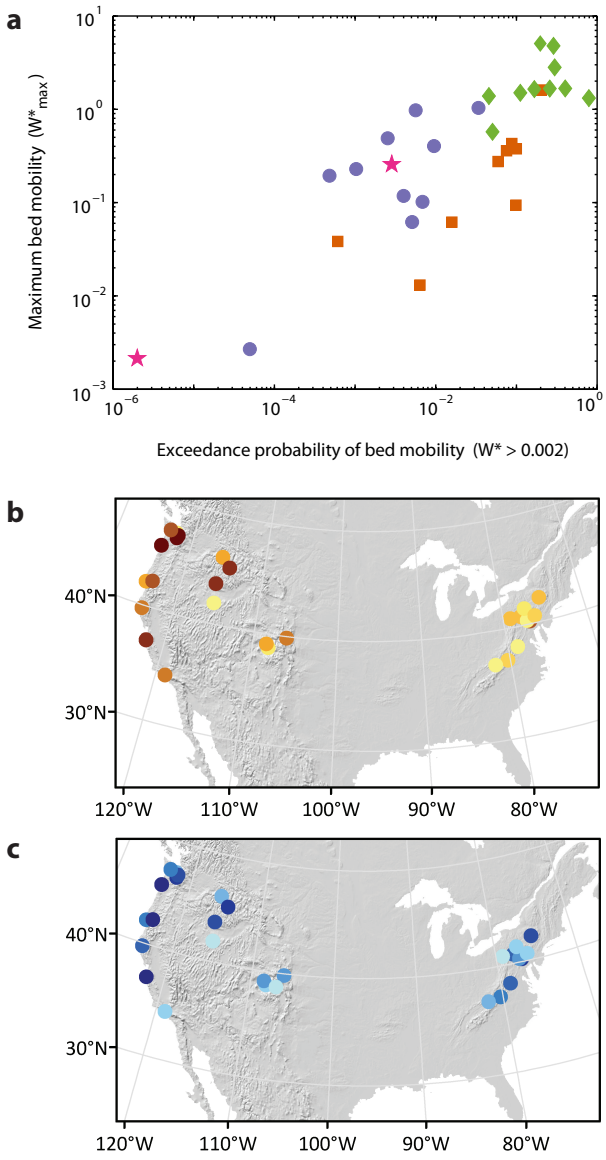

Figure 4.6: Regional clustering of the exceedance probability of bed mobility and the maximum bed mobility. These data can also be viewed in Figure 4.4. Comparison of the exceedance probability of mobility (W*>0.002) and the maximum bed mobility. Data are colored by region, as in Figure 4.1 (West Coast= green diamonds; Rocky = orange squares; Appalachian = purple circles; Dammed = fuchsia star). Note the strong regional clustering. B) Map of exceedance probability of mobility. Points colored by the logarithm of exceedance probability, with dark shading corresponding to higher values. C) Map of maximum bed mobility. Points colored by the logarithm of maximum W*, with dark shading corresponding to higher values.

mobility. There is not a strong mode to the wait time between bed mobilizing storms in the Appalachian rivers. Wait times vary from 2-2000 days, with two weak modes around 60 and 400 days.

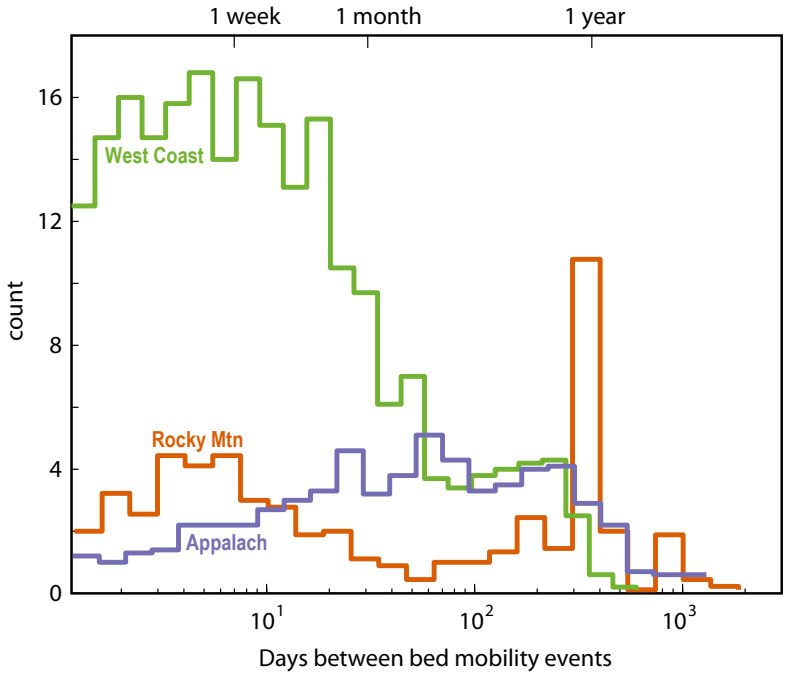

Figure 4.7: Histogram showing the number of days in between bed mobility events (W*>0.002), separated by region. Counts are normalized by the number of sites in that region. Colors match previous figures.

4.5 Discussion

There are several notable benefits to this approach to bed mobility. First, we are unconstrained by the need to define bankfull flow depth. While convenient in many situations, bankfull depth can be an imprecise metric of river

dimensions. 'Bankfull' flow has several different definitions (*Williams*, 1978), and does not have a characteristic recurrence interval across (or even within) regions (*Williams*, 1978). Some channels have poorly defined floodplains or multiple topographic breaks, complicating the characterization of a single bankfull channel. By characterizing the mobility of a riverbed in terms of exceedance probabilities and inter-storm wait times, we use metrics that have uniform meaning and biological relevance between regions. Furthermore, in the myriad rivers where upstream dams regulate flow, the bankfull channel may represent pre-dam conditions, rather than the flow and sediment supply that determine post-dam bed mobility. Bed mobility has biological relevance in regulated rivers as well as unregulated ones. Our method for characterizing bed mobility can be applied to regulated rivers.

Gravel riverbed mobility varies enormously among the rivers in our compilation. Given the importance of bed mobility to lotic ecosystems, it is an important dimension by which we can (and perhaps should) compare rivers. On one end of the spectrum captured in our data compilation, some rivers fail to reach reference mobility ($W^{\star}$=0.002; roughly, the threshold for motion) more than a few times over the course of decades (e.g. Trinity (dammed) and Mahoning (Appalachian) Rivers). On the other end, the Nisqually River, which drains the glaciers of Mt. Rainier, has a mobile bed the majority of the time.

While there is variation between rivers in a region, strong regional patterns exist in timing and intensity of bed mobility (e.g. Figure 4.6 and 4.7). *Hassan et al.* (2014) categorized streams according to the exceedance probability of effective discharge. Our analysis is focused on mobility thresholds rather than effective discharge, but we can apply a similar categorization scheme to the rivers in our analysis. In general, the West Coast rivers, with a median of 83 days above reference mobility (including a median of 4.3 cumulative annual days of 'full mobility')

annually, are 'frequently mobile' gravel rivers. The Rocky Mountain rivers, which tend to have a long period of marginal mobility during the spring snowmelt (average of 28 days of marginal mobility, 0.19 days of full mobility per year), tend to be 'frequently marginally mobile, rarely fully mobile'. We term the Appalachian rivers 'infrequently mobile', with a region-wide median of 1.7 days of marginal mobility (0.0034 days of full mobility).

The rivers just downstream of dams (Trinity and Bear) could also be characterized as 'infrequently mobile'. However, gravel augmentation is a common restoration practice in sediment starved reaches downstream of dams. Gravel augmentation is common in the Trinity River reach analyzed in this study (*Viparelli et al.*, 2011), but has not occurred in the Bear River reach (*Minear*, 2010). This practice causes fining of the bed surface during the high flow events following gravel additions, likely resulting in higher transport rates than we predict in this study. Historically, gravel augmentation in the Trinity has accounted for only 6% of the pre-dam annual sediment supply though proposed plans would greatly increase that number (*Viparelli et al.*, 2011). Our bed mobility estimates represent the predicted bed mobility associated with the surface grain size as measured on the riverbed, in the absence of gravel augmentation.

The regional trends in gravel river bed mobility can be explained by the combined effects of coarse sediment supply and basin hydrology. The intensity of bed surface mobility is primarily driven by sediment supply. The gradient in sediment supply represented by these three regions (336, 114, 22 mm/kyr average erosion rate for West, Rocky, Appalachian respectively (Pfeiffer et al. (2017)) is reflected in the patterns in the exceedance probability of bed mobility (Figure 4.6). The West Coast rivers have significantly higher peak transport intensity when compared to both Appalachian and Rocky Mountain rivers and significantly higher

exceedance probability of mobility when compared to Appalachian rivers. These findings build on the work by *Lisle et al.* (2000), who showed that bankfull bed mobility varied systematically with sediment supply. In addition, this supports the observation of *Pfeiffer et al.* (2017) that the ratio of bankfull to critical Shields stress varies with sediment supply, and that the ratio is substantially higher in West Coast rivers. In general, rivers that are supplied more sediment are mobile more often.

Basin hydrology is the other obvious driver of bed mobility differences between regions. The effects of hydrology are apparent in the relationship between peak mobility and exceedance probability of reference mobility (Figure 4.6). Appalachian and Rocky Mountain rivers have similar peak mobility intensity (difference in $W^{\star}$max is not statistically significant); however, moderate sediment transporting flows occur a greater portion of the time in Rocky Mountain streams than in Appalachian ones (significant difference in exceedance probability). This pattern results from the differences in hydrology between the two regions. Rocky Mountain rivers experience long periods of high flow during the spring snowmelt, whereas Appalachian rivers experience abrupt, brief floods (Figure 4.3).

We can use patterns in bed mobility intermittency to explore the relative importance of sediment supply and basin hydrology as drivers of bed mobility. Both West Coast and Appalachian rivers experience numerous brief high flow events compared to Rocky Mountain rivers (in the latter, hydrology is characterized by less intense but longer duration events), but West Coast rivers are subject to much higher sediment supply than their Appalachian counterparts. If hydroclimatic factors outweighed sediment supply, we might expect West Coast and Appalachian bed mobility intermittency to be more similar when compared to the Rocky Mountains. However, many of the moderate floods in Appalachian rivers fail to reach

reference mobility (Fig4.3 e and f). In contrast, the vast majority of modest floods in West Coast rivers exceed reference mobility. This pattern is reflected in the number of discrete bed mobilizing events (Figure 4.7). Appalachian rivers experience significantly fewer discrete events than West Coast rivers. These findings suggest that (across the spectrum of rivers examined here), sediment supply is the primary driver of bed surface mobility intensity, with hydrology as a secondary driver. This hierarchy of controls mirrors the conclusions of *Hassan et al.* (2006), who found that sediment supply was the first order control on bed surface grain size armoring, with hydrology playing a secondary role.

With these drivers in mind, we can begin to speculate about the departures from regional trends. For instance, Boise River is fully mobile 5% of the time, making it more similar to the West Coast rivers than the other Rocky Mountain rivers in in terms of mobility intensity. However, the mobility occurs over an average of only 3.5 discrete events per year, a result of the snowmelt-dominated hydrology. We suspect that high sediment supply is the primary driver of high bed mobility intensity in the Boise River when compared to other rivers in the region. The Nehalem River in the Oregon Coast Range (West Coast) represents another departure from regional patterns that can be explained by sediment supply. The Nehalem River is mobile 5% of the time, substantially less than the West Coast average (26%). A large portion of the Nehalem drainage basin is underlain by Coast Range sedimentary rocks, which are extremely friable, and abrade rapidly during bedload transport (*O'Connor et al.*, 2014). Despite high erosion rates in the Oregon Coast range, the bedload supply rate in the Nehalem is modest when compared to other rivers in the West Coast (*O'Connor et al.*, 2014).

4.5.1 Implications of variation in bed mobility

Our approach to bed surface mobility analysis could be used to test ecological disturbance theories, enabling first-order quantitative characterization of bed surface disturbance regimes without requiring extensive field surveys or 2-D flow models. Segura et al (*Segura et al.*, 2011) suggested that periphyton accumulation is controlled by both bed mobility and growth stimulation (e.g. temperature and nutrient availability). Viewed along these axes, we might expect the Rocky Mountain rivers (low temperatures limiting growth and moderate bed mobility) and West Coast rivers (higher temperatures but intense bed mobility) to have low periphyton growth compared to Appalachian rivers (higher temperatures, low bed mobility).

The regional differences in bed mobility timing have potential implications for memory effects (e.g. changes in sediment transport that depend on inter-storm wait times). Biologically-mediated memory effects almost certainly operate differently in Appalachian streams than in West Coast and/or Rocky Mountain ones. In most Rocky Mountain and West Coast streams, the high-flow season predictably brings (either marginal or full) bed-mobilizing flows. In most years, the late summer and early fall months are characterized by relative immobility. In these regions, the first bed-mobilizing flow following the dry season may be result in less intense bed mobility than we have predicted due to bed stabilization, both abiotic (e.g. (*Masteller and Finnegan*, 2017)) and biotic (*Johnson et al.*, 2009). We suggest that memory effects may have an even greater influence in Appalachian rivers. While floods in the West Coast and Rocky Mountain Rivers tend to occur in quick succession (median wait time between mobility events is 7 and 14 days, respectively), Appalachian Rivers have long periods of immobility between most storms (median = 45 days; mean = 115) (Figure 4.7). This allows more time for

macroinvertebrates to build bed-stabilizing silk nets and low flows to stabilize the bed through subtle grain reorganization (*Masteller and Finnegan*, 2017) before the next storm. Interestingly, these potential effects would further increase the discrepancy in bed mobility between regions, making the Appalachian streams even less mobile. Further work is needed to understand the magnitude of these memory effects, and the degree to which they vary between regions.

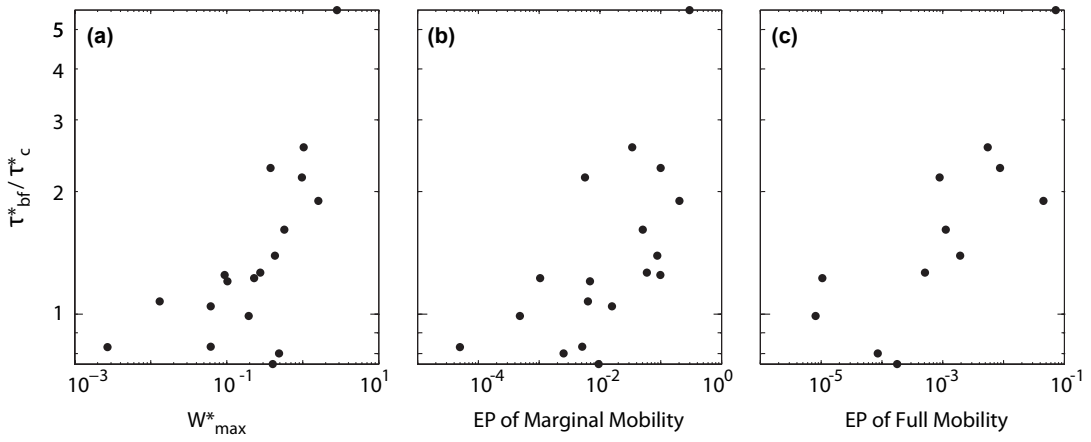

Figure 4.8: Comparing metrics of bed mobility to the ratio of bankfull Shields stress to critical Shields stress: a) maximum bed mobility ($W^\star$); b) exceedance probability of marginal mobility ($W^\star$=0.002); c) exceedance probability of full mobility ($W^\star$=0.1555). Note that there is a modest, positive relationship between $\tau^\star_{bf}/\tau^\star_c$ and all three metrics of bed mobility.

The method for characterizing bed surface mobility presented in this study requires long-term stream gage data, which is not available for many rivers. It would be convenient if commonly used metrics, such as the ratio of bankfull Shields

stress to critical Shields stress, were sufficient to distinguish between bed mobility regimes. To test this, we looked at the relationship between $\tau^{\star}_{bf}/\tau^{\star}_{c}$ and several metrics of bed mobility (Figure 4.8). In all cases, we find modest positive relationships between $\tau^{\star}_{bf}/\tau^{\star}_{c}$ and bed mobility. The relationship between hydrology, grain size, and sediment transport is complex, to say nothing of the complex drivers of 'bankfull' geometry. As a result, it is not surprising to find that $\tau^{\star}_{bf}/\tau^{\star}_{c}$ cannot be cleanly explained by bed mobility alone. That said, remarkably high or low $\tau^{\star}_{bf}/\tau^{\star}_{c}$ is likely a good indication of a highly mobile or immobile bed.

4.5.2 Caveats and uncertainties

We used published sediment supply data for a subset of sites in our compilation to check our sediment transport calculations. This check is valuable because sediment transport is notoriously difficult to predict and the sediment supply estimates have substantial uncertainty as well. The generally good agreement between average annual sediment supply and average annual sediment transport (4.2) is reassuring: it suggests that our bed mobility calculations are reasonable. The remarkably low predicted bedload transport rates in the Appalachian sites are intriguing. Unfortunately, we were unable to find independent published bedload sediment supply (or, for that matter, any individual bedload sample) data in the literature for rivers in the Appalachians. All of the sediment supply data used in 4.2 are from West Coast and Rocky Mountain sites. The lack of independent constraint for the Appalachian rivers is unfortunate, and points to a gap in the literature. That said, the good agreement between sediment supply and sediment transport in the West Coast and Rocky Mountain rivers suggests that our approach yields reasonable bed mobility estimates. Our method for calculating bed mobility assumes fixed channel geometry and bed surface grain size through time.

This simplification is common in calculations of sediment transport, though somewhat unsatisfying, as channel geometry and bed surface grain size often change during major flood events. Channels tend to widen during high-magnitude flood events and narrow over time during subsequent moderate discharge events *Pizzuto* (e.g. 1994). This suggests that in the years following an extreme event, our bed mobility estimates may be inaccurate. In addition, the grain size distribution of the bed surface may shift during floods (changing the sediment transport capacity independent of changes in flow). However, *Rubin and Topping* (2001) found that in alluvial rivers, discharge is the dominant driver of sediment transport, with changes in bed surface grain size playing a secondary role. While the exact values of bed mobility for a given site may vary depending on the antecedent high-magnitude flood history, the effects of variable grain size and channel geometry are unlikely to change the regional trends in bed mobility intensity and intermittency. Here, we have treated bed mobility as a reach-averaged problem. This is a substantial simplification, borne from the limited channel geometry and grain size patch information available in the literature. Both *Lisle et al.* (2000) and *Segura et al.* (2011) deal with the mobility of individual bed surface grain size patches within a reach. Both studies found that, even when the reach-averaged shear stresses were low, small fine-grained bed surface patches remained mobile. The patch-scale variations in bed surface mobility are certainly important for the benthic inhabitants living in those places. That said, *Lisle et al.* (2000) found that, while the details differed, reach-averaged bed mobility predictions were generally in agreement with the trends seen in patch-scale mobility. The simplified approach we propose here is, therefore, a good option for comparative studies between regions but not ideal for studies focused on sub-reach scale processes.

The method we used to process USGS channel geometry and gage data was

inspired by *Phillips and Jerolmack* (2016), but the results lead us to quite different conclusions. *Phillips and Jerolmack* (2016) argue that gravel bedded rivers adjust themselves to 'filter' climatic variation, such that a wide variety of hydroclimatic conditions all result in rivers that are, roughly, threshold channels. Their analysis focused on the central tendency of gravel bedded rivers. Here, we have focused on the variation between regions, viewing the problem through the lens of bed mobility. While the average river may indeed be a threshold channel, the wide variety of sediment supply and hydroclimatic conditions imposed on gravel bedded rivers yield statistically significant regional trends. Here, we show that gravel bedded rivers reach threshold mobility at a wide variety of stages relative to bankfull flow.

4.6 Conclusions

Viewing sediment transport through the lens of bed mobility, we show that there are substantial differences between regions across North America. Sediment transport appears to be the primary driver of the intensity of bed mobility, while the intermittency of bed mobility is largely determined by hydrologic regime. The regional differences have important implications for memory effects in rivers, and represent diverse physical habitat regimes for the benthic inhabitants of river ecosystems.

Appendix A

Scott Creek supplementary figures

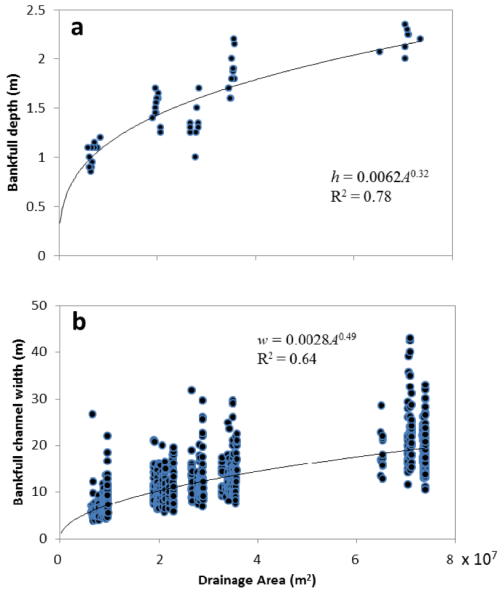

Figure A.1: a) At-a-station hydraulic geometry power-law scaling relationship between observed bankfull channel depth and drainage area. Measurements were made throughout the 11 study reaches. (b) At-a-station hydraulic geometry power-law scaling relationship between drainage area and bankfull width. Width measurements were made using ArcGIS and HEC-RAS at 15-m spaced cross sections throughout the extent of anadromous fish habitat in Scott Creek, Mill Creek, and Big Creek.

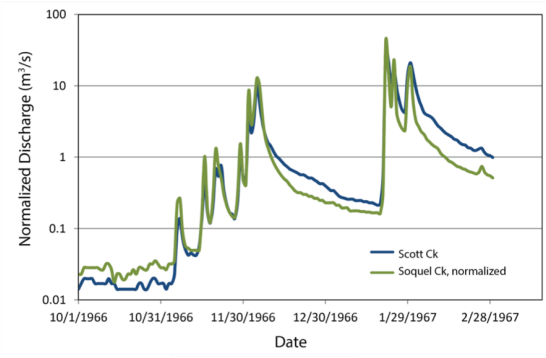

Figure A.2: Flood hydrographs for Scott Creek and Soquel Creek. Discharge values for Soquel Creek are normalized for the drainage area at the Scott Creek gauge using a linear discharge to drainage area scaling relationship.

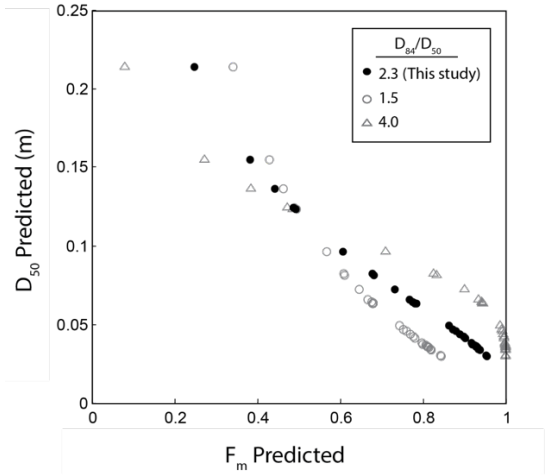

Figure A.3: Relationship between predicted D50 and predicted Fm, demonstrating the effect of D84/D50 ratio on Fm.

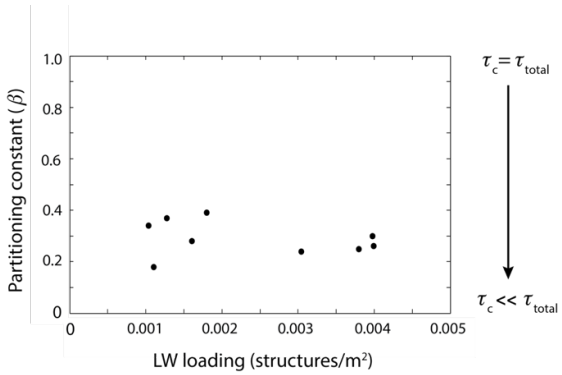

Figure A.4: LW loading and partitioning by reach (n = 9 reaches surveyed for LW). Note that these measurements of LW loading are reported in units of structures/m2 rather than pieces/m2 (e.g. Montgomery et al., 1995). Structures include jams of many pieces, so these numbers are lower than they would be if the data had been recorded in pieces/m2.

Appendix B

Sediment supply supplementary information

B.1 Basin Lithology

Using a geologic map of North America (*Garrity and Soller*, 2009), a 15 arc-second Digital Elevation Model (DEM), and a digital stream network (available online at: http://hydrosheds.cr.usgs.gov/), we extract basin lithology data for each basin in our data compilation, from which we calculate the percent of each basin underlain by sedimentary rock. This provides a rough estimate of the influence of lithology on the ratio of bedload to suspended load in our data compilation, as sedimentary rocks tends to abrade most rapidly (*Mueller et al.*, 2016). We note that the sedimentary rocks of the Appalachian Basin have undergone diagenesis during burial and exhumation from depths >5 km (*Friedman*, 1987), which tends to make them stronger than the younger sedimentary rocks of the West Coast. Thus, the comparison of lithologic effects between West Coast and Other sites is conservative, as sedimentary rocks on the West will tend to more rapidly abrade

into suspended load, decreasing the effective coarse sediment supply for a given erosion rate. Because a 15 arc-second grid imperfectly captures basin geometry, especially for smaller basins, we checked the output drainage areas against the drainage areas reported in the source literature. We discarded any basins with a mismatch in drainage area >15%, unless it was clear from visual inspection of the source data that the basin was underlain entirely by one lithologic category. In total, we retained 51 West Coast sites and 156 sites on the rest of the continent for our lithologic analysis.

B.2 *Recking* (2013) sediment transport equations

We use channel geometry and grain size data to estimate volumetric bankfull sediment transport capacity per unit channel width, Q_t (m^2/s), for sites in our data compilation using the (*Recking*, 2013) surface-based transport relation. These transport estimates appear in Figure 3.3 (colored points) and in Figure B.1. The Recking equations are well suited to our purposes because they are designed specifically for situations in which data on channel grain size are limited (e.g. incomplete knowledge of the surface, subsurface, or bedload grain size distribution), as is the case in our data compilation. Secondly, in this model, Q_t is not a function of excess bed surface shear stress (i.e. $\tau^\star_{bf} - \tau^\star_c$), but instead assumes partial mobility at low-to-moderate flows. Thus, with the knowledge of only channel slope (S), bankfull width (w (m)), bankfull depth (h (m)), and median bed surface grain size (D_{50} (m)), we can predict non-zero transport even in channels where $\tau^\star_{bf}/\tau^\star_c < 1$.

Recking frames transport in terms of the mobility of the 84th percentile bed surface grain size, D_{84}. Lacking knowledge of D_{84} for most of our sites, we follow the suggestion of Recking and estimate D_{84} from D_{50}:

$$D_{84} = 2.1 D_{50} \tag{B.1}$$

Recking approximates the Shields stress corresponding to the transition from partial to full mobility of the bed surface grains as:

$$\tau_m^\star = (5S + 0.06)(\frac{D_{84}}{D_{50}})^{4.4\sqrt{S}-1.5} \tag{B.2}$$

The bankfull Shields stress associated with D_{84} is:

$$\tau_{84}^\star = \frac{SR_{bf}}{(s-1)D_{84}} \tag{B.3}$$

where s is the relative density of the sediment (ρ_s/ρ), for which we assume a value of 2.65.

Using $\tau_m^\star$ and $\tau_{84}^\star$ Recking approximates the dimensionless sediment discharge, $q^\star$, as:

$$q^\star = \frac{14(\tau_{84}^\star)^{2.5}}{[1 + (\frac{\tau_m^\star}{\tau_{84}^\star})^4]} \tag{B.4}$$

from which we calculate the volumetric sediment flux per unit width (m^2/s):

$$Q_t = \sqrt{(s-1)gD_{84}^3}q^\star \tag{B.5}$$

B.3 Parker (1990) sediment transport model

Parker (1990b) presents a transformation from the subsurface-based relation of *Parker* (1990b) to a sediment transport model based on the grain size distribution of the bed surface. Using the equations presented in his transformation, we can relate the transport stage $\tau^\star/\tau_c^\star$ to both bed surface armoring (D_{50}/D_{50ss}) and

sediment flux, Q_t. These data are presented in the colored curve in Figure 3.3. We note that we are not using the final surface-based transport relation to determine these values, but rather the intermediate equations in ref (*Parker*, 1990b). We calculate Q_t based on the subsurface grain size distribution, then determine the surface grain size distribution (and therefore, armor ratio) from the equations derived by *Parker* (1990b) as a part of the subsurface-to-surface transformation. Below, we use notation that is consistent with that used above and in the main manuscript, not the notation used by Parker.

Our goal is to predict the bed surface armor ratio (D_{50}/D_{50ss}) and sediment flux (Q_t) for an example river at a variety of transport stages $\tau^\star/\tau_c^\star$. As inputs for the model, we used the Oak Creek channel slope, S, and subsurface grain size distribution, as in *Parker* (1990b). The subsurface grain size distribution is broken into n size classes, each of which is described by its diameter, D_i, and fraction of the total subsurface grain size distribution, f_i.

We used the following steps for a range of substrate-based transport stages (ϕ_{50}),

$$\phi_{50} = \frac{\tau_{ss}^\star}{\tau_{rss}^\star} \tag{B.6}$$

where the subsurface Shields stress, $\tau_{ss}^\star$, is

$$\tau_{ss}^\star = \frac{\tau}{(\rho_s - \rho) g D_{50ss}} \tag{B.7}$$

and $\tau_{rss}^\star$ is a reference Shields stress associated with the mobility of D_{50ss} with an assumed value of 0.0876. Ultimately, we transform these ϕ_{50} values to the surface-based transport stage ϕ_{sg0} (nearly equivalent to $\tau^\star/\tau_c^\star$) for display in Figure 3.3.

For each ϕ_{50}, we determine the substrate-based transport stage associated with

each individual grain size fraction (f_i)

$$\phi_i = g_{si}\phi_{50} \tag{B.8}$$

using the substrate-based hiding function (g_{si}),

$$g_{si} = 1.048(\frac{Di}{D_{50ss}})^{-0.0951} \tag{B.9}$$

For each ϕ_i we determine the dimensionless bedload transport rate ($W_i^\star$) according to Parker:

$$W_i^\star = 0.00218G_i \tag{B.10}$$

In which G_i is the piecewise empirical transport function:

$$G_i = \begin{cases} 5474(1 - \frac{0.853}{\phi_i})^{4.5} & \phi_i > 1.59 \\ exp[14.2(\phi_i - 1) - 9.28(\phi_i - 1)^2] & 1 \leq \phi_i \leq 1.59 \\ \phi_i^{14.2} & \phi_i < 1 \end{cases} \tag{B.11}$$

The total dimensionless bedload transport rate across all grain size fractions for the given ϕ_{50} is then

$$W_{tot}^\star = \sum_{i=1}^{n} W_i^\star \tag{B.12}$$

The dimensionless transport rate is then converted to a volumetric sediment transport rate per unit channel width, Q_t (m^2/s):

$$Q_t = \frac{W_{tot}^\star(\tau/\rho)^{3/2}}{Rg} \tag{B.13}$$

R is the submerged specific gravity of sediment ($(\rho_s - \rho)/\rho$), assumed to be 1.65. The bed surface shear stress, τ (N/m^2), can be obtained by combining and rear-

ranging equations 6 and 7, above:

$$\tau = \phi_{50}\tau^{\star}_{rss}(\rho_s - \rho)gD_{50ss} \tag{B.14}$$

In order to determine the surface median grain size, D_{50}, we first solve for the surface grain size distribution, which is described as grain size fractions, F_i, using the same diameter bins, D_i, as above.

$$F_i = \frac{f_i}{G_i}G_{tot} \tag{B.15}$$

where

$$G_{tot} = \frac{1}{\sum_{i=1}^{n} f_i/G_i} \tag{B.16}$$

Using the calculated bed surface grain size fractions, we determine the surface median grain size

$$D_{50} = e^{\sum_{i=1}^{n} F_i \ln D_i} \tag{B.17}$$

from which we calculate the armor ratio D_{50}/D_{50ss}. Because we want to compare armor and Q_t to a surface-based measure of transport stage, i.e. $\tau^{\star}/\tau^{\star}_c$, rather than a substrate based one (ϕ_{50}), we calculate ϕ_{sg0} for each case of ϕ_{50} according to:

$$\phi_{sg0} = \frac{\tau^{\star}_{sg}}{\tau^{\star}_{rsg0}} \tag{B.18}$$

Where the surface based Shields stress, $\tau^{\star}_{sg}$, and the reference surface-based Shields stress, $\tau^{\star}_{rsg0}$, are:

$$\tau^{\star}_{sg} = \frac{\tau}{(\rho_s - \rho)gD_{50}} \tag{B.19}$$

and

$$\tau^{\star}_{rsg0} = 0.0386 \tag{B.20}$$

We note that when we compare the output of the Parker model to our data in Figure 3.3, we are equating the surface-based reference Shields stress ($\tau^{\star}_{rsg0}$) to the critical Shields stress ($\tau^{\star}_{c}$). These two values are very nearly similar. Additionally, we equate the surface based Shields stress ($\tau^{\star}_{sg}$) to the bankfull Shields stress ($\tau^{\star}_{bf}$). For a discussion of this comparison, see the Methods section of the main text.

B.4 Notation

D_{50} - median grain size on the bed surface

D_{50ss} - median grain size in the subsurface

D_{84} - 84th percentile grain size on the bed surface

Di - characteristic diameter of grain size bin i

fi - fraction of subsurface grain size distribution within bin i

Fi - fraction of surface grain size distribution within bin i

g - gravitational acceleration (9.8 m^2/s)

Gi - value of the empirical transport function for grain size fraction i

gsi - value of the hiding function for grain size fraction i

G_{tot} - total empirical transport G for all grain size fractions

$q^{\star}$ - dimensionless bedload transport rate (Recking)

Q_t - volumetric sediment transport capacity per unit channel width

$R - (\rho_s - \rho)/\rho$

S - channel slope

s - relative density of sediment ρ_s/ρ

$W^{\star}_i$ - dimensionless bedload transport rate (Parker) for grain size fraction i

$W^{\star}_{tot}$ - total dimensionless bedload transport rate

ρ - density of water (1000 kg/m^3)

ρ_s - density of water (1000 $kg/^3$)

τ - bed surface shear stress (Pa)

$\tau^{\star}_{84}$ - Shields stress associated with D_{84}

$\tau^{\star}_{m}$ - Shields stress associated with the transition from partial to full mobility of the bed surface

$\tau^{\star}_{rsg0}$ - reference Shields stress associated with the bed surface

$\tau^{\star}_{rss}$ - reference Shields stress associated with the subsurface

$\tau^{\star}_{sg}$ - Shields stress associated with the D_{50}

$\tau^{\star}_{ss}$ - Shields stress associated with the D_{50ss}

ϕ_{50} - substrate based transport stage (associated with D_{50ss})

ϕ_{i} - transport stage of subsurface grain size fraction i

ϕ_{sg0} - surface based transport stage (associated with D_{50})

B.5 Supplementary Figures

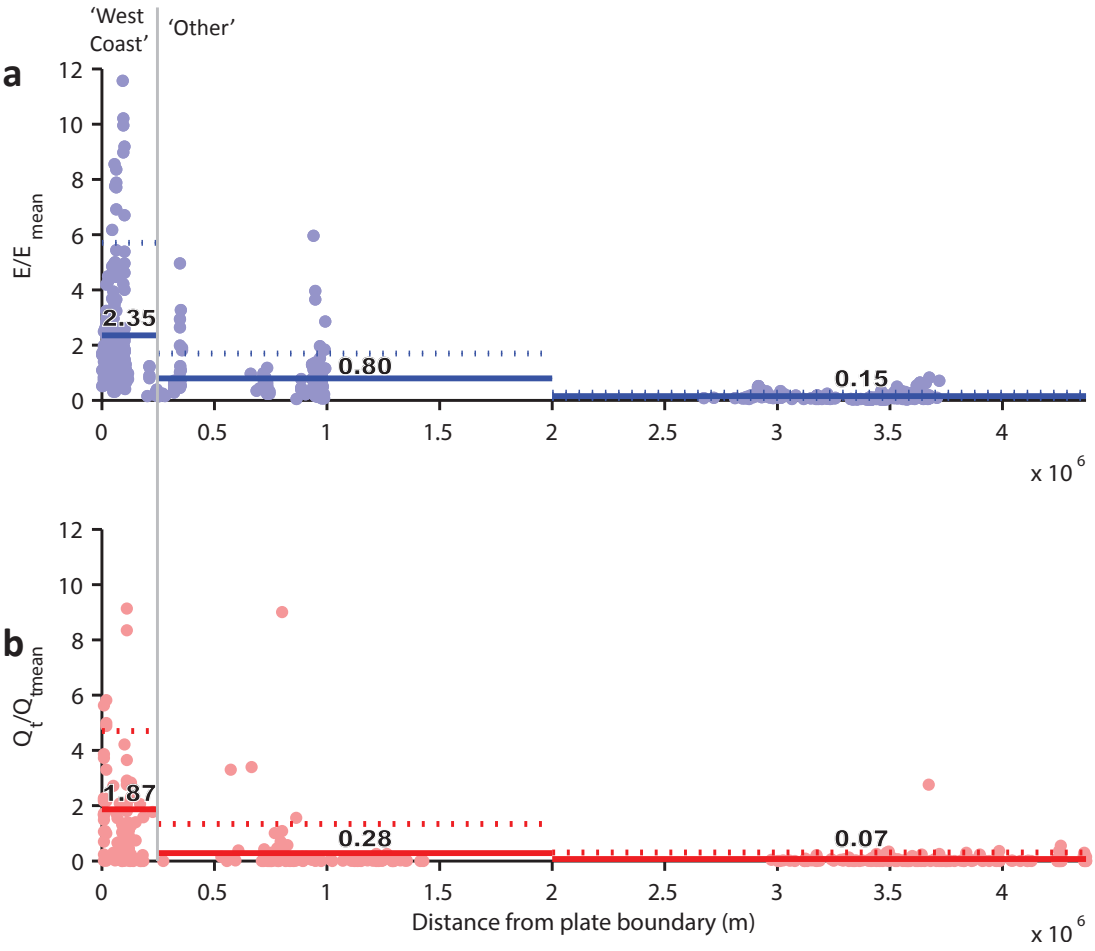

Figure B.1: Transport capacity and erosion rate away from the Pacific Plate boundary. a, Erosion rate as a proportion of mean erosion rate and, b, calculated sediment transport capacity as a proportion of mean sediment transport capacity plotted by distance from the plate boundary. Solid lines mark the means of each region, dotted lines mark one standard deviation. Means for each region are marked in black text. Three high E and one high Q_t points, all within the 'West Coast' region plot off the axes. Sespe Creek, CA and Fish Creek, AK, with Q_t/Q_{tmean} of 93 and 36 respectively, plot above the axes.

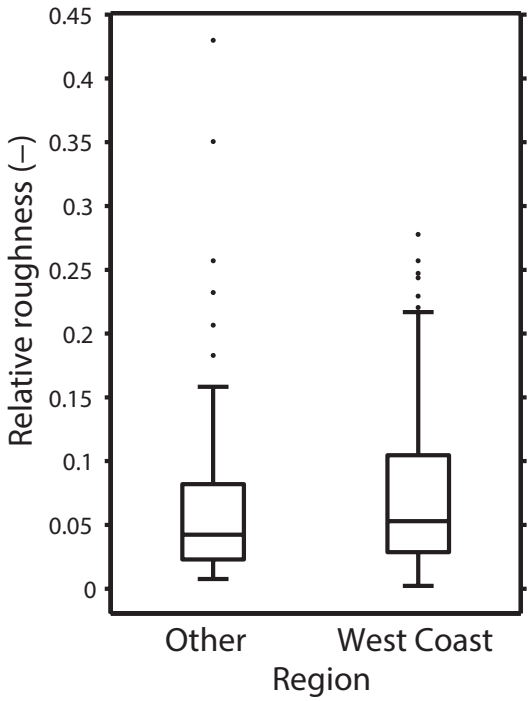

Figure B.2: Boxplot of relative roughness (D_{50}/h) measured at each site in the data compilation, separated by region.

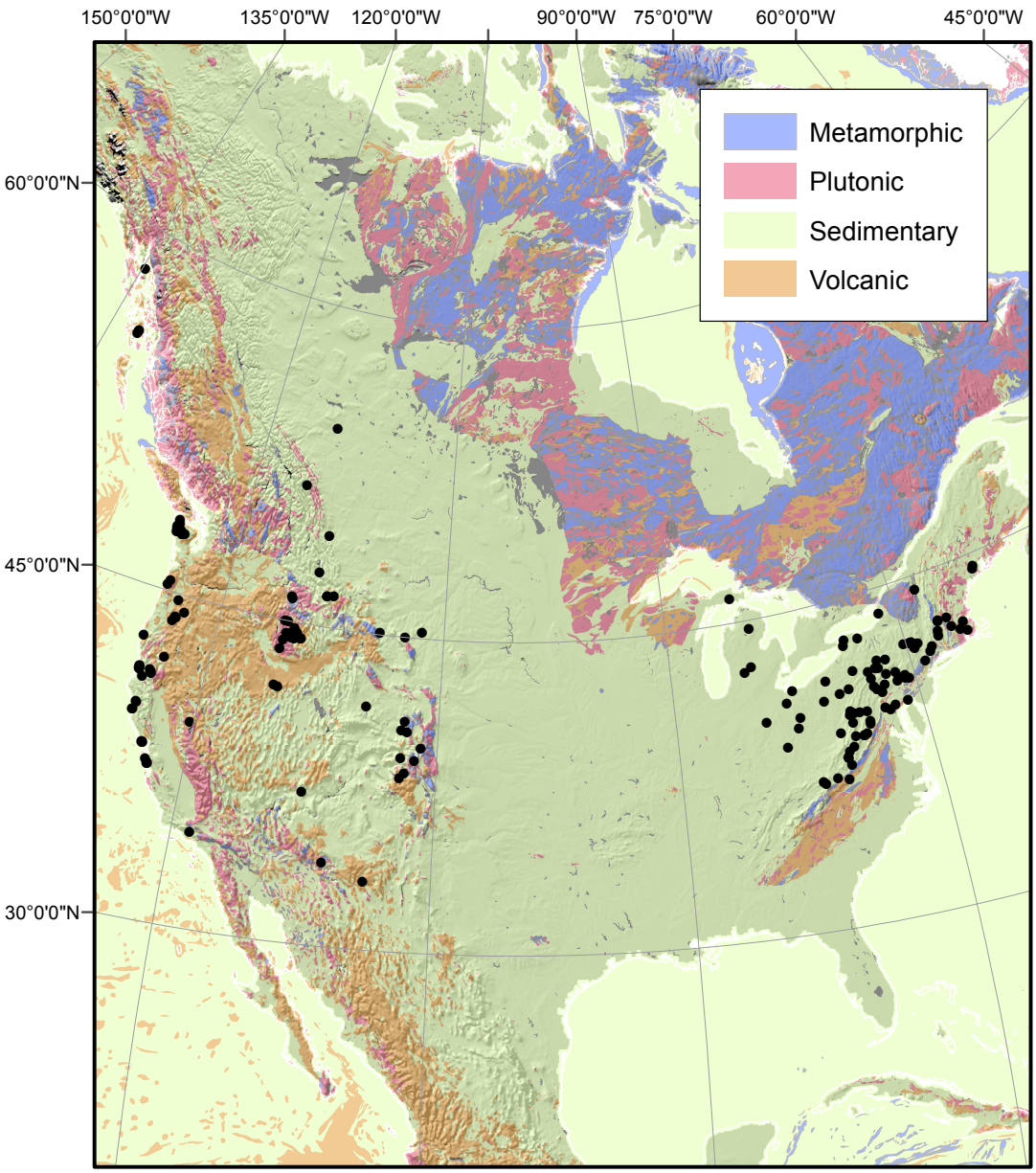

Figure B.3: Shaded relief model overlain by the USGS Geologic Map of North America, separated into broad lithologic categories. Black dots mark the location of sites within our data compilation for which we calculated percent sedimentary bedrock.

Appendix C

Bed mobility supplementary information

C.1 Appendix 1: Sediment Transport Models

C.1.1 Parker (1990)

The sediment transport rate at a given flow is a function of the bed surface grain size distribution, described by fractions (f_i) of median diameters (D_i), as well as the bed surface shear stress, τ:

$$\tau = \rho g R_h S \tag{C.1}$$

Where ρ = the density of water, and R_h is the hydraulic radius. We estimate hydraulic radius as

$$R_h = \frac{wh}{2h + w} \tag{C.2}$$

where h and w are the average flow depth and width associated with the

given discharge. We use hydraulic radius instead of depth in order to more fairly compare between large and small streams.

This stress is non-dimensionalized using the median bed surface grain size to find the Shields stress ($\tau^{\star}_{50}$):

$$\tau^{\star}_{50} = \frac{\tau}{(\rho_s - \rho)gD_{50}} \tag{C.3}$$

where we assume a sediment density, ρ_s, of 2650 kg/m3. Parker defines a non-dimensional (Shields) reference stress ($\tau^{\star}_r$):

$$\tau^{\star}_r = 0.0386 \tag{C.4}$$

ϕ_o is the ratio of the Shields stress of the median grain size to the reference Shields stress:

$$\phi_o = \tau^{\star}_{50}/\tau^{\star}_r \tag{C.5}$$

Straining functions, σ_o and ω_o, are graphical functions of ϕ that are intended to account for changes in bed sorting as transport rate increases. We interpolate values of σ and ω based on tables available online via Parker (1990b).

σ_o is the arithmetic standard deviation of the surface grain size distribution on the phi scale:

$$\sigma_o = \sqrt{\sum \frac{\ln \frac{D_i}{D_{50}}^2}{\ln 2} f_i} \tag{C.6}$$

ω, the straining parameter, varies with σ_ϕ

$$\omega = 1 + \frac{\sigma_\phi}{\sigma_{\phi o}}(\omega_o - 1) \tag{C.7}$$

Parker's hiding function, g_s, comes in the form:

$$g_{si} = 1.048 \frac{D_i}{D_{50ss}}^{-0.0951} \tag{C.8}$$

and is calculated for each grain size fraction (denoted by the subscript i).

The sediment transport rate for each grain size fraction is a function of ϕ_i, which is the product of the straining function, bed surface arithmetic standard deviation, and the hiding function:

$$\phi_i = \phi_o \omega g_{si} \tag{C.9}$$

Finally, the dimensionless transport parameter for each grain size fraction, $W^\star$i is:

$$W_i^\star = 0.00218 G_i \tag{C.10}$$

Where G, the piecewise transport function, is:

$$G_i = \begin{cases} 5474(1 - \frac{0.853}{\phi_i})^{4.5} & \phi_i > 1.59 \\ exp[14.2(\phi_i - 1) - 9.28(\phi_i - 1)^2] & 1 \leq \phi_i \leq 1.59 \\ \phi_i^{14.2} & \phi_i < 1 \end{cases} \tag{C.11}$$

To characterize full-bed mobility, we define a single dimensionless transport parameter, $W^\star$:

$$W^\star = \sum_{i=1}^{n} W_i^\star f_i \tag{C.12}$$

Sediment flux, Q_t, is then:

$$Q_t = W^\star(\tau/\rho)^{3/2} R_s g \tag{C.13}$$

Where R_s is the dimensionless submerged specific gravity of sediment ($(\rho_s - \rho)/\rho$).

C.1.2 Wilcock and Crowe (2003)

The Wilcock and Crowe (2003) transport equations are based on surface mean grain size (D_{sm}):

$$D_{sm} = \sum D_i f_i \tag{C.14}$$

Of note, we calculated D_{sm} using the full grain size distribution, but only calculated transport for gravel size fractions (excluding sand transport).

Wilcock and Crowe suggest a reference Shields stress that varies with the sand content of the bed surface:

$$\tau^\star_{rm} = 0.021 + 0.015 exp(-20F_s) \tag{C.15}$$

Where F_s is the fraction of the bed surface grain size distribution <2mm. Dimensionalizing the reference transport rate, τ_{rm} is:

$$\tau_{rm} = \tau^\star_{rm}(\rho_s - \rho) g D_{sm} \tag{C.16}$$

The hiding function exponent proposed by Wilcock and Crowe (2003) is:

$$b = \frac{0.67}{1 + exp(1.5 - \frac{D_i}{D_{sm}})} \tag{C.17}$$

The reference shear stress used for calculating transport for each grain size

fraction, τ_{ri}, is:

$$\tau_{ri} = \frac{D_i}{D_s m}^{b} \tau_{rm} \tag{C.18}$$

We note that there is some ambiguity in the notation in the original paper, in which D_{50} is used here in place of D_{sm}. We have used D_{sm} in all cases, as Parker (2004) and Cui (2007) in their implementation of the Wilcock and Crowe (2003) equations.

The transport parameter for any given flow and grain size fraction, ϕ_i, is:

$$\phi_i = \frac{\tau_i}{\tau_{ri}} \tag{C.19}$$

The dimensionless transport parameter, $W_i^\star$is:

$$W_i^\star = \begin{cases} 0.002\phi_i^{7.5} & \phi < 1.35 \\ 14(1 - \frac{0.894}{phi_i^{0.5}}) & \phi \geq 1.35 \end{cases} \tag{C.20}$$

Full-distribution transport parameter ($W^\star$) and the dimensional transport rate (Q_t) are calculated as above.

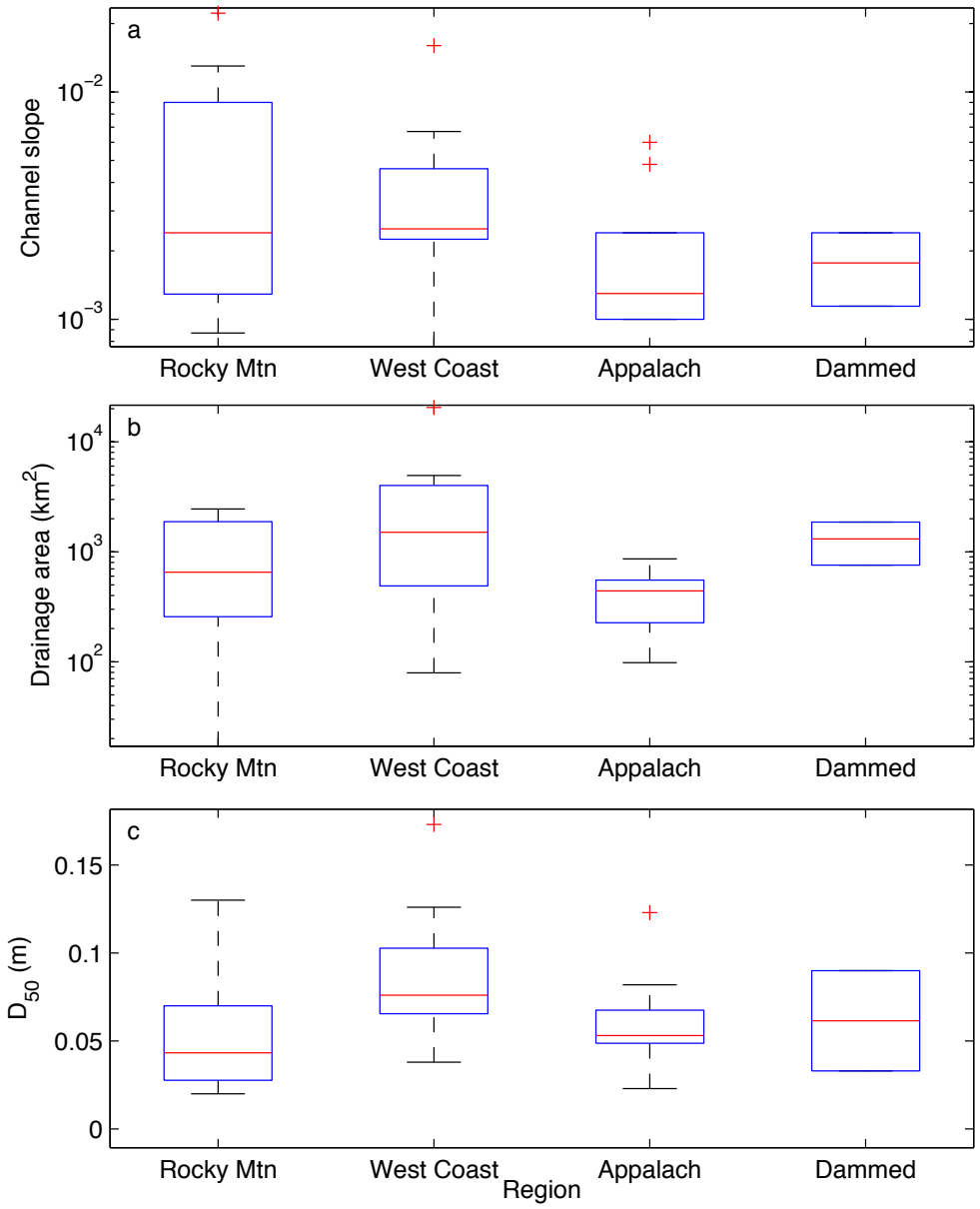

Figure C.1: Channel characteristics separated by region: a) channel slope, b) drainage area, c) median grain size.

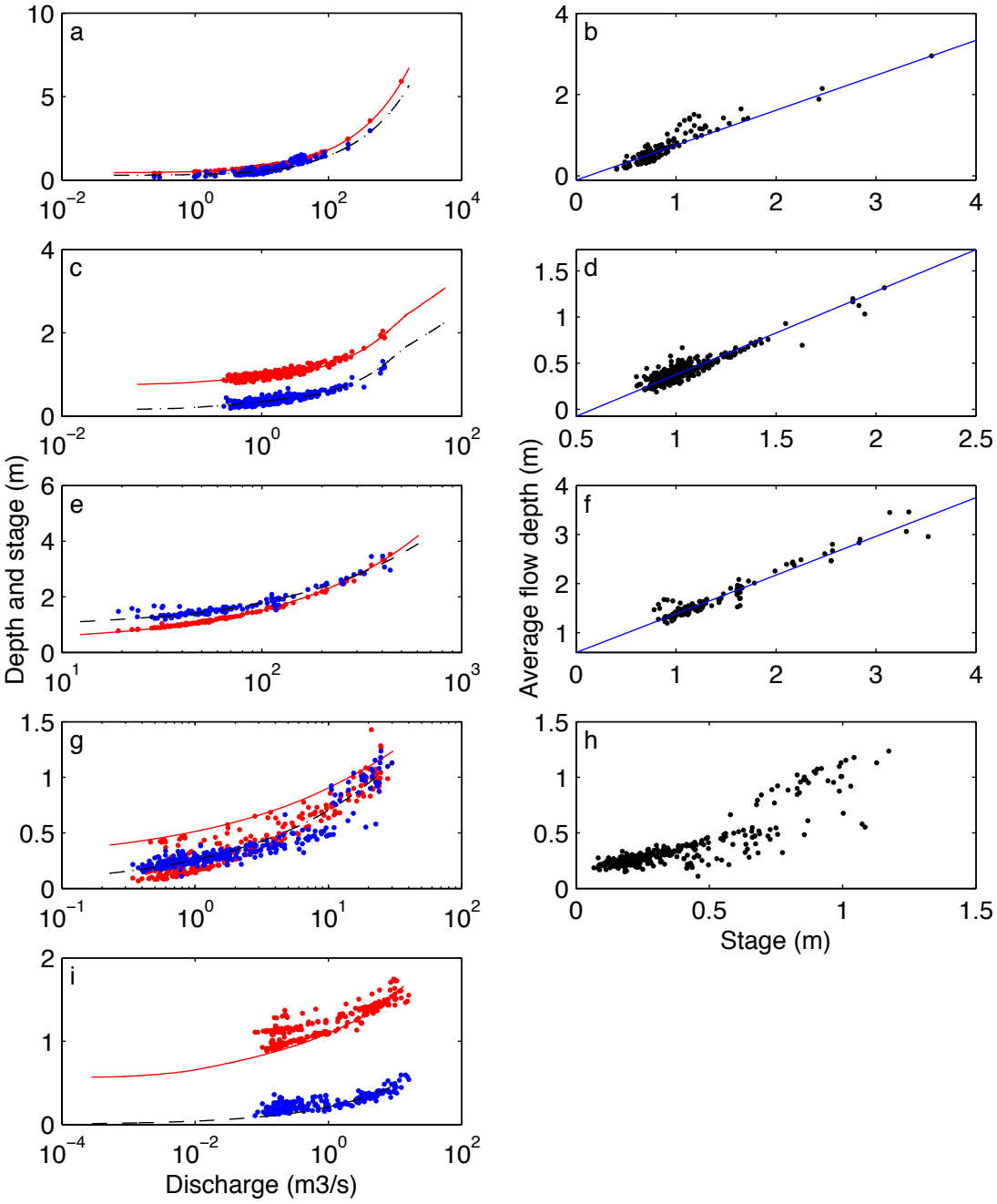

Figure C.2: Modified techniques for converting from stage to average flow depth using USGS field data. Stage shown in red dots, measured average depth in blue dots. USGS rating curve shown in red. Dashed black line marks our average depth rating curve. Plots on the right show the relationship between stage and average flow depth used to determine the average depth rating curve. Figures a-d: depth-stage regression forced through the maximum stage value (default method used in our analysis). Figures e-f: simple regression between depth and stage (unmodified Phillips and Jerolmack (2016) method). Figures g-h: logarithm of data taken before regression. Figure i: measured power-law relationship between discharge and average flow depth (no depth-stage regression required).

Table C.1: Data sources and explanation of sediment supply calculations.

Site	Drainage Area (km^2)	Erosion rate (mm/kyr)	Bedload fraction	Coarse sed supply (m^3/yr)	Sources	Explanation
Lochsa	3056	4.1	0.03	375	Kirchner et al. (2001); USFS BAT	Bedload fraction calculated from USFS bedload and suspended load rating curves for bankfull flow. Short term erosion rate is an average from detention basins in nearby small drainages.
Selway	4947	4.1	0.06	1214	Kirchner et al. (2001); USFS BAT	
Salmon	855	4.1	0.5	1748	Kirchner et al. (2001); USFS BAT	
Sespe	652	600	0.1	39120	Stillwater Sciences	Erosion rate based on sediment retention basins in the Sespe Creek watershed.
Chetco	702			48458	O'Connor (2014)	Coarse sediment load modeled
Applegate	1994			52344	O'Connor (2014)	same as above
Nehalem	1844			11350	O'Connor (2014)	same as above
Puyallup	2455		0.12	64630	Czuba et al (2010)	Total sediment load is the average of 3 independent estimates reported by Czuba et al. (2010)
Nisqually	344			124362	Anderson and Pitlick (2014)	Based on bed material estimated from downstream reservoir, minus the proportion of sediment contributed by one minor tributary.

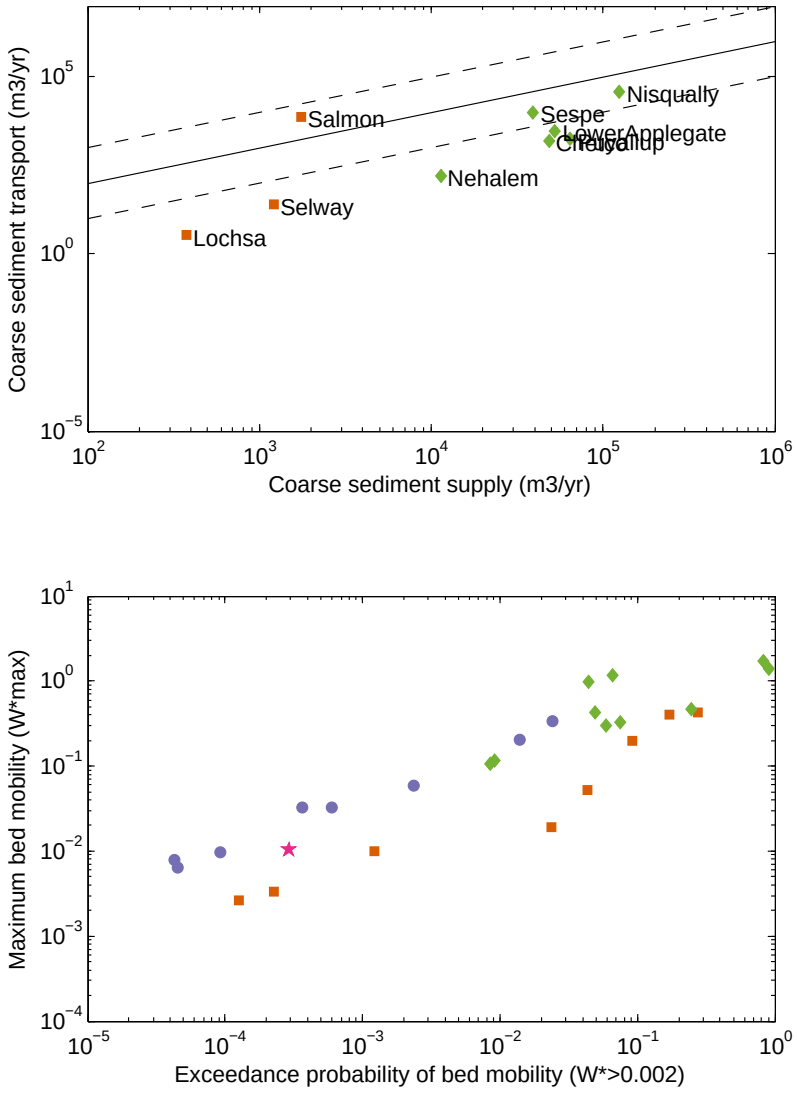

Figure C.3: Output from model results using Wilcock and Crowe (2003), no modifications. See Figures 5 and 7 for legend information. Note the consistent under-prediction of transport, relative to supply.

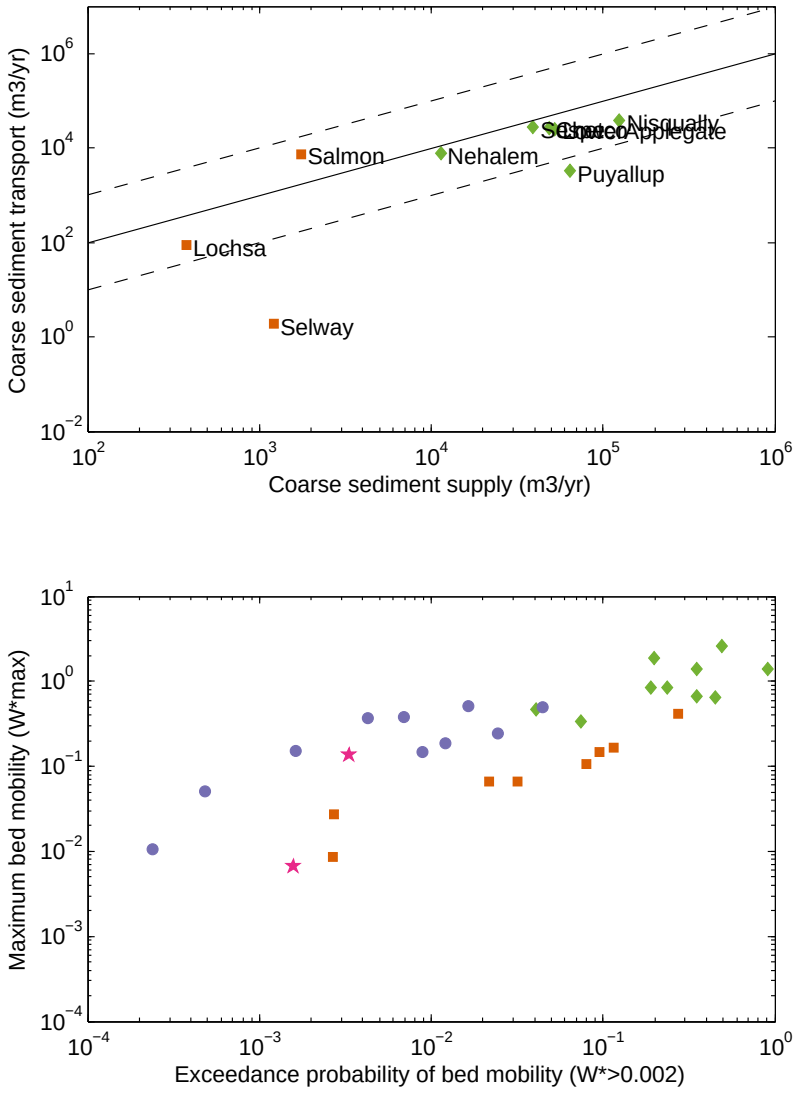

Figure C.4: Wilcock and Crowe (2003), modified with Lamb et al. (2008) reference Shields stress.

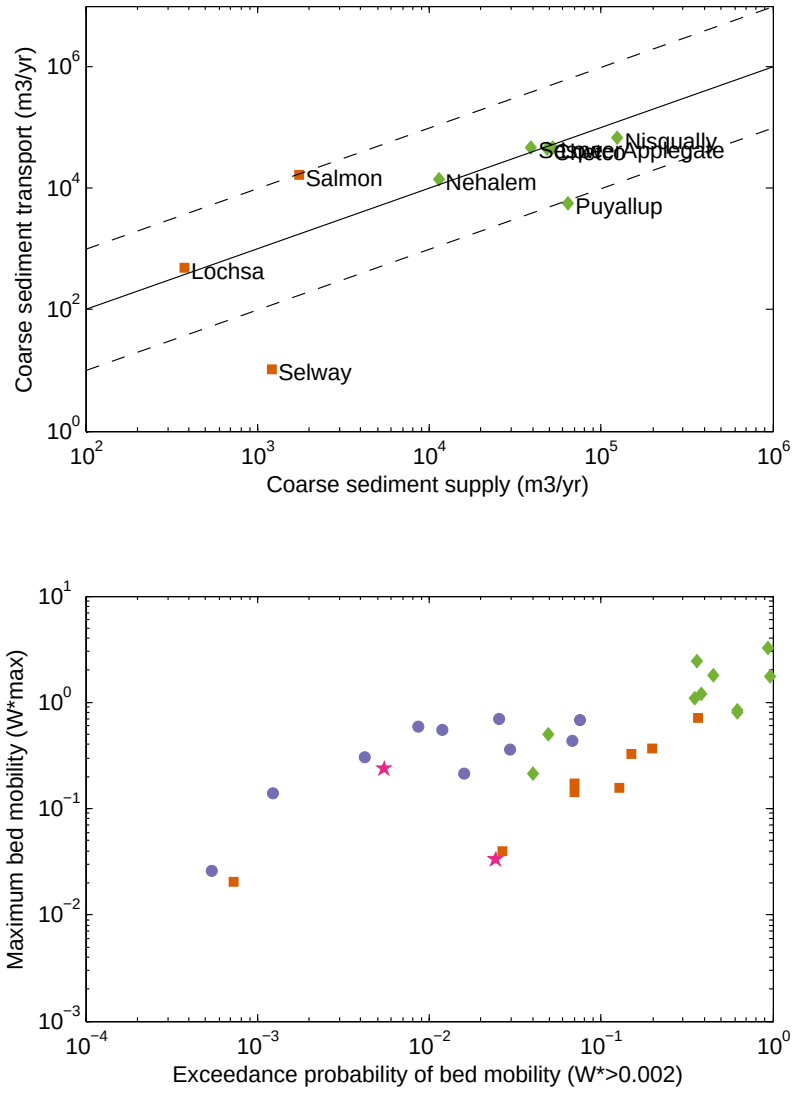

Figure C.5: Wilcock and Crowe (2003), modified with Mueller et al. (2005) reference Shields stress. Note that several West Coast rivers have mobile beds more than 50% of the time.

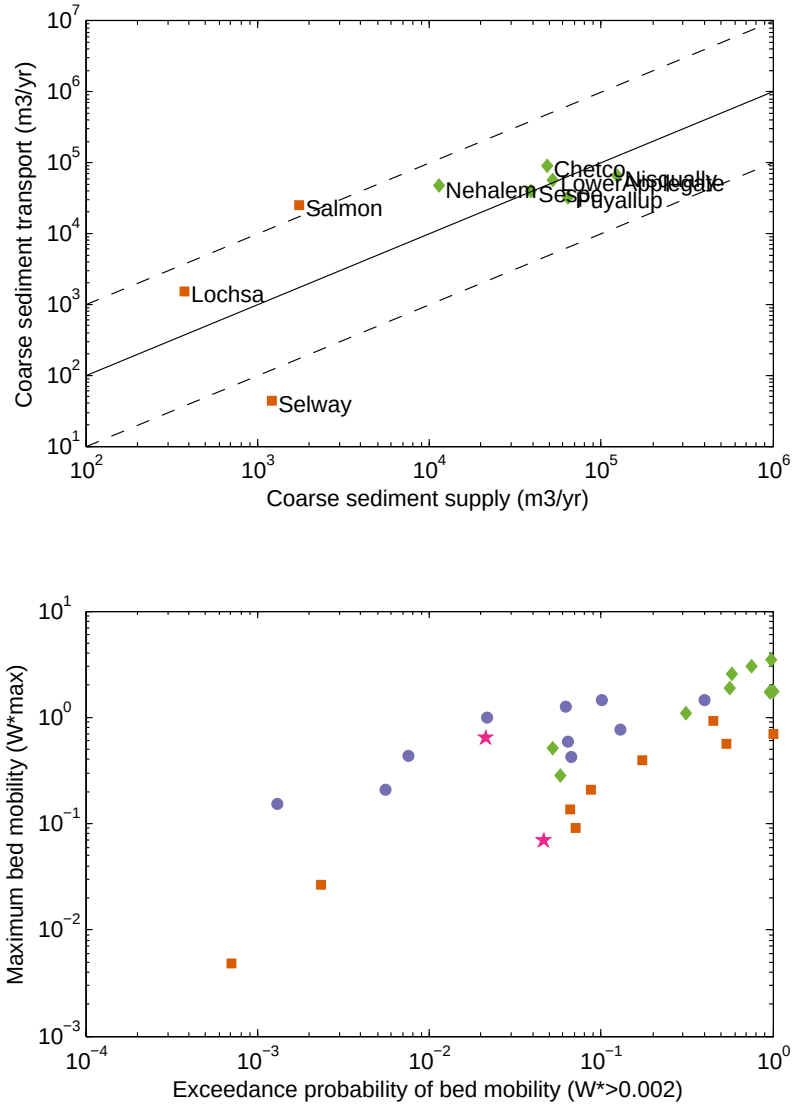

Figure C.6: Wilcock and Crowe (2003), modified with Pitlick et al. (2008) reference Shields stress. Again, note that many rivers are mobile more than 50% of the time.

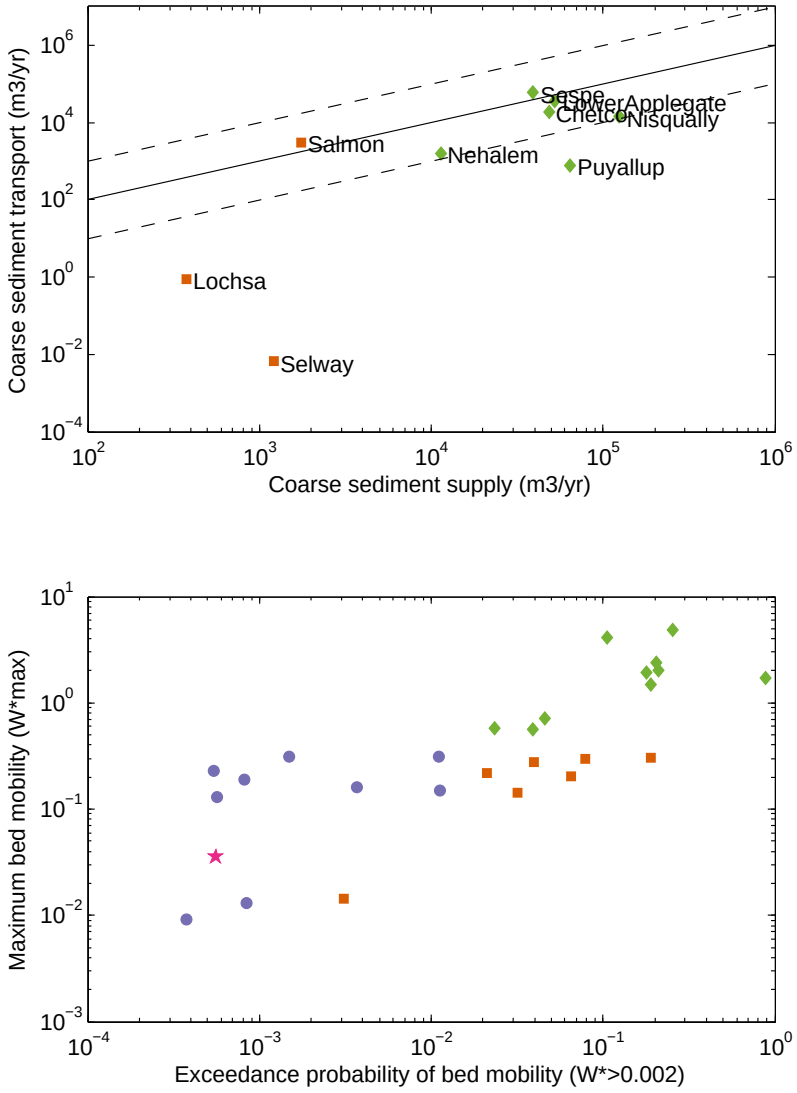

Figure C.7: Unmodified Parker (1990).

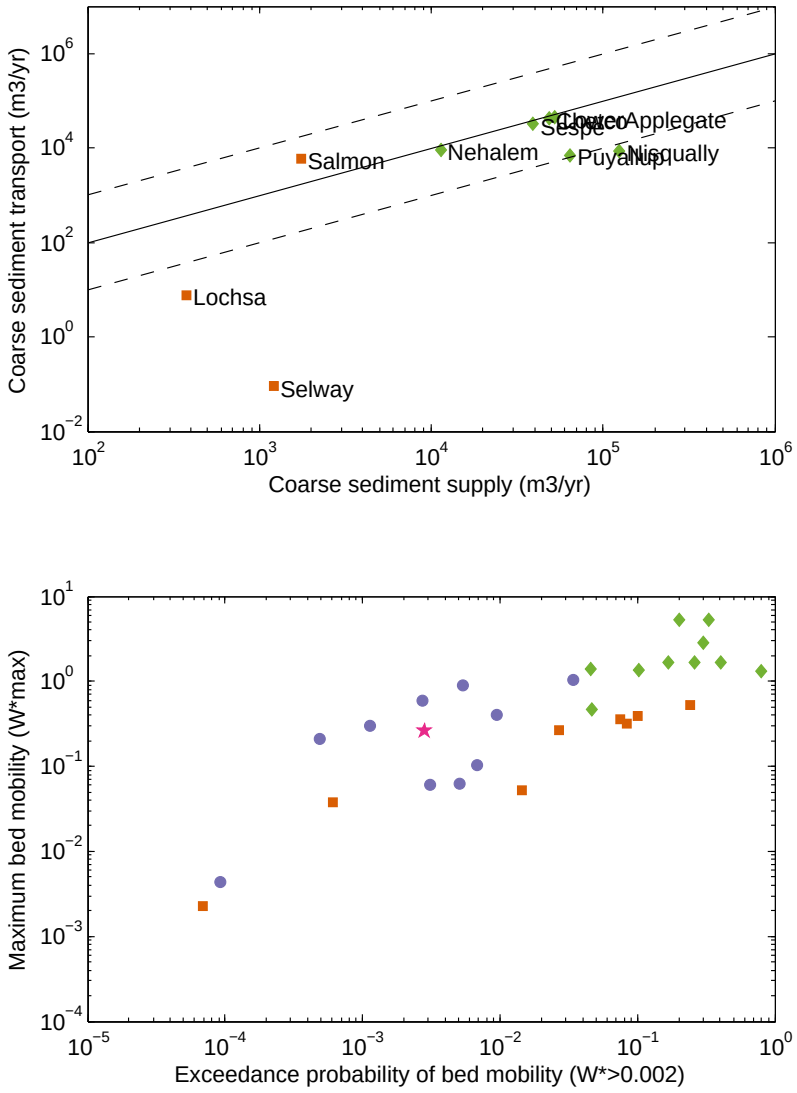

Figure C.8: Parker (1990), modified with Lamb et al. (2008) reference Shields stress.

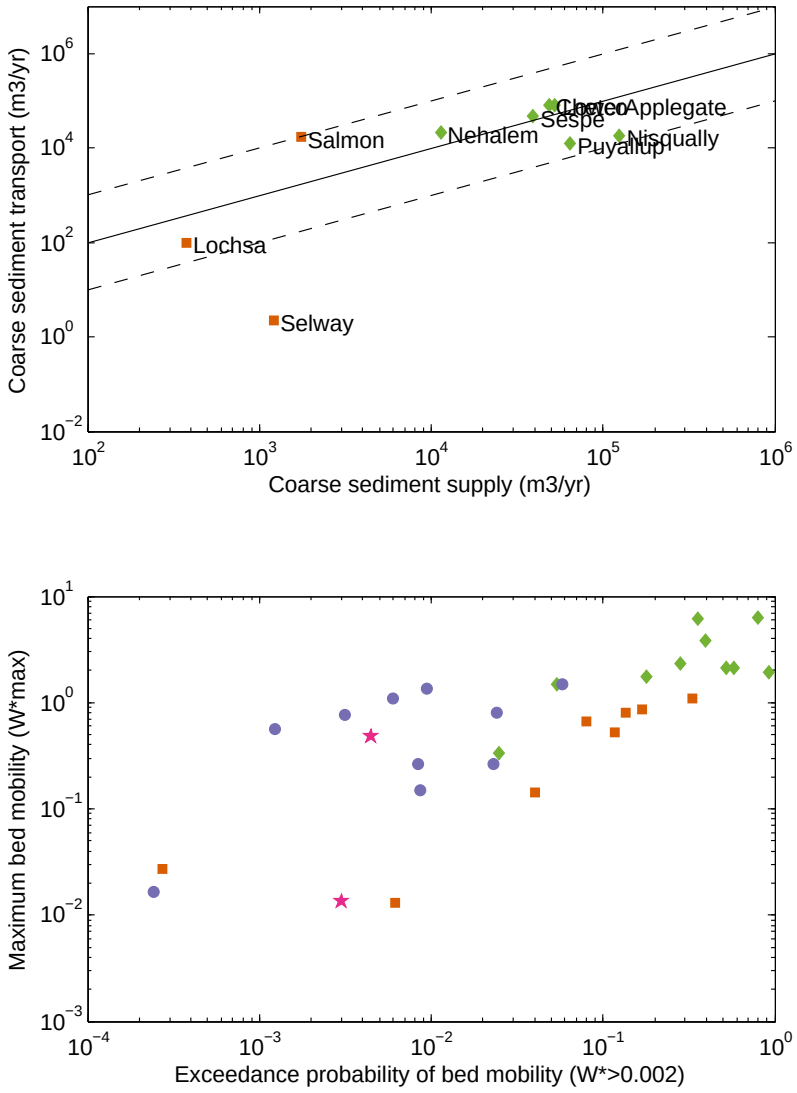

Figure C.9: Parker (1990), modified with Mueller et al. (2005) reference Shields stress. Note that several West Coast rivers are mobile more than 50% of the time.

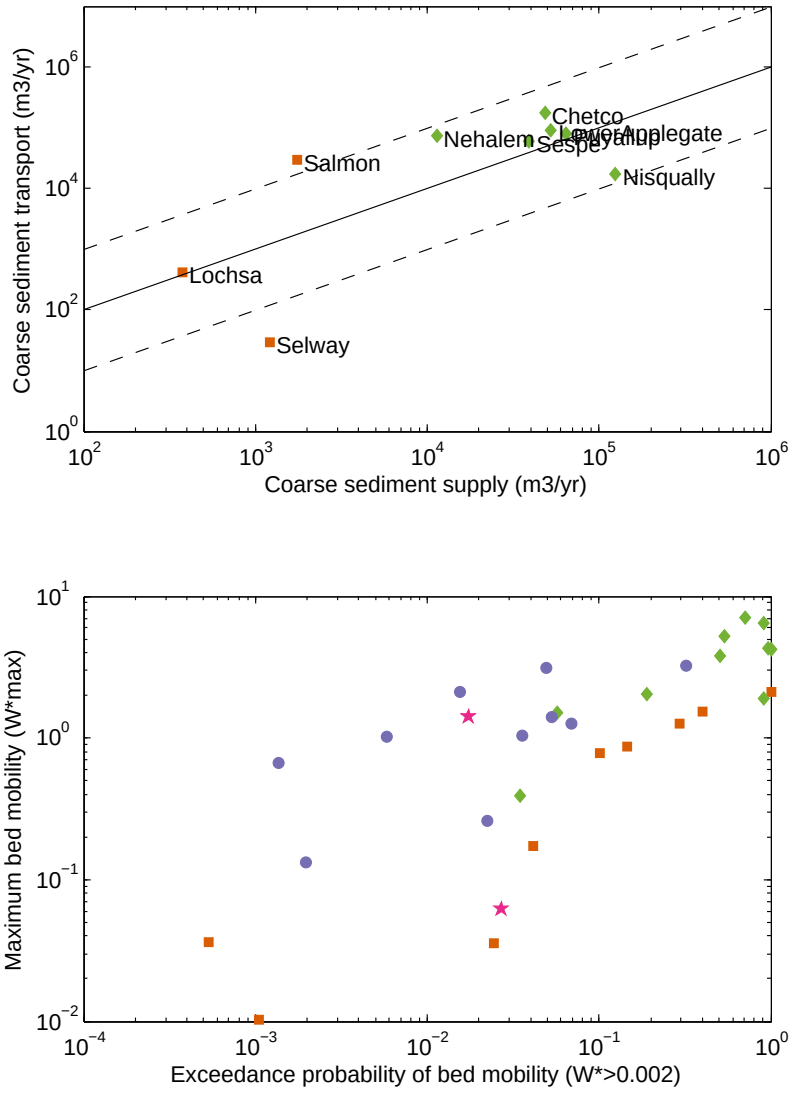

Figure C.10: Parker (1990), modified with Pitlick et al. (2008) reference Shields stress. Note that most West Coast rivers are mobile more than 50% of the time.

Bibliography

Albertson, L. K., B. J. Cardinale, and L. S. Sklar (2014), Non-additive increases in sediment stability are generated by macroinvertebrate species interactions in laboratory streams, *PLoS ONE*, *9*(8), doi: 10.1371/journal.pone.0103417.

Anderson, R. S. (1990), Evolution of the Northern Santa Cruz Mountains by advection of crust past a San Andreas Fault bend., *Science (New York, N.Y.)*, *249*(4967), 397–401, doi: 10.1126/science.249.4967.397.

Andrews, E. (1984), Bed-material entrainment and hydraulic geometry of gravel-bed rivers in Colorado, *Geological Society of America Bulletin*, *95*, 371–378, doi: 10.1130/0016-7606(1984)95<371.

Andrews, E. (1994), Marginal bed load transport in a gravel bed stream, *Water Resources Research*, *30*(7), 2241–2250.

Balco, G., N. Finnegan, A. Gendaszek, J. O. H. Stone, and N. Thompson (2013), Erosional response to northward-propagating crustal thickening in the coastal ranges of the U.S. Pacific Northwest, *American Journal of Science*, *313*(8), 790–806, doi: 10.2475/11.2013.01.

Barnes, H. H. (1967), Roughness Characteristics of Natural Channels, *Technical Report, Geological Survey Water-Supply, United States Government Printing Office, Washington, U.S.A*, p. 219, doi: 10.1016/0022-1694(69)90113-9.

Benda, L., and P. Bigelow (2014), On the patterns and processes of wood in northern California streams, *Geomorphology*, *209*, 79–97, doi: 10.1016/j.geomorph.2013.11.028.

Benda, L. E., and J. C. Sias (2003), A quantitative framework for evaluating the mass balance of in-stream organic debris, *Forest Ecology and Management*, *172*(1), 1–16, doi: 10.1016/S0378-1127(01)00576-X.

Bilby, R., and J. Ward (1991), Characteristics and function of large woody debris in streams draining old-growth, clear-cut, and second-growth forests in southwestern Washington, *Canadian Journal of Fisheries and Aquatic Sciences*, *48*, 2499–2508.

Bjornn, T., and D. Reiser (1991), Habitat requirements of salmonids in streams, in *Influences of Forest and Rangeland Management on Salmonid Fishes and Their Habitats. American Fisheries Society Special Publication 19*, edited by W. Meehan, pp. 83–183, American Fisheries Society, Bethesda, MD.

Booker, D. J., M. J. Dunbar, and A. Ibbotson (2004), Predicting juvenile salmonid drift-feeding habitat quality using a three-dimensional hydraulic-bioenergetic model, *Ecological Modelling*, *177*(1-2), 157–177, doi: 10.1016/j.ecolmodel.2004.02.006.

Brabb, E. E. (1989), Geologic map of Santa Cruz County, California.

Braudrick, C., W. Dietrich, G. Leverich, and L. Sklar (2009), Experimental evidence for the conditions necessary to sustain meandering in coarse-bedded rivers, *Proceedings of the National Academy of Sciences*, *106*(40), 16,936–16,941, doi: 10.1073/pnas.0909417106.

Brewin, P., S. Buckton, and S. Ormerod (2000), The seasonal dynaimcs and presistence of stream macroinvertebrates in Nepal: Do monsoon flood represent disturbance?, *Freshwater Biology*, *44*, 581–594.

Briggs, J. (1953), Fish Bulletin No. 94. The Behavior and Reproduction of Salmonid Fishes in a Small Coastal Stream, *Marine Fisheries Branch Bulletin*, pp. 1–66.

Buffington, J., and D. Montgomery (1999a), Effects of hydraulic roughness on surface textures of gravel-bed rivers, *Water Resources Research*, *35*(11), 3507–3521.

Buffington, J., and D. Montgomery (1999b), Effects of sediment supply on surface textures of gravel-bed rivers, *Water Resources Research*, *35*(11), 3523–3530.

Buffington, J., D. R. Montgomery, and H. M. Greenberg (2004), Basin-scale availability of salmonid spawning gravel as influenced by channel type and hydraulic roughness in mountain catchments, *Canadian Journal of Fisheries and Aquatic Sciences*, *61*, 2085–2096, doi: 10.1139/F04-141.

Buffington, J. M., and D. R. Montgomery (1997), A systematic analysis of eight decades of incipient motion studies, with special reference to gravel-bedded rivers, *Water Resources Research*, *33*(8), 1993–2029, doi: 10.1029/96WR03190.

Buffington, J. M., D. J. Isaak, and R. F. Thurow (2003), Hydraulic control on the spatial distribution of Chinook salmon spawning gravels in central Idaho: Integrating reach-scale predictions via digital elevation models, *Eos, Transactions, American Geophysical Union,*, *84*(46), Fall Meeting Supplement, Abstract H32F–01.

Bunte, K., and S. R. Abt (2001), Sampling Surface and Subsurface Particle-Size Distributions in Wadable Gravel- and Cobble-Bed Streams for Analyses in Sediment Transport, Hydraulics, and Streambed Monitoring, *General technical report rmrs-gtr-74*, USDA Forest Service, Rocky Mountain Research Station, Fort Collins, Colorado, doi: 10.1017/CBO9781107415324.004.

Bunte, K., S. R. Abt, K. W. Swingle, D. A. Cenderelli, and J. M. Schneider (2013), Critical Shields values in coarse-bedded steep streams, *Water Resources Research*, *49*(11), 7427–7447, doi: 10.1002/2012WR012672.

Bürgmann, R., R. Arrowsmith, T. Dumitru, and R. McLaughlin (1994), Rise and fall of the southern Santa Cruz Mountains, California, from fission tracks, geomorphology, and geodesy, doi: 10.1029/94JB00131.

Burnett, K. M., G. H. Reeves, D. J. Miller, S. Clarke, K. Vance-Borland, and K. Christiansen (2007), Distribution of salmon-habitat potential relative to landscape characteristics and implications for conservation., *Ecological applications : a publication of the Ecological Society of America*, *17*(1), 66–80.

Cal Poly Swanton Pacific Ranch (2012), Mission & History - The History of Swanton Ranch as told by Al Smith, July, 1990.

Carling, P. A., and H. G. Orr (2000), Morphology of riffle-pool sequences in the River Severn, England, *Earth Surface Processes and Landforms*, *25*, 369–384.

Church, M., and M. a. Hassan (2002), Mobility of bed material in Harris Creek, *Water Resources Research*, *38*(11), 19–1–19–12, doi: 10.1029/2001WR000753.

Crisp, D. T., and P. a. Carling (1989), Observations on siting, dimensions and structure of salmonid redds, *Journal of Fish Biology*, *34*(1), 119–134.

Davey, C., and M. Lapointe (2007), Sedimentary links and the spatial organization of Atlantic salmon (Salmo salar) spawning habitat in a Canadian Shield river, *Geomorphology*, *83*(1-2), 82–96, doi: 10.1016/j.geomorph.2006.06.011.

DiBiase, R. A., K. X. Whipple, A. M. Heimsath, and W. B. Ouimet (2010), Landscape form and millennial erosion rates in the San Gabriel Mountains, CA, *Earth and Planetary Science Letters*, *289*(1-2), 134–144, doi: 10.1016/j.epsl.2009.10.036.

Dietrich, W. E., J. W. Kirchner, H. Ikeda, and F. Iseya (1989), Sediment supply and the development of the coarse surface layer in gravel-bedded rivers, *Nature*, *340*(6230), 215–217, doi: 10.1038/340215a0.

Eaton, B. C., and M. Church (2009), Channel stability in bed load-dominated streams with nonerodible banks: Inferences from experiments in a sinuous flume, *Journal of Geophysical Research: Earth Surface*, *114*(1), 1–17, doi: 10.1029/2007JF000902.

Eaton, B. C., and T. R. Giles (2008), Assessing the effect of vegetation-related bank strength on channel morphology and stability in gravel-bed streams using numerical models, *Earth Surface Processes and Landforms*, *34*(5), 712–724, doi: 10.1002/esp.

Efron, B. (1987), Better bootstrap confidence intervals, *Journal of the American statistical Association*, *82*(397), 171–185.

Fernandez-Luque, R., and R. Van Beek (1976), Erosion and Transport of Bed-Load Sediment, *Journal of Hydraulic Research*, *14*(2), 127–144.

Finnegan, N. J., and G. Balco (2013), Sediment supply, base level, braiding, and bedrock river terrace formation: Arroyo Seco, California, USA, *Geological Society of America Bulletin*, *125*(7-8), 1114–1124, doi: 10.1130/B30727.1.

Friedman, G. M. (1987), Vertical movements of the crust: Case histories from the northern Appalachian Basin, *Geology*, *15*(12), 1130–1133, doi: 10.1130/0091-7613(1987)15<1130:VMOTCC>2.0.CO;2.

Ganti, V., C. V. Hagke, D. Scherler, M. P. Lamb, W. W. Fischer, and J.-p. Avouac (2016), Time scale bias in erosion rates of glaciated landscapes, *Science Advances*, *2*.

Garrity, C. P., and D. R. Soller (2009), Database of the Geologic Map of North America; adapted from the map by J.C. Reed, Jr. and others (2005), *U.s. geological survey data series 424*, U.S. Geological Survey Data Series 424.

Geist, D. R., and D. D. Dauble (1998), Redd Site Selection and Spawning Habitat Use by Fall Chinook Salmon: The Importance of Geomorphic Features in Large Rivers, *Environmental management*, *22*(5), 655–69.

Geist, D. R., J. Jones, C. J. Murray, and D. D. Dauble (2000), Suitability criteria analyzed at the spatial scale of redd clusters improved estimates of fall chinook salmon (Oncorhynchus tshawytscha) spawning habitat use in the Hanford Reach , Columbia River, *Canadian Journal of Fisheries and Aquatic Sciences*, *57*, 1636–1646.

Gibbins, C., D. Vericat, and R. J. Batalla (2007), When is stream invertebrate drift catastrophic? The role of hydraulics and sediment transport in initiating drift during flood events, *Freshwater Biology*, *52*(12), 2369–2384, doi: 10.1111/j.1365-2427.2007.01858.x.

Gomez, B., and M. Church (1989), An assessment of bed load sediment transport formulae for gravel bed rivers, *Water Resources Research*, *25*(6), 1161–1186, doi: 10.1029/WR025i006p01161.

Gorman, A. M., P. J. Whiting, T. M. Neeson, and J. F. Koonce (2011), Channel substrate prediction from GIS for habitat estimation in Lake Erie tributaries, *Journal of Great Lakes Research*, *37*(4), 725–731, doi: 10.1016/j.jglr.2011.08.008.

Gudmundsdottir, M. H., K. Blisniuk, Y. Ebert, N. M. Levine, D. H. Rood, A. Wilson, and G. E. Hilley (2013), Restraining bend tectonics in the Santa Cruz Mountains, California, imaged using 10Be concentrations in river sands, *Geology*, *41*(8), 843–846, doi: 10.1130/G33970.1.

Hanrahan, T. P. (2007), Bedform morphology of salmon spawning areas in a large gravel-bed river, *Geomorphology*, *86*(3-4), 529–536, doi: 10.1016/j.geomorph.2006.09.017.

Hassan, M. A., R. Egozi, and G. Parker (2006), Experiments on the effect of hydrograph characteristics on vertical grain sorting in gravel bed rivers, *Water Resources Research*, *42*(9), 1–15, doi: 10.1029/2005WR004707.

Hassan, M. A., D. Brayshaw, Y. Alila, and E. Andrews (2014), Effective discharge in small formerly glaciated mountain streams of British Columbia: Limitations and implications, *Water Resources Research*, *50*(5), 4440–4458, doi: 10.1002/2013WR014529.

Hayes, S., M. Bond, C. Hanson, and R. MacFarlane (2004), Interactions between endangered wild and hatchery salmonids: can the pitfalls of artificial propagation be avoided in small coastal streams?, *Journal of Fish Biology*, *65*, 101–121, doi: 10.1111/j.1095-8649.2004.00547.x.

Hilldale, R., and D. Raff (2008), Assessing the ability of airborne LiDAR to map river bathymetry, *Earth Surface Processes and Landforms*, *783*, 773–783, doi: 10.1002/esp.

Hirschboeck, K. K. (1991), Climate and floods: National Water Summary 1988-1989-Hydrologic events and floods and droughts, *United States Geological Survey Water Supply Paper*, *2375*, 67–88.

Isaak, D. J., and R. F. Thurow (2006), Network-scale spatial and temporal variation in Chinook salmon (Oncorhynchus tshawytscha) redd distributions: patterns inferred from spatially continuous replicate surveys, *Canadian Journal of Fisheries and Aquatic Sciences*, *63*(2), 285–296, doi: 10.1139/f05-214.

Isaak, D. J., R. F. Thurow, B. E. Rieman, and J. B. Dunham (2007), Chinook salmon use of spawning patches: relative roles of habitat quality, size, and connectivity., *Ecological applications : a publication of the Ecological Society of America*, *17*(2), 352–64.

Johnson, M. F., I. Reid, S. P. Rice, and P. J. Wood (2009), Stabilization of fine gravels by net-spinning caddisfly larvae, *Earth Surface Processes and Landforms*, *34*(3), 413–423, doi: 10.1002/esp.1750.

Keller, E., and W. Melhorn (1978), Rhythmic spacing and origin of pools and riffles, *Geological Society of America Bulletin*, *89*(5), 723–730, doi: 10.1130/0016-7606(1978)89<723.

King, J., W. W. Emmett, P. J. Whiting, R. P. Kenworthy, and J. J. Barry (2004), Sediment transport data and related infornation for selected coarse-bed streams and rivers in Idaho, *Tech. rep.*, U.S. Department of Agriculture, Forest Service, Rocky Mountain Research Station., Fort Collins, CO.

Kirchner, J. W. (2001), Data Repository, *Geology*.

Kirchner, J. W., W. E. Dietrich, F. Iseya, and H. Ikeda (1990), The variability of critical shear stress, friction angle, and grain protrusion in water worked sediments, *Sedimentology*, *37*, 647–672.

Klier, R. (2014), A field test of the influence of grain size in determining bedrock river channel slope, Ms, University of California Santa Cruz.

Knapp, R. A., and H. K. Preisler (1999), Is it possible to predict habitat use by spawning salmonids? A test using California golden trout (Oncorhynchus mykiss aguabonita), *Canadian Journal of Fisheries and Aquatic Sciences*, *56*(9), 1576–1584, doi: 10.1139/f99-081.

Kondolf, G., and G. Cada (1991), Distribution and stability of potential salmonid spawning gravels in steep boulder-bed streams of the eastern Sierra Nevada, *Transactions of the American Fisheries Society*, *120*(2), 177–186, doi: 10.1577/1548-8659(1991)120.

Kondolf, G. M., and M. G. Wolman (1993), The sizes of salmonid spawning gravels, *Water Resources Research*, *29*(7), 2275, doi: 10.1029/93WR00402.

Lamb, M. P., W. E. Dietrich, and J. G. Venditti (2008), Is the critical Shields stress for incipient sediment motion dependent on channel-bed slope?, *Journal of Geophysical Research*, *113*(F2), F02,008, doi: 10.1029/2007JF000831.

Larsen, C. F., K. A. Echelmeyer, J. T. Freymueller, and R. J. Motyka (2003), Tide gauge records of uplift along the northern Pacific-North American plate boundary, 1937 to 2001, *Journal of Geophysical Research*, *108*(B4), doi: 10.1029/2001JB001685.

Leopold, L. B., and T. Maddock (1953), The Hydraulic Geomtry of Stream Channels and Some Physiographic Implications, *Geological Survey Professional Paper 252*, p. 57.

Leopold, L. B., M. G. Wolman, and J. P. Miller (1964), *Fluvial Processes in Geomorphology*, 522 pp., W. H. Freeman, New York.

Li, C., M. J. Czapiga, E. C. Eke, E. Viparelli, and G. Parker (2014), Variable Shields number model for river bankfull geometry: bankfull shear velocity is viscosity-dependent but grain size-independent, *Journal of Hydraulic Research*, *1686*(January), 1–13, doi: 10.1080/00221686.2014.939113.

Li, C., M. Czapiga, E. Eke, E. Viparelli, and G. Parker (2016), Closure to "Variable Shields number model for river bankfull geometry: Bankfull shear velocity is viscosity-dependent but grain size-independent", *Journal of Hydraulic Research*, *54*(2), doi: 10.1080/00221686.2015.1137088.

Li, R. M. (1975), Mathematical modeling of response from small watershed, Unpublished phd dissertation, Colorado State University, Fort Collins, Colorado.

Lisle, T. E., J. M. Nelson, J. Pitlick, M. A. Madej, and B. L. Barkett (2000), Variability of bed mobility in natural, gravel-bed channels and adjustments to sediment load at local and reach scales, *Water Resources Research*, *36*(12), 3743–3755, doi: 10.1029/2000WR900238.

Madej, M. A., D. G. Sutherland, T. E. Lisle, and B. Pryor (2009), Channel responses to varying sediment input: A flume experiment modeled after Redwood Creek, California, *Geomorphology*, *103*(4), 507–519, doi: 10.1016/j.geomorph.2008.07.017.

Manga, M., and J. Kirchner (2000), Stress partitioning in streams by large woody debris, *Water Resources Research*, *36*(8), 2373–2379.

Manning, R. (1891), On the flow of water in open channels and pipes, *Transactions of the Institute of Civil Engineering of Ireland*, *20*, 161–207.

Mark, D. M., and M. Church (1977), On the misuse of regression in earth science, *Mathematical Geology*, *9*(1), 63–75.

Masteller, C. C., and N. J. Finnegan (2017), Interplay between grain protrusion and sediment entrainment in an experimental flume, *Journal of Geophysical Research: Earth Surface*, *122*(1), 274–289, doi: 10.1002/2016JF003943.

Matmon, A., P. R. Bierman, J. Larsen, S. Southworth, M. Pavich, and M. Caffee (2003), Temporally and spatially uniform rates of erosion in the southern Appalachian Great Smoky Mountains, *Geology*, *31*(2), 155–158, doi: 10.1130/0091-7613(2003)031<0155:TASURO>2.0.CO;2.

May, C. L., and T. E. Lisle (2012), River profile controls on channel morphology, debris flow disturbance, and the spatial extent of salmonids in steep mountain streams, *Journal of Geophysical Research*, *117*, 1–15, doi: 10.1029/2011JF002324.

May, C. L., B. Pryor, T. E. Lisle, and M. Lang (2009), Coupling hydrodynamic modeling and empirical measures of bed mobility to predict the risk of scour and fill of salmon redds in a large regulated river, *Water Resources Research*, *45*(5), 1 – 22, doi: 10.1029/2007WR006498.

McKean, J. A., D. J. Isaak, and C. W. Wright (2008), Geomorphic controls on salmon nesting patterns described by a new, narrow-beam terrestrialâĂŞaquatic lidar, *Frontiers in Ecology and the Environment*, *6*(3), 125–130, doi: 10.1890/070109.

Milne, J. (1982), Bed-material size and the riffle-pool sequence, *Sedimentology*, *29*, 267–278.

Minear, J. T. (2010), The Downstream Geomorphic Effect of Dams: A Comprehensive and Comparative Approach, Dissertation, University of California, Berkeley.

Moir, H. J., and G. B. Pasternack (2008), Relationships between mesoscale morphological units, stream hydraulics and Chinook salmon (Oncorhynchus tshawytscha) spawning habitat on the Lower Yuba River, California, *Geomorphology*, *100*(3-4), 527–548, doi: 10.1016/j.geomorph.2008.02.001.

Moir, H. J., and G. B. Pasternack (2010), Substrate requirements of spawning chinook salmon (Onchorhyncus tshawytscha) are dependent on local channel hydraulics, *River Research and Applications*, *26*, 456–468, doi: 10.1002/rra.

Montgomery, D., and J. Buffington (1997), Channel-reach morphology in mountain drainage basins, *Geological Society of America Bulletin*, *109*(5), 596–611.

Montgomery, D. R., J. M. Buffington, R. D. Smith, K. M. Schmidt, and G. Pess (1995), Pool Spacing in Forest Channels, *Water Resources Research*, *31*(4), 1097–1105, doi: 10.1029/94WR03285.

Montgomery, D. R., J. M. Buffington, N. P. Peterson, D. Schuett-Hames, and T. P. Quinn (1996), Stream-bed scour, egg burial depths, and the influence

of salmonid spawning on bed surface mobility and embryo survival, *Canadian Journal of Fisheries and Aquatic Sciences*, *53*(5), 1061–1070, doi: 10.1139/f96-028.

Montgomery, D. R., E. M. Beamer, G. R. Pess, and T. P. Quinn (1999a), Channel type and salmonid spawning distribution and abundance, *Canadian Journal of Fisheries and Aquatic Sciences*, *56*(3), 377–387, doi: 10.1139/cjfas-56-3-377.

Montgomery, D. R., M. S. Panfil, and S. K. Hayes (1999b), Channel-bed mobility response to extreme sediment loading at Mount Pinatubo, *Geology*, *27*(3), 271–274, doi: 10.1130/0091-7613(1999)027<0271:CBMRTE>2.3.CO;2.

Mueller, E. R., and J. Pitlick (2013), Sediment supply and channel morphology in mountain river systems: 1. Relative importance of lithology, topography, and climate, *Journal of Geophysical Research: Earth Surface*, *118*(4), 2325–2342, doi: 10.1002/2013JF002843.

Mueller, E. R., J. Pitlick, and J. M. Nelson (2005), Variation in the reference Shields stress for bed load transport in gravel-bed streams and rivers, *Water Resources Research*, *41*(4), doi: 10.1029/2004WR003692.

Mueller, E. R., M. E. Smith, and J. Pitlick (2016), Lithology-controlled evolution of stream bed sediment and basin-scale sediment yields in adjacent mountain watersheds, Idaho, USA, *Earth Surface Processes and Landforms*, *1883*(May), 1869–1883, doi: 10.1002/esp.3955.

Nelson, P. a., W. E. Dietrich, and J. G. Venditti (2010), Bed topography and the development of forced bed surface patches, *Journal of Geophysical Research*, *115*(F4), F04,024, doi: 10.1029/2010JF001747.

Neville, H. M., D. J. Isaak, J. B. Dunham, R. F. Thurow, and B. E. Rieman (2006), Fine-scale natal homing and localized movement as shaped by sex and spawning habitat in Chinook salmon: insights from spatial autocorrelation analysis of individual genotypes., *Molecular Ecology*, *15*(14), 4589–602, doi: 10.1111/j.1365-294X.2006.03082.x.

NOAA (2011), North-Central California Coast Recovery Domain Summary and Evaluation of Central California Coastal Steelhead DPS, *Tech. rep.*, National Marine Fisheries Service, Southwest Region, Long Beach, California.

NOAA (2012), Final Recovery Plan for Central California Coast Coho Salmon Evolutionarily Significant Unit, *Tech. rep.*, National Marine Fisheries Service, Southwest Region, Santa Rosa, California.

O'Connor, J. E., J. F. Mangano, S. W. Anderson, J. R. Wallick, K. L. Jones, and M. K. Keith (2014), Geologic and physiographic controls on bed-material yield, transport, and channel morphology for alluvial and bedrock rivers, western Oregon, *Bulletin of the Geological Society of America*, *126*(X), 377–397, doi: 10.1130/B30831.1.

Paola, C., and D. Mohrig (1996), Palaeohydraulics revisited: palaeoslope estimation in coarse-grained braided rivers, *Basin Research*, *8*, 243–254.

Parker, G. (1978), Self-formed straight rivers with equilibrium banks and mobile bed. Part 2. The gravel river, *Journal of Fluid Mechanics*, *89*(1), 127–146.

Parker, G. (1990a), Surface-based bedload transport relation for gravel rivers Surface-based bedload transport relation for gravel rivers, *Journal of Hydraulic Research*, *28*(4), 417–436.

Parker, G. (1990b), The ACRONYM series of PSACAL programs for computing bedload transport in gravel rivers.

Parker, G., P. Klingeman, and D. L. McLean (1982), Bedload and size distribution in paved gravel bed streams, *Journal of Hydraulics Division, ASCE*, *108*, 544–571.

Parker, G., M. Hassan, and P. Wilcock (2006), Adjustment of the Bed Surface Size Distribution of Gravel-Bed Rivers in Response To Cycled Hydrographs, in *Gravel-Bed Rivers VI: From Process Understanding to River Restoration*, edited by H. Habersack, H. Pieglay, and M. Rinaldi, pp. 1–46, Elsevier B.V.

Parker, G., P. R. Wilcock, C. Paola, W. E. Dietrich, and J. Pitlick (2007), Physical basis for quasi-universal relations describing bankfull hydraulic geometry of single-thread gravel bed rivers, *Journal of Geophysical Research*, *112*, F04,005, doi: 10.1029/2006JF000549.

Pazzaglia, F. J., and M. T. Brandon (2001), A fluvial record of long-term steady-state uplift and erosion across the Cascadia forearc high, western Washington State, *American Journal of Science*, *301*, 385–431, doi: 10.2475/ajs.301.4-5.385.

Pfeiffer, A. M., and N. J. Finnegan (2017), Basin-scale methods for predicting salmonid spawning habitat via grain size and riffle spacing, tested in a California coastal drainage, *Earth Surface Processes and Landforms*, *42*(6), 941–955, doi: 10.1002/esp.4053.

Pfeiffer, A. M., N. J. Finnegan, and J. K. Willenbring (2017), Sediment supply controls equilibrium channel geometry in gravel rivers, *Proceedings of the National Academy of Sciences*, *114*(13), 3346–3351, doi: 10.1073/pnas.1612907114.

Phillips, C. B., and D. J. Jerolmack (2016), Self-organization of river channels as a critical filter on climate signals, *Science*, *352*(6286), 694–697, doi: 10.1126/science.aad3348.

Pitlick, J., E. R. Mueller, C. Segura, R. Cress, and M. Torizzo (2008), Relation between flow, surfaceâĂŘlayer armoring and sediment transport in gravelâĂŘbed rivers, *Earth Surface Processes and Landforms*, *33*(8), 1192–1209, doi: 10.1002/esp.1607.

Pizzuto, J. E. (1994), Channel adjustments to changing discharges, Powder River, Montana, *Geological Society of America Bulletin*, *106*(11), 1494–1501, doi: 10.1130/0016-7606(1994)106<1494:CATCDP>2.3.CO;2.

Power, M. E., M. S. Parker, and W. E. Dietrich (2008), Seasonal Reassembly of a River Food Web: Floods, Droughts, and Impacts of Fish, *Ecological Monographs*, *78*(2), 263–282.

Prancevic, J. P., and M. P. Lamb (2015), Unraveling bed slope from relative roughnessin initial sediment motion, *Journal of Geophysical Research: Earth Surface*, *120*, 474–489, doi: 10.1002/2014JF003323.Received.

PRISIM Climate Group (2004), 30-year Normal: annual precipitation.

Recking, A. (2013), Simple Method for Calculating Reach-Averaged Bed-Load Transport, *Journal of Hydraulic Engineering*, *139*(1), 70–75, doi: 10.1061/(ASCE)HY.1943-7900.0000653.

Reusser, L., P. Bierman, and D. Rood (2015), Quantifying human impacts on rates of erosion and sediment transport at a landscape scale, *Geology*, *43*(2), 171–174, doi: 10.1130/G36272.1.

Rickenmann, D., and A. Recking (2011), Evaluation of flow resistance in gravel-bed rivers through a large field data set, *Water Resources Research*, *47*(7), W07,538, doi: 10.1029/2010WR009793.

Riebe, C., L. Sklar, B. Overstreet, and J. Wooster (2014), Optimal reproduction in salmon spawning substrates linked to grain size and fish length, *Water Resources Research*, *50*, 898–918, doi: 10.1002/2013WR014231.Received.

Robinson, C. T., S. Aebischer, and U. Uehlinger (2004), Immediate and habitat-specific responses of macroinvertebrates to sequential, experimental floods, *Journal of the North American Benthological Society*, *23*(4), 853–867, doi: 10.1899/0887-3593(2004)023<0853:IAHROM>2.0.CO;2.

Roni, P., and T. P. Quinn (2001), Density and size of juvenile salmonids in response to placement of large woody debris in western Oregon and Washington streams, *Canadian Journal of Fisheries and Aquatic Sciences*, *58*(2), 282–292, doi: 10.1139/cjfas-58-2-282.

Rosenfeld, J., M. Porter, and E. Parkinson (2000), Habitat factors affecting the abundance and distribution of juvenile cutthroat trout (Oncorhynchus clarki) and coho salmon (Oncorhynchus kisutch), *Canadian Journal of Fisheries and Aquatic Sciences*, *57*(4), 766–774, doi: 10.1139/f00-010.

Rubin, D. M., and D. J. Topping (2001), Quantifying the relative importance of flow regulation and grain size regulation of suspended sediment transport α and tracking changes in grain size of bed sediment β, *Water Resources Research*, *37*(1), 133–146, doi: 10.1029/2000WR900250.

Scrimgeour, G. J., R. J. Davidson, and J. M. Davidson (1988), Recovery of benthic macroinvertebrate and epilithic communities following a large flood, in an unstable, Braided, New Zealand River, *New Zealand Journal of Marine and Freshwater Research*, *22*(3), 337–344, doi: 10.1080/00288330.1988.9516306.

Segura, C., J. H. McCutchan, W. M. Lewis, and J. Pitlick (2011), The influence of channel bed disturbance on algal biomass in a Colorado mountain stream, *Ecohydrology*, *4*(3), 411–421, doi: 10.1002/eco.142.

Shapovalov, L., and A. Taft (1954), *Fish Bulletin No. 98. Life histories of steelhead Rainbow Trout (Salmo gairdneri gairdneri) and Silver Salmon (Oncorhynchus kisutch)*, State of California Department of Fish and Game.

Sklar, L. S., and W. E. Dietrich (2006), The role of sediment in controlling steady-state bedrock channel slope: Implications of the saltationâĂŞabrasion incision model, *Geomorphology*, *82*(1-2), 58–83, doi: 10.1016/j.geomorph.2005.08.019.

Sklar, L. S., and W. E. Dietrich (2008), Implications of the Saltation âĂŞ Abrasion Bedrock Incision Model for Steady-State River Longitudinal Profile Relief and Concavity, *Earth Surface Processes and Landforms*, *1151*, 1129–1151, doi: 10.1002/esp.

Smith, B. K., and J. A. Smith (2015), The Flashiest Watersheds in the Contiguous United States, *Journal of Hydrometeorology*, *16*(6), 2365–2381, doi: 10.1175/JHM-D-14-0217.1.

Snyder, N. P., A. O. Nesheim, B. C. Wilkins, and D. A. Edmonds (2013), Predicting grain size in gravel-bedded rivers using digital elevation models: Application to three Maine watersheds, *Geological Society of America Bulletin*, *125*(1-2), 148–163, doi: 10.1130/B30694.1.

Sogard, S. M., J. E. Merz, W. H. Satterthwaite, M. P. Beakes, D. R. Swank, E. M. Collins, R. G. Titus, and M. Mangel (2012), Contrasts in Habitat Characteristics and Life History Patterns of Onchorynchus mykiss in California's Central Coast and Central Valley, *Transactions of the American Fisheries Society*, *141*(March 2015), 747–760, doi: 10.1080/00028487.2012.675902.

Soulsby, C., A. F. Youngson, H. J. Moir, and I. A. Malcolm (2001), Fine sediment influence on salmonid spawning habitat in a lowland agricultural stream: a preliminary assessment., *The Science of the Total Environment*, *265*(1-3), 295–307.

Thurow, R. F. (2000), Dynamics of Chinook Salmon Populations Within Idaho's Frank Church Wilderness: Implications for Persistence, *Usda forest service proceedings*, USDA Forest Service.

Tonina, D., and J. M. Buffington (2009), A three-dimensional model for analyzing the effects of salmon redds on hyporheic exchange and egg pocket habitat, *Canadian Journal of Fisheries and Aquatic Sciences*, *66*(12), 2157–2173, doi: 10.1139/F09-146.

Townsend, C. R., M. R. Scarsbrook, and S. Dolédec (1997), The intermediate disturbance hypothesis, refugia, and biodiversity in streams, *Limnology and Oceanography*, *42*(5), 938–949, doi: 10.4319/lo.1997.42.5.0938.

Turowski, J. M., D. Rickenmann, and S. J. Dadson (2010), The partitioning of the total sediment load of a river into suspended load and bedload: A review of empirical data, *Sedimentology*, *57*(4), 1126–1146, doi: 10.1111/j.1365-3091.2009.01140.x.

Viparelli, E., D. Gaeuman, P. Wilcock, and G. Parker (2011), A model to predict the evolution of a gravel bed river under an imposed cyclic hydrograph and its application to the Trinity River, *Water Resources Research*, *47*(2), 1–22, doi: 10.1029/2010WR009164.

Whipple, K. X. (2004), Bedrock Rivers and the Geomorphology of Active Orogens, *Annual Review of Earth and Planetary Sciences*, *32*(1), 151–185, doi: 10.1146/annurev.earth.32.101802.120356.

Wilcock, P., and J. Crowe (2003), Surface-based transport model for mixed-size sediment, *Journal of Hydraulic Engineering*, *129*(2), 120–128.

Wilcock, P. R., and B. T. DeTemple (2005), Persistence of armor layers in gravel-bed streams, *Geophysical Research Letters*, *32*(8), 1–4, doi: 10.1029/2004GL021772.

Wilkins, B., and N. Snyder (2011), Geomorphic comparison of two Atlantic coastal rivers: toward an understanding of physical controls on Atlantic salmon habitat, *River Research and Applications*, *27*, 135–156, doi: 10.1002/rra.

Willenbring, J. K., A. T. Codilean, and B. McElroy (2013), Earth is (mostly) flat: Apportionment of the flux of continental sediment over millennial time scales, *Geology*, *41*(3), 343–346, doi: 10.1130/G33918.1.

Williams, G. P. (1978), Bank-full discharge of rivers, *Water Resources Research*, *14*(6), 1141, doi: 10.1029/WR014i006p01141.

Wolman, M. G. (1954), A method of sampling coarse river-bed material, *Transactions, American Geophysical Union*, *35*, 951–956.

Wyrick, J. R., and G. B. Pasternack (2014), Geospatial organization of fluvial landforms in a gravel-cobble river: Beyond the riffle-pool couplet, *Geomorphology*, *213*, 48–65, doi: 10.1016/j.geomorph.2013.12.040.

Yager, E. M., J. W. Kirchner, and W. E. Dietrich (2007), Calculating bed load transport in steep boulder bed channels, *Water Resources Research*, *43*, W07,418, doi: 10.1029/2006WR005432.